TECHNISCHE UNIVERSITÄT MÜNCHEN
Lehrstuhl für Anorganische Chemie mit Schwerpunkt Neue Materialien

Synthesis and Characterization of Tin Polyanions Endohedrally Filled with Transition Metal Group 9 Atoms

Haiyan He

Vollständiger Abdruck der von der Fakultät für Chemie der Technischen Universität München zur Erlangung des akademischen Grades eines Doktors der Naturwissenschaften genehmigten Dissertation.

Vorsitzender: Univ.- Prof. Dr. Tom Nilges
Prüfer der Dissertation: 1. Univ.- Prof. Dr. Thomas F. Fässler
2. Univ.- Prof. Dr. Lukas Hintermann

Die Dissertation wurde am 05.08.2014 bei der Technischen Universität München eingereicht und durch die Fakultät für Chemie am 02.09.2014 angenommen.

For My Parents and Yang

Die vorliegende Arbeit wurde zwischen September 2010 und Juli 2014 am Lehrstuhl für Anorganische Chemie mit Schwerpunkt Neue Materialien der Technischen Universität München unter wissenschaftlicher Anleitung durch Prof. Dr. Thomas F. Fässler angefertigt.

Ich erkläre hiermit an Eides statt, dass ich die vorliegende Arbeit ohne unzulässige Hilfe Dritter und ohne Benutzung anderer als der angegebenen Hilfsmittel angefertigt habe. Die aus anderen Quellen direkt oder indirekt übernommenen Daten und Konzepte sind unter Angabe des Literaturzitates gekennzeichnet.

Garching, den 2014

Acknowledgement

I would like express my deepest gratitude to my supervisor,

Prof. Dr. Thomas F. Fässler

for providing me an opportunity to work in his group. I am appreciated for his dedicated guidance and thoughtful ideas throughout the whole project.

My gratitude also goes:

To Dr. **Wilheim Klein** for the supportive assistance with crystallographic complicated matters and all kind helps, especially great support in the manuscripts preparation and revisions.

To Dr. **Viktor Hlukhyy** for all the helps in solid state synthesis and paper revisions and the guidance of crystallographic structure refinements.

To Priv.-Doz. Dr. **Florian Kraus** and Dr. **Christian Benda** for all the discussions and friendly support.

To Dr. **Annette Schier** for her kindly experimental and mental support.

To Dr. **Lei Zhang** and Dr. **Shengping Guo** for paper revisions and their friendship.

To **Hanpeng Jin** for his help in solid state synthesis and the friendship.

To Prof. Dr. **Klaus Köhler**, **Oliver Dachwald** and Dr. **Carmen Haeßner** for their assistance in EPR measurements

To Prof. Dr. **Reinhard Niessner** and **Haibo Zhou** for their assistance in Raman spectroscopy measurements.

To Ms. **Ingrid Werner** and **Andrea Hoffmann** for their assistance in EDX and REM analysis.

To **Kerstin Mayer**, **Christina Fischer** and Dr. **Sergei Vagin** for their assistance in Mass spectroscopy measurements.

To Ms. **Georgetta Krutsch**, Dr. **Magnus Buchner**, Mr. **Jürgen Kudermann** and **Maria Weindl** for their assistances in NMR measurements.

To Ms. **Manuela Donaubauer** and Ms. **Lucia Weissenborn** for their kind assistance in organizational issues and all the helps in my life.

To my student **André Utrap** in practice training for his hard work and the friendship.

To all my **colleagues** in Prof. Thomas Fässler's, P.D. Florian Kraus's and Prof. Tom Nilges's research group and all my friends with whom I spent a nice time in Munich.

To **Chinese Scholarship Council** for the financial support in Germany.

Finally, to my parents and Yang for supporting me as always.

Zusammenfassung

Endohedral gefüllte Tetrelatom-Zintl-Cluster werden üblicherweise aus Lösungen der binären Phasen A_4E_9 (homoatomare E_9 Cluster, E = Ge, Sn und Pb) durch Reaktion mit metallorganischen Reagenzien erhalten. Die Darstellungsvariante endohedraler Zintl-Cluster durch die Extraktion intermetallischer Phasen, welche bereits gefüllte Cluster erhalten, bringt Vorteile, wenn größere gefüllte Zintl-Cluster aus Lösung isoliert wer den sollen.

Die Extraktion der endoedralen Zintl-Phase $K_{4.79}Co_{0.79}Sn_9$ mit Ethylendiamin in Gegenwart von komplexierenden Reagenzien führt unter verschiedenen Reaktionsbedingungen zu drei Typen Co-zentrierter Polyanionen, von welchen [Co@Sn_9], [Co@Sn_{10}] und [Co_2@Sn_{17}] als K[2.2.2]crypt Salze isoliert wurden. Eine unendlich ausgedehnte Zick-Zack Kette $^1_\infty\{$ [K(Co@Sn_9)]$_{0.68}$[KSn_9]$_{0.32}\}$ mit verbrückenden Kaliumatomen treten in der Verbindung **K[K([2.2.2]crypt)]$_3$[Co@Sn_9]$_{0.68}$[Sn_9]$_{0.32}$** auf. Zwei dimere Einheiten von [Co_2@Sn_{17}]$^{5-}$ in welcher zwei Co@Sn_9-Cluster über ein gemeinsames Sn-Atom und mit unterschiedlicher Anordnung verknüpft sind, kristallisieren in **[K([2.2.2]crypt)]$_5$[Co_2@Sn_{17}]** und **[K[2.2.2]crypt]$_5$[Co_2@Sn_{17}]·en·tol**. Zwei weitere monomere Einheiten wurden in der Verbindung **[K([2.2.2]crypt)]$_6$[Sn_9]$_{1.21}$[Co@Sn_9]$_{0.12}$[Co@Sn_{10}]$_{0.67}$·3en·tol** charakterisiert.

Die Reaktion der ternären Phase mit der nominellen Zusammensetzung "K_3RhSn_6" in Ethylendiamin führt zum ersten Rh-zentrierten Cluster in der Verbindung **[K([2.2.2]crypt)]$_6$[Sn_9]$_{1.53}$[Rh@Sn_{10}]$_{0.47}$·3en·tol**, welch isotrukturell zu Kristallen von [K([2.2.2]crypt)]$_6$[Sn_9]$_{1.21}$[Co@Sn_9]$_{0.12}$[Co@Sn_{10}]$_{0.67}$·3en·tol ist. Der paramagnetische Charakter der Verbindung wurde mittels EPR Spektroskopie nachgewiesen. Ein Iridium-zentrierter Cluster [Ir@Sn_{12}]$^{3-}$ in dem Salz **[Rb([2.2.2]crypt)]$_3$[Ir@Sn_{12}]·en·2tol** wurde direkt aus einer Lösung des Festkörpers der nominellen Zusammensetzung "Rb_3IrSn_{12}" erhalten. Das Derivat [K([2.2.2]crypt)]$_3$[Ir@Sn_{12}]·en·tol wurde früher durch schrittweise Synthese aus einer Lösung von Sn_9^{4-} dargestellt.

Aus Lösungen von Rb_4Sn_9 oder $K_{4.79}Co_{0.79}Sn_9$ mit $SbPh_3$ in

Ethylendiamin ließen sich zwei Arten von heteroatomaren Clustern $\mathbf{[\mathit{E}_{9-x}\mathit{E}'_x]^{2-}}$ und $\mathbf{[Co@\mathit{E}_{9-x}\mathit{E}'_x]^{2-}}$ (**E = Sn, E' = Sb**) in den Verbindungen **[Rb([2.2.2]crypt)]$_2$[Sn$_{9-x}$Sb$_x$]·3tol·2en** (**x≈2**), sowie in **[K([2.2.2]crypt)]$_2$[Co$_x$@Sn$_{7-x}$Sb$_{2+x}$] (x≈0.58)** isolieren.

Schließlich wurde ein weiterer zweifach vinylierter dimerer Ge_9-Cluster in der Verbindung **K(18-crown-6)en$_2$][K(18-crown-6)]$_3$[Ge$_9$(CH=CH$_2$)]$_2$·2en** kristallisiert und durch Ramanspektroskopie charakterisiert. Zum ersten Mal wird ein $[Sn_9]^{4-}$ Cluster, welcher mit zwei verschiedenen Kronenethern kristallisiert, in der Verbindung **[K(18-crown-6)]$_2$[K([2.2.2]crypt)][KSn$_9$]·1.5en** isoliert.

Alle Verbindungen wurden mittels Einkristallröntgenstrukturanalyse charakterisiert.

Abstract

Group 14 Zintl clusters with transition metal inserted, namely endohedral Zintl ions, are commonly obtained from the dissolution of A_4E_9 phases (containing unfilled homoatomic E_9 clusters, E = Ge, Sn, Pb) and subsequent reaction with organometallic compounds in solution. Endohedrally filled Zintl ions synthesized by solid state routes show great advantages as a potential precursor to build larger species of endohedral clusters.

By the extraction of endohedral Zintl phase $K_{4.79}Co_{0.79}Sn_9$ with ethylenediamine in presence of sequestering reagent under different reaction conditions, three types of crystals with cobalt-centered clusters appear in K[2.2.2]crypt-salts: [Co@Sn_9], [Co@Sn_{10}] and [Co_2@Sn_{17}]. A infinite zigzag chain with potassium atoms as bridging linkers $^1_\infty$[K($Co_{0.68}$@Sn_9)] appear in **K[K([2.2.2]crypt)]$_3$[Sn$_9$]$_{0.32}$[Co@Sn$_9$]$_{0.68}$**, two [Co_2@Sn_{17}]$^{5-}$ dimer clusters in which two Co@Sn_9 units share one common Sn atom, with different tortuosity are formed in **[K([2.2.2]crypt)]$_5$[Co$_2$@Sn$_{17}$]** and **[K[2.2.2]crypt]$_5$[Co$_2$@Sn$_{17}$]·en·tol**. Further two monomeric clusters were characterized in **[K([2.2.2]crypt)]$_6$[Sn$_9$]$_{1.21}$[Co@Sn$_9$]$_{0.12}$[Co@Sn$_{10}$]$_{0.67}$·3en·tol**.

The reaction of the ternary phase with the nominal composition "K_3RhSn_6" in ethylenediamine lead to the first Rh-filled clusters in **[K([2.2.2]crypt)]$_6$[Sn$_9$]$_{1.53}$[Rh@Sn$_{10}$]$_{0.47}$·3en·tol**. The crystals are isostructural to [K([2.2.2]crypt)]$_6$[Sn_9]$_{1.21}$[Co@Sn_9]$_{0.12}$[Co@Sn_{10}]$_{0.67}$·3en·tol. The paramagnetic nature of the clusters was further analyzed by EPR spectroscopy. An Iridium-capsuled cluster [Ir@Sn_{12}]$^{3-}$ was directly isolated in **[Rb([2.2.2]crypt)]$_3$[Ir@Sn$_{12}$]·en·2tol** by the extraction of the phase with nominal composition "Rb_3IrSn_{12}", whose analogue derivative [K([2.2.2]crypt)]$_3$[Ir@Sn_{12}]·en·tol was achieved before by a stepwise synthesis in solution from Sn_9^{4-} ions.

From the reactions of the compounds Rb_4Sn_9 and $K_{4.79}Co_{0.79}Sn_9$ with $SbPh_3$ in ethylenediamine, two kinds of heteroatomic clusters **[$E_{9-x}E'_x$]$^{2-}$** and **[Co@$E_{9-x}E'_x$]$^{2-}$** (**E = Sn, E' = Sb**), respectively, were isolated in the compounds **[Rb([2.2.2]crypt)]$_2$[Sn$_{9-x}$Sb$_x$]·3tol·2en** (**x≈2**) and **[K([2.2.2]crypt)]$_2$[Co$_x$@Sn$_{7-x}$Sb$_{2+x}$]** (**x≈0.58**), respectively.

Finally, a novel bisvinylated dimeric Ge_9 cluster was characterized in form of crystals of **[K(18-crown-6)en$_2$][K(18-crown-6)]$_3$[Ge$_9$(CH=CH$_2$)]$_2$·2en** and further investigated by Raman spectroscopy. A $[Sn_9]^{4-}$ cluster with mixed sequestering reagents was found in **[K(18-crown-6)]$_2$[K([2.2.2]crypt)][KSn$_9$]·1.5en**.

All compounds were structurally characterized by single crystal X-ray diffraction methods.

Table of Contents

1 Introduction

1.1 Bimetallic Compounds and their Application

The intermetallic compound is a kind of alloy phase without distinct boundary, which has been suggested to be the promising material species for their chemical and physical properties. Bimetallic compounds, especially transition metal stannides, have been widely used as technological important materials for various applications.[1] For example, the binary intermetallic Cu-Sn phases show great importance in artbronzes with large amounts of utilizations in daily life. The Co-Sn composites can be applied in a variety of negative electrode materials for rechargeable lithium batteries.[2] The functional nanomaterial of group 14 atoms (Si to Pb elements) can serve as an important role in catalytic progress or fuel/solar cells.

By the introduction of bimetallic compounds as catalysis application, the high temperature (250-300 ℃) and high pressure (20-35 MPa) of reactions can be significantly reduced. Generally, monometallic catalysts such as Raney nickel or $Pt(Pd)/Al_2O_3$ are classic catalysts for the hydrogenation of C=C double bond.[3] While the bimetallic catalysts or/and promoter with mono-metallic catalysts show great ability to enhance the hydrogenation of C=O bond by selective hydrogenation of α, β unsaturated carbonyl compounds. Especially, the preparation of composing the metal and the addictive has important influence on their catalytic ability. In 1989, Narasimhan reported a mixed ruthenium-tin boride over alumina for selective hydrogenations of methyl oleate to oleyl alcohol efficiently under relatively low pressure.[4] The catalyst $RuSn/Al_2O_3$ (with Sn/Ru=2) was synthesized by the impregnation of

$RuCl_3$ and $SnCl_2$ and then reduced by sodium boronhydride, which could bring 80% conversion with 80% selectivity for the hydrogenation. Mizukami and coworkers improved the synthetic methodology for this kind of catalyst *via* a sol-gel method without boron.[5] Based on Narasimhan's method, Barrault *et al.* developed cobalt-tin catalyst system, which is less active but presents comparable selectivity catalyst to Ru-Sn catalyst.[6] Nowadays, Co-Sn and Ru-Sn catalysts are also widely utilized in heterogeneous catalytic synthesis of fatty alcohols. The platinum stannides Pt_3Sn and Pt_2Sn have been investigated to convert cyclohexane to benzene effectively.[7]

The tin-based intermetallic compounds and alloys also bring bright prospects for their potential application as new anode materials in lithium-ion batteries. A series of such materials have been explored and studied, such as Cu_6Sn_5, $MnSn_2$, Mn_3Sn, FeSn, $CoSn_2$, Ag_3Sn, Ni_3Sn_2, and etc.[8-17] The aforementioned reductive precipitation with $NaBH_4$ has been also exploited to synthesize alloyed and intermetallic powders for Li-ion batteries. This "bottom-up" approach is different from the "top-down" method of the mechanical grinding and alloying by ball-milling. With the assistance of electrostatic spray pyrolysis, ultrafine powder with particular particle size and size distribution can be obtained, which is crucial for the high storage capacity and cyclic performance stability of these multiphase materials.[18]

1.2 Tetrel Zintl Phase and Zintl Ions

Group 14 elements in the periodic table are consisted of elements carbon, silicon, germanium, tin and lead, and the properties of these individual homologues differ significantly. The non-metal carbon atom tends mainly to the formation of covalent bonds; in compounds with the semiconducting properties, silicon exhibits the polar bond character. As the heaviest element of this group, lead is a metal that crystallizes in cubic closest packing crystallizes and forms electronegative reactants salts. According to the general rules of the periodic table, it is assumed that the electronegativity of the elements will decrease with increasing atomic number. However, later tetrel atoms show great advantages to form compounds where they carry a negative charge.

1.2.1 The Structure of Tetrel Zintl Phase

The homoatomic polyanions have attracted great research interest over a century, since Joannis observed the reduction of elemental lead in liquid ammonia solutions by sodium metal with a change in color, and Smyth suggested the existence of $Pb_{2.25}^{-}$ or Pb_9^{4-} anions.[19-21] In the early 1930s, Zintl and coworkers investigated atomic volume contraction to predict formation of the alkali metal cations and determined the composition of different polyanions $[E_9]^{4-}$ (E = Sn, Pb) and $[E_7]^{3-}$ (E = Sb, As) by employing potentiometric titration.[22-24] It was a great breakthrough that lead was introduced to form an ionic compound with a negative oxidation state instead of any oxidation state +2 or +4, in which the more electropositive metal completely transfer valence electrons to the electronegative atoms.[25] Due to the pioneering work of Zintl in this area, the term "Zintl Phases" was first used by Laves in 1941 and posthumously named after him to describe these species of compounds.[26]

Zintl phases are intermetallic compounds composed by an electropositive alkali metals or alkaline-earth metals (without Be) or lanthanides (A) and an electronegative post transition metals or metalloids from group 13 to group 16 elements (E, without sulfur and period 2), which can be described by the general formula $[A^{+}]_m[E_n]^{m-}$ with fixed stoichiometry. [27] Because of their electronic bonding nature somewhere between metallic bonding and covalent bonding, Zintl phases exhibit special physical properties such as high melting points, metallic luster, high brittleness, high hardness, and poor conductivity or good semi-conductivity (band gap 2-2.5 eV) with Landau diamagnetic or Pauli paramagnetic.[28,29]

The *Zintl line*, the hypothetical boundary separating element group 13 and 14, substantiates the formation of isoelectronic substructures from other group accompanying with a formal electron transfer. These electron-rich solid state compounds can be obtained by reducing elements beyond Zintl line with electropositive elements in solid state synthesis at high temperature. In the case of Zintl phases from alkali metal and group 14 elements, the characteristic of their structure is the formation of $[E_n]^{m-}$ polyanions with diverse networks besides cage-like polyhedron depending on the degree of reduction: isolated E^{4-} ions in Mg_2Si, [30] dumbbell-like $[E_2]^{6-}$ in Li_7Ge_2,[31] and ring $[E_6]^{10-}$ in $Ba_4Li_2Si_6$.[32]

The bonding situation and observed formulas of Zintl clusters elucidated by the Zintl-Klemm concept at an earlier time,[33] then the Mooser-Pearson extended (8-*N*) rule.[34] Later the Wade-Mingos rules developed to understand the skeletal electrons to build the Zintl clusters.[35,36]

1.2.2 Electronic Structure of Polyanionic E_9 Zintl Clusters

In cluster chemistry, as fundamental building blocks, the deltahedra are polyhedra with only triangular faces. Deltahedral Zintl clusters with more than four vertices in $[E_n]^{m-}$ (*E* = Si-Pb, n = 4, 5, 9, 10, 12, m = 2, 3, 4) are electron-deficient. The bonding in many these kinds of clusters cannot be understood by means of two-center-two-electron bonds. The delocalization of valence electrons can be considered to compensate the electron deficiency. The relationship between the structure of a cluster and its valence electrons can be illustrated by Wade-Mingos rules (Wades' rules), which were originally developed to understand the bonding in delocalized electron-deficient boranes.[37-39] According to Wade-Mingos rules, a *closo*-cluster with n vertices atoms is particularly stable when it has 2n+2 skeletal electrons. The structure of a *nido*-cluster is derived from the structure of a *closo*-cluster with a missing polyhedral and possesses 2n+4 skeletal electrons. An *arachno*-cluster with two missing polyhedral has 2n+6 skeletal electrons, while a *hypo*-cluster with three polyhedral vertices disappeared possesses 2n+8 skeletal electrons.

Specifically, the nine-atom clusters $[E_9]^{x-}$ (*E* = Si-Pb , x = 2, 3, 4) can display flexible structures. Two ideal structure types are: (i) the tricapped trigonal prism with D_{3h}-symmetry, representative of a *closo*-cluster with 20 skeletal electrons in $[E_9]^{2-}$; (ii) a monocapped square antiprism with C_{4v}-symmetry, giving a *nido*-cluster with 24 skeletal electrons in $[E_9]^{4-}$. Meanwhile, the intermediate $[E_9]^{3-}$ with 21 skeletal electrons cannot be classified by Wades' rules, whose structure should be between two forms above.

Although the observed structures are often between these two ideal structures, it can be well discussed by applying structural parameters associated with slight distortions in the structure of an ideal example.[40] This system for description of the shapes of empty nine-vertex clusters

was established by Corbett with specific edge ratios and developed by Fässler with additional dihedral angles.[40-42] In Figure 1.1, the letter *e* stands for the edge length of the prism basal plane and *h* represents the height of the trigonal prism. The letter α is the torsion angle over *h*. The letters d_1 and d_2 stand for the diagonal lengths of the open square face. (i) $[E_9]^{2-}$ cluster with D_{3h}-symmetry shows a structure of a tricapped trigonal prism, when $h_1=h_2=h_3$, $e_1=e_2=e_3$ and $\alpha_1=\alpha_2=\alpha_3$. (ii) $[E_9]^{4-}$ cluster with C_{4v}-symmetry has a monocapped square antiprism, when $d_1=d_2$ and $\alpha_1=0$. The movement of the atom 2 and atom 4 out of the plane 1-2-3-4 will change d_2 and cause the symmetry transformation from C_{4v} through C_{2v} to D_{3h}, which occurs during oxidation. Sevov suggested that the Zintl clusters in solution represent equilibrium between different charges through releasing solvated electrons, which can be described by the equation:

$[E_9]^{4-} \rightleftharpoons [E_9]^{3-} + e^- \rightleftharpoons [E_9]^{2-} + 2\ e^-$.[43]

In spite of the charge differences, the geometries and the electronic structures of $[E_9]^{x-}$ show no significant difference. Ab initio calculations shows that the two structures C_{4v} and D_{3h} of $[Sn_9]$ only differ slightly in energy, with a gap of -3.5~+4.7 kJ/mol under the smallest basis set.[44]

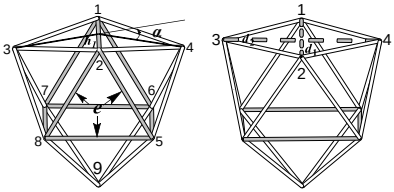

Figure 1.1 Structures of $[E_9]^{x-}$ clusters with C_{4v} and D_{3h} symmetries.[45]

1.2.3 Chemistry of Zintl Anions Containing Group 14 Clusters in Solution

The aforementioned term "Zintl phases" mainly represents the solid state intermetallic compounds, which are soluble in polar aprotic solvents sometimes; while "Zintl anions" is applied to describe the discrete polyanions in Zintl phases. Zintl phases and Zintl anions had not been discriminated as two separate concepts until the discovery of

the phases Cs_4Ge_9 and $A_{12}E_{17}$ (A = Na - Rb; E = Si, Ge, Sn) at the end of the nineteenth century, [46-49] whose solid and solution structures are consisted of the same $[E_9]^{4-}$ clusters. The $A_{12}E_{17}$ phases are composed with $[E_4]^{4-}$ and $[E_9]^{4-}$ clusters in the ratio of 2:1.[40] Generally, Zintl anions can be synthesized by dissolving the phases with nominal composition A_4E_9 (A = K – Cs; E = Ge, Sn, Pb) in liquid ammonia or polar aprotic solvents such as ethylenediamine, dmf, acetonitrile, THF, *etc.*, which are resilient against the reduction and can stabilize high charges. The usage of cation-sequestering reagents, the macropolycyclic ligands such us [2.2.2]crypt and 18-crown-6, promotes the crystallization and crystallographic characterization of Zintl anions by single crystal X-ray diffraction.[50-54] The $[A(18\text{-crwon-}6)]^+$ units can contact triangular or rectangular faces of E_9 clusters with η^3- or η^4- coordination.[24,55]

In solution, the polyanions are extensively used as molecular building blocks for different types of reactions, e.g., oxidation to polymers or larger aggregates, or reaction with organometallic compounds, and organic ligands modifications.[43,55-60] From the last century until now, a large and still growing number of publications about polyhedral Zintl anions in polar and aprotic solvents have been reported, indicating that these compounds and reactions attract great attention from chemists. A number of reviews on the subject "Zintl chemistry in solution" have been published, illustrating new findings in experimental methodologies, novel structures and complementary theories.[43,45,53,55,61-64]

Unfilled Zintl Clusters

In 1970, Diehl and Kummer discovered a Na-Sn alloy with a nominal composition between Na_2Sn_4 and Na_2Sn_5 in liquid ammonia and some other amines (e.g. ethylenediamine, N-dimethyl-ethylenediamine, diethylenetriamine and triethylenetetramine) at room temperature. [65] The produced clusters feature *nido*-type $[Sn_9]^{4-}$ polyhedral with diamagnetic properties. In 1975, Corbett and Edwards investigated suspicious $[Sn_9]^{4-}$ clusters in crystal $[Na([2.2.2]crypt)]_4[Sn_9]$ formed in the presence of sequestering reagent, whose structure was determined by X-ray diffraction.[66] The *closo*-type $[E_9]^{2-}$ clusters can be obtained after subsequent oxidation of $[E_9]^{4-}$ units in solution. [40,55,56,62,67-69] Till now, only two $[Si_9]^{2-}$ and $[Ge_9]^{2-}$ are exclusively accessible with a

charge of 2-.[68,69] While the paramagnetic $[E_9]^{3-}$ intermediates are the common acquisitions of most solvent-based oxidation reactions.[37,49,50,70-74] The $[Si_9]^{3-}$ anion was isolated firstly in 2004 by Sevov *et al.* [70]

The number of publications about new solvate structures of $[E_9]^{x-}$ (x = 2, 3, 4) still keeps growing. The clusters $[E_n]^{x-}$ with homogenious elements tolerate inceasing atomic number n = 4, 5, 9, 10 and 12, consequently with distinct charges x = 2, 3 and 4. The anion $[Pb_{10}]^{2-}$ is the largest unfilled cluster until now, which was found in solid crystal $[K([2.2.2]crypt)]_2[Pb]_{10}$.[75] The clusters $[E_{12}]^{2-}$ (E = Sn, Pb) were only detected in gas phase but not in solution and solid state yet (Figure 1.2).[76-79]

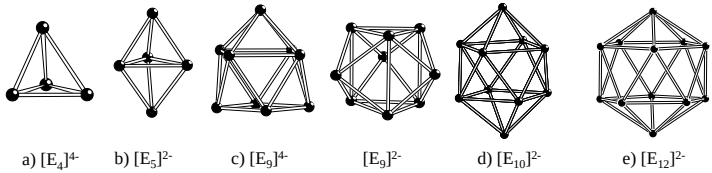

Figure 1.2 Homoatomic polyanions of group 14 elements: (a) tetrahedral $[E_4]^{4-}$ (E = Si - Pb); (b) trigonal bipyramidal $[E_5]^{2-}$ (E = Si – Pb); (c) nine-atom cages $[E_9]^{n-}$ (n = 2 – 4; E = Si – Pb); (d) $[Pb_{10}]^{2-}$ in crystal $[K([2.2.2]crypt)]_2[Pb]_{10;}$ [75] (e) $[E_{12}]^{2-}$ (E = Sn, Pb) in gas phase. [76-79]

Oligo-and Polymers of Zintl Clusters

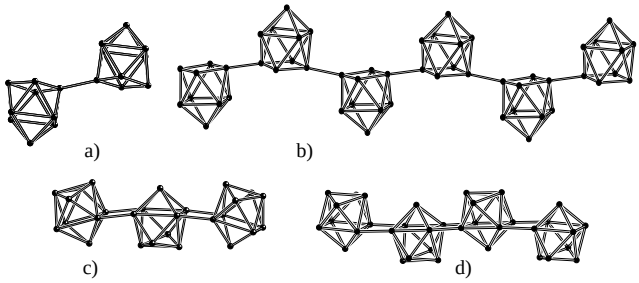

Figure 1.3 Oligo-and polymers of Zintl clusters. (a) dimer $[Ge_9\text{-}Ge_9]^{6-}$ [80,86,87] (b) polymer $^1_\infty[Ge_9]^{2-}$ [81,82] (c) trimer $[Ge_9{=}Ge_9{=}Ge_9]^{6-}$ [78] (d) tetramer $[Ge_9{=}Ge_9{=}Ge_9{=}Ge_9]^{8-}$.[79]

With mild oxidation, $[Ge_9]^{4-}$ clusters are able to form radicals and connect to each other to give oligomers or polymers. The first dimer $[Ge_9\text{-}Ge_9]^{6-}$ was reported in 1999, which could be considered as two covalently linked $[Ge_9]^{3-}$ clusters.[80] Guloy *et al.* obtained the polymer $^1_\infty[\ Ge_9]^{2-}$ with different sequestering agents 18-crown-6 and [2.2]diaza-(18-crown-6), which was formed via *exo*-bond of *nido*-type $[Ge_9]^{2-}$ clusters (Figure 1.3).[81,82] Trimer $[Ge_9{=}Ge_9{=}Ge_9]^{6-}$ and tetramer $[Ge_9{=}Ge_9{=}Ge_9{=}Ge_9]^{8-}$ have also been discovered with delocalized 2-electron multi-center bonds.[83,84] The isolation of oligomers or polymers of $[Si_9]$ and $[Pb_9]$ cluster anions has not been reported yet. While the anion $[Sn_9AgSn_9]^{5-}$ exhibits an *exo*-bond between two Sn_9 clusters stabilized by one Ag atom, indicating the existence of $[Sn_9\text{-}Sn_9]^{6-}$ dimers.[85]

Zintl clusters functionalized with main-group complexes

It has been reported that $[Ge_9]$ clusters can be functionalized by main group fragments *via* nucleophilic additions to clusters, such as reactions with triphenyl bismuth or triphenyl antimony. Sevov *et al.* described $[Ph_2Sb\text{-}Ge_9\text{-}SbPh_2]^{2-}$ and $[Ph_2Bi\text{-}Ge_9\text{-}BiPh_2]^{2-}$ clusters with *exo*-bonds generated between Ge and Sb/Bi atoms, and the two ligands bind to the open square of the *nido*-typed clusters. [88,89] $[Ph_2Sb\text{-}Ge_9\text{-}Ph]^{2-}$ is the first case of organically and main-group functionalized Zintl ions with Ge-C covalent bond, and dimer cluster $[Ph_2Sb\text{-}Ge_9\text{-}Ge_9\text{-}SbPh_2]^{4-}$ with the formation of one inter-cluster bond, shown in Figure 1.4.[89] Other derivatized Zintl ion bonds with group 14 elements have been established as well, like $[Ge_9\text{-}ER_3]^{3-}$, $[ER_3\text{-}Ge_9\text{-}ER_3]^{2-}$ and $[ER_3\text{-}Ge_9\text{-}Ge_9\text{-}ER_3]^{2-}$ (E = Ge, Sn; R = Me, Ph).[90] Especially, through silylation reaction of K_4Ge_9 by $Si(SiMe_3)_3Cl$ [tris(trimethylsilyl)silane chloride] in acetonitrile, a reduced anion $[Ge_9(SiR_3)_3]^-$ with a charge of -1 is obtained, which can be relatively stable in nonpolar solvent due to the large silyl group.[91] Another synthetic method taking advantage of disproportion reaction of subvalent metastable halide SnCl can be applied to build such as $[Sn_9(Si(SiR_3)_3)_2]^{2-}$ and $[Sn_9(Si(SiR_3)_3)_3]^-$ clusters.[92-94] The first case of tetra-substituted neutral cluster $[Ge_9(Si(SiMe_3)_3)_3(SnPh_3)]$ has been synthesized by $[Ge_9(Si(SiR_3)_3)_3]^-$ with Ph_3SnCl in the same year 2012.[95]

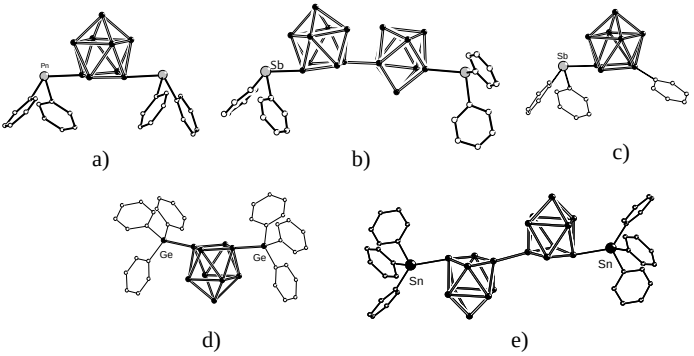

Figure 1.4 Selective cases of Zintl clusters functionalized with main group element compounds: (a) $[Ph_2Pn\text{-}Ge_9\text{-}PnPh_2]^{2-}$ (Pn = Sb, Bi),[88,89] (b) $[Ph_2Sb\text{-}Ge_9\text{-}Ge_9\text{-}SbPh_2]^{4-}$,[89] (c) $[Ph_2Sb\text{-}Ge_9\text{-}Ph]^{2-}$,[89] (d) $[Ph_3Ge\text{-}Ge_9\text{-}GePh_3]^{2-}$,[90] (e) $[Ph_3Sn\text{-}Ge_9\text{-}Ge_9\text{-}SnPh_3]^{4-}$.[90]

Zintl Clusters Functionalized with Organic Reagents

The alkylation or vinylation reaction of Zintl clusters is a novel exploitation area in Zintl chemistry, which leads to the formation of carbon-cluster *exo*-bonds. Some results are shown in Figure 1.5. Sevov and coworkers reported the first case in 2007, where the alkylation of K_4Ge_9 by *t*BuCl generate the two-fold functionalized dimer $[t\text{Bu-}Ge_9\text{-}Ge_9\text{-}t\text{Bu}]^{6-}$.[96] The applied organic reagents for vinylation have extended from halogenated hydrocarbons (*t*BuCl, *i*PrCl, *c*PrMeCl, *etc*.) to alkyne, e.g. $Me_3Si\text{-}C{\equiv}C\text{-}SiMe_3$ HC≡C-Ph, HC≡C-Ph-OMe, $Me_3Si\text{-}C{\equiv}C\text{-}Im\text{-}CH_3$, HC≡C-Fc, $HC{\equiv}C\text{-}CH_2NH_2$, $H_3C\text{-}C{\equiv}C\text{-}CH_2\text{-}CH_3$ and so on.[97-102]

Based on $Me_3Si\text{-}C{\equiv}C\text{-}SiMe_3$ [bis(trimethylsilyl)acetylene, BTMSA], mono- or bis- additional vinyl group can bind to Ge_9 clusters. The mechanism of the vinylation reaction is elucidated in Sevov's publication.[60] The vinylations of Zintl clusters give rise to hybrid building blocks consisted of organic functional groups and inorganic clusters, which provide a possibility for further reactive spot.

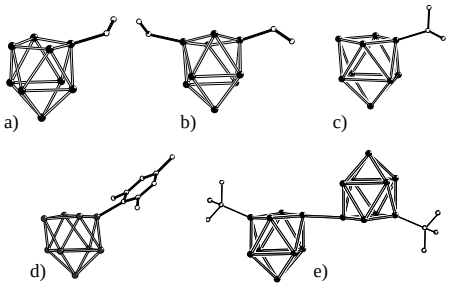

Figure 1.5 Zintl clusters with organic radicals. (a) $[Ge_9\text{-}CH{=}CH_2]^{3-}$ [103] (b) $[Ge_9\ (CH{=}CH_2)_2]^{2-}$ [98,103] (c) $[Sn_9\text{-}^{i}Pr]^{3-}$ [102] (d) $[Ge_9\text{-}Mes]^{3-}$ [103] (e) $[t\text{Bu-}Ge_9\text{-}Ge_9\text{-}t\text{Bu}]^{6-}$ [96].

Zintl Clusters Decorated with Transition Metal Complexes

Among the group 14 atom polyhedrons, nine-atom clusters $[E_9]$ are usually obtained as small charged nanoparticles of uniform size. [55] The atomic mobility of transition metal in bare metal clusters and small metallic nanoparticles (NPs) is of fundamental significance to show possibilities for the development of nano-scaled materials. As shown in Table 1.1, the distribution map reveals different reactive capabilities of the diverse transition metal derivatives with group 14 Zintl ions, which can be synthesized from the intermetallic precursors A_4E_9 (A = Na to Cs; E = Ge to Pb) or their derivatives.

Table 1.1 The distributions of transition metal derivatives of Group 14 Zintl ions sorted by elements.

Group	**3**	**4**	**5**	**6**	**7**	**8**	**9**	**10**	**11**	**12**
Period 4	Sc	Ti	V	Cr	Mn	Fe	Co	Ni	Cu	Zn
Period 5	Y	Zr	Nb	Mo	Tc	Ru	Rh	Pd	Ag	Cd
Period 6		Hf	Ta	W	Re	Os	Ir	Pt	Au	Hg
Inserted metal			**Capped/Ligated metal**				**Metal with both connection**			

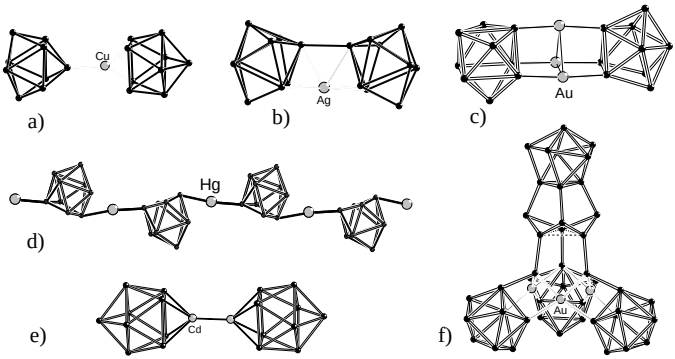

Figure 1.6 Selective cases of Zintl clusters with transition metal as linkers: (a) $[(\eta^4\text{-}Ge_9)Cu(\eta^1\text{-}Ge_9)]^{7-}$ [139] (b) $[(Sn_9)Ag(Sn_9)]^{5-}$, [85] (c) $[Au_3(Ge_9)_2]^{5-}$, [140] (d) $^1_\infty[Hg(Ge_9)]^{2-}$,[147] (e) $[(Pb_9)Cd\text{-}Cd(Pb_9)]^{6-}$, [142] and (f) $[Au_3Ge_{45}]^{9-}$.[140]

The functionalization with transition metal-introduced E_9 clusters includes directly atom insertion, capped by ligated various metal-organic fragments, linkage with naked metal, and reconstruction of an increasing nuclearity by fusion with two original clusters, or lose deltaheral-shape to form pentagonal clusters or the some combination (Figure 1.6, 1.7 and 1.8). In the field of group VIIIB elements, transition metals are apt to reside in the clusters due to the structures and reactivity of the metal cores. In Group 10 elements, atoms displace flexible ability to decorate the deltahedral clusters, resulting in rich resource of Ni-centered clusters ($[Ni@Sn_9H]^{3-}$,[104,105] $[Ni@Sn_9]^{4-}$,[106] $[Ni_2@Sn_{16}Ge]^{4-}$,[106] $[Ni@Sn_9Tl]^{3-}$,[104] $[Ni@Pb_{10}]^{2-}$,[107] $[Ni@Pb_{12}]^{2-}$,[76] $[Ni_2@Sn_{17}]^{4-}$,[108] $[Ni_3@Ge_{18}]^{4-}$,[109] $[Ni@Ge_9(PdPPh_3)]^{2-}$,[110]), Pd-centered clusters ($[Pd@Pb_{12}]^{2-}$,[76] $[Pd_2@Ge_{18}]^{4-}$,[111] $[Pd_2@Sn_{18}]^{4-}$,[112,113] $[Pd@Sn_9(SnCy_3)]^{3-}$,[114]), and Pt-centered clusters ($[Pt@Sn_9H]^{3-}$,[115] $[Pt@Pb_{12}]^{2-}$,[76] $[Pt_2@Sn_{17}]^{4-}$,[115]), as well as metal-ligand (ML) capped clusters ($[Ge_9Ni(CO)]^{3-}$,[116] $[Ge_9Pd(PPh_3)]^{3-}$,[110] $[Sn_9Pt(PPh_3)_x]^{4-}$,[118]) and both the transition metal centered and ML-capped species ($[Ni@Ge_9Ni(PPh_3)]$[152] $[Ni@Ge_9(PdPPh_3)]^{2-}$,[110] $[Pd@Sn_9(PdSnCy_3)]^{3-}$,[114,119] $[Ni@Sn_9Ni(CO)]^{3-}$,[120] $[Pt@Sn_9Pt(PPh_3)]^{2-}$,[120]). The diversity models of clusters with group 8-9 elements nosedives: $[Ge_8Fe(CO)_3]^{3-}$,[121] a heavy-disordered deltahedra cluster $[Fe@Sn_{10}]^{3-}$;[122] two analogues of non-deltahedra

pentagonal prismatic cage $[Fe@Ge_{10}]^{3-}$ [123] and $[Co@Ge_{10}]^{3-}$;[124] more complexes such as monomer $[Co@Sn_9]^{5-}$,[125] dimers clusters $[Co_2@Sn_{17}]^{5-}$[125]; as well as icosahedral cluster $[Ir@Sn_{12}]^{3-}$,[126] which is made from ligated heteroatoms $[Sn_9Ir(cod)]^{3-}$.[126] Recently, a unique anion $[Ru@Ge_{12}]^{3-}$ with D_{2h} symmetry has been described.[149] Aside from group VIIIB, only a few of metal-centered clusters have been reported, including: 36-electron close-shell icosahedral paramagnetic $[Mn@Pb_{12}]^{3-}$;[127] $[Cu@Pb_9]^{3-}$,[128] and $[Cu@Sn_9]^{3-}$ with different C_{4v}/D_{3h} geometries; [56] the clusters with metal immerged $[(\eta^4\text{-}Sn_8)Ti(Cp)]^{3-}$ like half-centered-half-capped phase and metal complexes mono-bound anions $[(\eta^1\text{-}Sn_9)TiCp_2(NH_3)]^{3-}$.[129] More examples of ML_n capped clusters were obtained as $[E_9M(CO)_3]^{4-}$ with different coordination modes η^4 and η^5 where M= Cr, Mo, W; *E* = Sn, Pb,[130-134] $[Ge_9Cr(Si(SiMe_3)_3)_3(CO)_3]^-$,[135] neutral clusters $[Ge_{18}M(Si(SiMe_3)_3)_6]$ (M= Zn, Cd, Hg) *closo*-$[E_9ZnR]^{3-}$ (*E* = Si, Ge, Sn, Pb; R = Mes, ^{i}Pr, Ph),[136,137] $[E_9CdPh]^{3-}$ (*E* = Sn, Pb) and $[Sn_9CdSn[(CH_2)_3CH_3]_3]^{3-}$,[138] $[Ge_9Cu(PR_3)]^{3-}$ (R = ^{i}Pr, Cy)[139]. Regarding the metal-linked clusters, examples are $[(Ge_9)Cu(Ge_9)]^{7-}$ adopting $\eta^4+\eta^1$ connection,[139] *exo*-bond clusters $[Sn_9AgSn_9]^{5-}$,[85] $[Au_3Ge_{18}]^{5-}$ with triangular metals joint,[140] large aggregation clusters $[Au_3Ge_{45}]^{9-}$,[141] $[Pb_9CdCdPb_9]^{6-}$ with double metals linkage,[142] discrete chains $[Hg_3(Ge_9)_4]^{10-}$,[143] two infinite chains $[Ge_9Hg]^{2-}$,[144] discrete particles $[Sn_9HgSn_9]^{6-}$,[145] and a polymer $[Zn(Ge_9)]^{2-}$ adopting $\eta^3+\eta^3$ connection.[146]

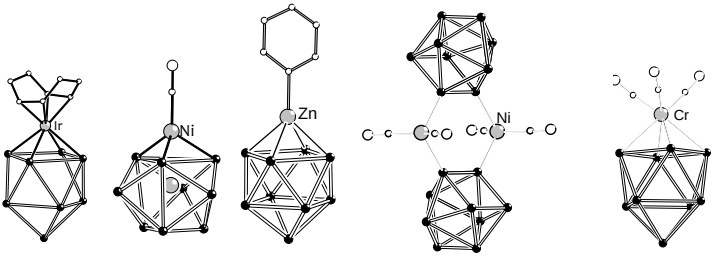

Figure 1.7 Selective examples of Zintl clusters connected with transition-metal complexes: (a) $[Sn_9Ir(cod)]^{3-}$,[126] (b) $[(Ni@Sn_9)Ni(CO)]^{3-}$, [120] (c) $[(E_9)(ZnPh)]^{3-}$ (*E* = Si, Ge, Sn, Pb), [137] (d) $[(Si_9)_2(Ni(CO)_2)_2]^{8-}$,[147] (e) $[(Sn_9)Cr(CO)_3]^{4-}$.[130]

1.3 Endohedrally Filled Group 14 Atom Clusters with Insertion of Transition Metals

Group 14 Zintl clusters containing transition metal centers are named as endohedral Zintl ions, the most common synthetic route is their extraction in solution accompanied with the reaction of an organometallic compound.[40,43,148] Endrohedrally filled Zintl ions have been generated from the A_4E_9 phase with unfilled clusters and transition metal compounds with the occasion of releasing organic ligands. For instance, $[Ni@Sn_9]^{3-}$, $[Ni_2@Sn_{17}]^{4-}$ and $[Ni@Sn_9]^{4-}$ could be isolated by the corresponding reactions of intermetallic precursors K_4Sn_9 phase with $Ni(cod)_2$ in slightly varied conditions. The reported intermetalloid clusters mainly adopt an isolate cage or congregation of two or more cages, and rare examples of polymer or oglimer of endohedral filled cluster have been reported (Figure 1.8).

Recent progress in the synthesis of endohedral clusters put the basis of the idea from stepwise in solution to establish directly corresponding species in solid state route. Consequently, solid state synthetic products can be developed as a potential precursor to build more complicated novel phases of endohedral clusters. The first solid state synthesis of endohendral metal-filled cluster $K_{4.79}Co_{0.79}Sn_9$ was established in 2012,[125] which can be dissolved in polar ethylenediamine to form another distinct intermetalloid dimer $[Co_2@Sn_{17}]^{5-}$ (***chapter 3.1.4***, page 34).

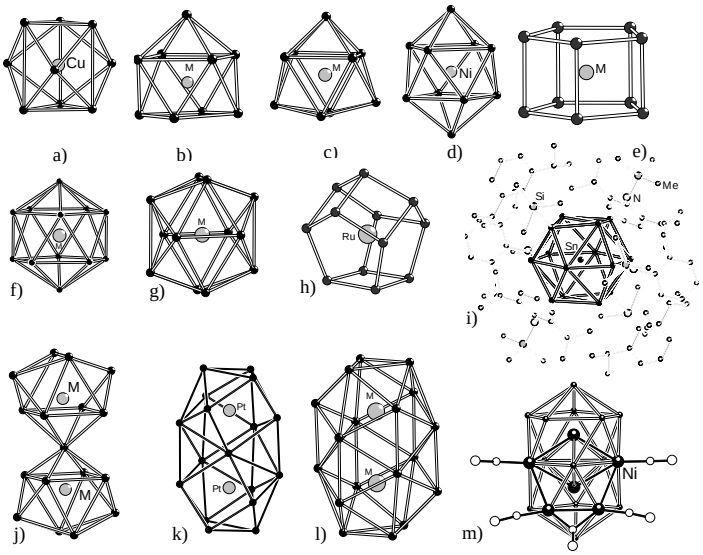

Figure 1.8 Representative Zintl ions with one endohedral metal atom: (a) $[Cu@E_9]^{3-}$ (E=Sn, Pb) with D_{3h} symmetry, [128] (b) $[Cu@E_9]^{3-}$ (E=Sn, Pb) with C_{4v} symmetry, [79] (c) $[Ni@Sn_9]^{n-}$ (n=3, 4) or $[Co@Sn_9]^{5-}$ with C_{2v} symmetry,[104,106,125] (d) $[Ni@Pb_{10}]^{2-}$,[107] (e) $[M@Ge_{10}]^{3-}$ (M=Co, Fe), [123,124] (f) $[Ir@Sn_{12}]^{3-}$ [126] and $[M@Pb_{12}]^{2-}$ (M=Ni, Pd, Pt) with I_h symmetry, [76] (g) $[Mn@Pb_{12}]^{3-}$ with D_{2h} symmetry,[127] (h) $[Ru@Ge_{12}]^{3-}$ with D_{2h} symmetry,[149] (i) $[Sn@(Sn_8[SnN(2,6\text{-}i\text{Pr}_2C_6H_3)(SiMe_3)]_6)]$,[150] (j) $[Ni_2@Sn_{17}]^{4-}$ [108] and $[Co_2@Sn_{17}]^{5-}$,[125] (k) $[Pt_2@Sn_{17}]^{4-}$,[151] (l) $[Pd@E_{18}]^{4-}$ (E=Ge, Sn), [111-113] and (m) $[Ni_6Ge_{13}(CO)_5]^{4-}$.[152]

1.4 Heteroatomic Tetrel Zintl Clusters in Material Science

The chemistry of homo- and hetero-metallic cluster has intrigued inorganic chemists due to the progressively established basic chemistry, based on these clusters and their potential utility as nanoparticle preparation.

The nine-atom deltahedral Zintl ions of Group 14 have received a large amount of interests during the past decade, because of their

chemical applications in diversified types of reactions. These reactions proceed rapidly and were well developed in functionalization with organic and organometallic groups, captain and insertion of transition metal atoms, coupling or fusion of clusters, *etc*. The concept of metal doping has also been used to these molecular compounds not only in materials chemistry. Heteropolyatomic species $[TlSn_9]^{3-}$, $[TlSn_8]^{3-}$, $[TlSn_8]^{5-}$, $[Sn_{9-x}E_x]^{4-}$ (x = 0-9, *E* = Ge, Pb), $[SnTe_4]^{4-}$ could be observed for different p-electrons contribution per atom to the skeletal bonding.[153-155] Sevov's group exhibit additional ability of Zintl clusters to exchange the vertex atoms partially to build heteroatomic clusters with *exo*-bonded functional groups. The homoatomic Ge_9 clusters can react with $SbPh_3$ or $BiPh_3$ at higher temperatures to give rise to substituted monomer of $[Ge_7Sb_2]^{2-}$ and dimers of $[(Ge_8Bi)_2]^{4-}$ with Ge-Ge intercluster bonds.[156] Lately, trimetallic deltahedral ions $[(Sn_6Ge_2Bi)_2]^{4-}$ evidenced that Sn_9-clusters show the similar potential property with Bi atoms.[157,158] Cluster $[Zn_6Sn_3Bi_8]^{4-}$ has introduced the intermetalloid Zintl ions into ternary phase, which is followed by a series of endohedral-shaped clusters anions including $[LnSn_7Bi_7]^{4-}$, $[LnSn_4Bi_9]^{4-}$ (Ln = La, Ce), $[Pd_3Sn_8Bi_6]^{4-}$, $[Ni_2Sn_7Bi_5]^{3-}$ and $[EuSn_6Bi_8]^{4-}$.[159-162] Although the above four clusters are obtained from the reactions of tetrahedral $[Sn_2Bi_2]^{2-}$ with organometallic compounds, the resulted structures lose original deltahedral shape. $[Sn_2Sb_2]^{2-}$, $[Sn_3Sb_4]^{6-}$ and $[Sn_2Sb_5(ZnPh)_2]^{3-}$ display heterometallic anions structures which are isoelectronic with homoatomic $[E^{14}{}_4]^{4-}$ or $[E^{15}{}_4]$ and $[E^{15}{}_7]^{3-}$ cages, shown in Figure 1.9.[163] Mixed Zintl clusters can react with organometallic compounds to produce metal complex decorated Zintl ions, such as the nominal compound "$K_4Ge_{4.5}Sn_{4.5}$" with $Ni(cod)_2$ to form $[Ni_2@GeSn_{16}]^{4-}$ anion,[106] and "$Rb_{12}Si_{12}Ge_5$" with MesCu to receive $[(MesCu)_2Si_{3.3}Ge_{0.7}]^{4-}$.[164]

In general, the heteroatomic clusters can be assembled by melting mixed elements stoichiometrically according to a solid state synthetic approach. $[E_9]^{3-}$ (*E* = Si/Ge) and $[E_4]^{4-}$ (*E* = Si/Ge) can be obtained in $A_{12}E_{17}$ (*A* = K-Cs; *E* = Si/Ge) and A_4E_4 (*A* = K, Rb; *E* = Si/Ge) from the corresponding elements heating at high temperature.[165] In solution, the homoatomic clusters gain more chances to react with main-group elements complex occasionally accompanied by element substitution, such as the formations of the clusters $[Sb_2Ge_7]^{2-}$ and $[TlSn_9]^{3-}$.[104,156] There are multitude of advantages to study heteroatomic clusters: (i) the charge of the heteroatomic clusters can simply regulate by the ratio between the two elements with different numbers of valence electron;

(ii) the substituted atom of the cluster may provide different reactivities due to the resulting polarity of the chemical bonds; (iii) heteroatomic clusters can provide a different perspective to study the chemistry of these elements which cannot build cluster by themselves. [166]

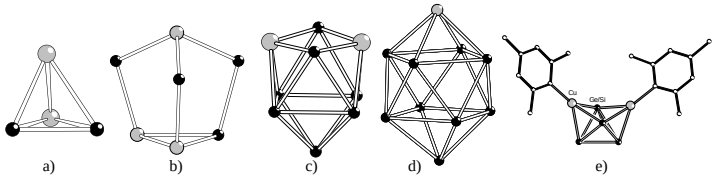

Figure 1.9 Selective cases of heteroatomic Zintl clusters: (a) $[E_4]^{2-}$ (E =Sn/Sb, Sn/Bi, Pb/Sb, In/Bi, Tl/Te)[155,163,167-169] or $[E_4]^{4-}$ (E = Si/Ge),[165] (b) $[Sn_3Sb_4]^{6-}$,[163] (c) $[E_9]^{3-}$ (E = Si/Ge),[165] $[TlSn_8]^{5-}$,[153] $[In_4Bi_5]^{3-}$,[170] $[Sb_2Ge_7]^{2-}$ [156] or $[Bi_2Pb_7]^{2-}$,[171] (d) $[TlGe_9]^{3-}$,[104] or $[TlSn_9]^{3-}$,[153] (e) $[(MesCu)_2Si_{3.3}Ge_{0.7}]^{4-}$.[164]

2 Motivation and Scope

2.1 Motivation

Applications of Co-Sn binary or ternary systems can be found in various fields: conductive materials, electrode materials for lithium batteries, catalysts and other application for advanced technologies, due to their semi- or super-conductive properties, optoelectronic, and catalysis effect for particular reactions.[2]

The traditional synthesis processes of Co-Sn alloys mainly focus on fusions of stoichiometric amounts of the elements. According to the Co-Sn phase diagram reported by Vassilev and Lilova in 2006,[172] four kinds of intermetallic phases were included: CoSn, $CoSn_2$, Co_3Sn_2 [173]and $CoSn_3$ [174]. Among these phases, $CoSn_3$ has been recently synthesized by peritectic reactions or tin flux methods, which is found to be only stable to 275 ℃.[175,176] The electrochemical tests of $Sn_{1-x}Co_x$ ($0.28< x < 0.43$) system result in an amorphous phase with specific capacity.[177] These samples could be prepared by mechanical alloying, electro-deposition, vacuum deposition and so on. Among these methods, the template-based strategies could apply non- or reactive templates (metal nanoparticle) to produce shape-controlled nanoscale complexes with morphologies.[178] For instance, Schaak and Chou started with β-Sn nanocrystals as seeds to react with Co^{2+} salts under reducing conditions to form a mixture of binary intermetallic species, including cubic/spherical α-$CoSn_3$ (main phase), $CoSn_2$ and β-Sn precursors. Recently, the aforementioned reducing precipitation, the conversion chemistry route was also applied to generate $CoSn_5$ nanospheres or analogous phase by reducing $SnCl_2$ in surfactant and suspending with $CoCl_2{\cdot}6H_2O$.[179] The intermetallic $CoSn_5$ nanocluster represents a new binary structure through this method, which was not existent in the recording Co-Sn phase diagram. Consequently, this chemical conversion synthesis method displays great advantages as an effective routine strategy to produce nano-structrured, nano-composite,

or even amorphous nano-metallic materials.

Series of compounds formed by germanium, tin and lead in solid state synthesis or in solution chemistry are introduced in literature (***chapter 1.2-1.4***, page 2-16 and Figure 1.2-1.9). While the mechanism and reactivity of polyanionic (tin and germanium) towards transition metal complexes still remains unexplained.[112,113]

The intermetallic compounds with different nominal compositions $K_{4.79}Co_{0.79}Sn_9$, "K_3RhSn_6" and "Rb_3IrSn_{12}" were synthesized in solid state reactions, which can be further studied to apply as potential precursors for the building of more distinct phases of endohedral clusters. The above mentioned mechanism of chemical conversion synthesis can be employed in the reducing reaction of Zintl ions. Based on trials under different conditions, a series of endohedral polyanions were isolated in solution.

2.2 Scope and Outline

The synthesis and characterization described in ***chapter 3.1*** show that the solutions of $K_{4.79}Co_{0.79}Sn_9$ Zintl phase can lead to four distinct types of cobalt-centered polyanions, which abundantly provide the complexity and multiformity of metal-introduced clusters: 1D infinite zigzag chain with potassium atoms as bridge linkers $^1_\infty[(KCo_{0.67}@Sn_9)^{3-}]$ in K(K[2.2.2]crypt)$_3$[$Co_{0.67}$@Sn_9] (**1**); another two kinds of monomer clusters with increased charge in [K([2.2.2]crypt)]$_6$[Sn_9]$_{1.21}$[Co@Sn_9]$_{0.12}$[Co@Sn_{10}]$_{0.67}$·3en·tol (**2**); and two types of $[Co_2@Sn_{17}]^{5-}$ dimers with different tortuosity in (K[2.2.2]crypt)$_5$[Co_2@Sn_{17}] (**3**) and [K[2.2.2]crypt]$_5$[Co_2@Sn_{17}]·en·tol (**4**).

The Rh analogue $[Rh_x@Sn_9]^{3-}$ is presented in ***chapter 3.2*** in terms of electron paramagnetic resonance spectrum and mass spectroscopy. This compound can be synthesized from a nominal intermetallic compounds "KRhSn".

Another similar Iridium-centered cluster $[Ir@Sn_{12}]^{3-}$ can be isolated directly from the extraction solution of nominal compounds "Rb_3IrSn_{12}", which is discussed in ***chapter 3.3*** in terms of mass spectroscopy.

In ***chapter 3.4***, further studies about heteroatomic $[E_9]^{2-}$ and $[Co@E_9]^{2-}$ (E = Sn/Sb) clusters show the derivative species from the

neat solid state compound Rb_4Sn_9 and $K_{4.79}Co_{0.79}Sn_9$, respectively.

Chapter 3.5 describes an organo-functional tetrel-atomic cluster $[(CH_2CH)Ge_9Ge_9(CHCH_2)]^{2-}$ in terms of Raman spectroscopy and also one $[Sn_9]^{4-}$ cluster with mixed sequestering reagents based on an organometallic compound $[K(18\text{-crown-6})(THF)_2][Co(anthracene)_2](THF)$.

3 Results and Discussion

3.1 Homoatomic Endohedral Cobalt-centered Polystannides Clusters

The first endohedral metal-filled cluster $[Co@Sn_9]^{5-}$ was established by solid state route in 2012.[125] This promising compound exhibits great potential to be developed as a precursor in solution chemistry of Zintl ions. The $[Co@Sn_9]^{5-}$ cluster with a charge of cobalt (-1) shows multiple possible reactive sites for redox reaction or as building block for polymerization. Thus, applying different reaction conditions and approaches, distinct intermetalloid clusters with cobalt centered were found in four novel compounds, respectively.

3.1.1 Synthesis and Characterization of Compounds 1-4

Single crystals of the four compounds presented here have been obtained via quite similar preparation routes (synthesis details see ***chapter 5.3.2.1***, page 93). The solid sample prepared with a nominal composition of $K_5Co_{1.2}Sn_9$, containing $K_{4.79}Co_{0.79}Sn_9$ as main phase, was used as precursor. [125] For all syntheses the solid precursor has been dissolved in ethylenediamine (en) by means of cryptand, after filtration of insoluble parts, toluene was added for crystallization. Some important variations of the synthesis conditions are the temperature during reactions, and the time, which has been spent for reaction and/or crystallization. $K(K[2.2.2]crypt)_3[Co_{0.68}@Sn_9]$ (**1**), which include isolated, but with respect to the starting compound partially oxidized, $[Co_{0.68}@Sn_9]^{4-}$ clusters, has been obtained after a crystallization time of only three hours at 60 ℃, while the more oxidized $[Co@Sn_{9/10}]^{3-}$ clusters in crystals of $[K([2.2.2]crypt)]_6[Sn_9]_{1.21}[Co@Sn_9]_{0.12}$ $[Co@Sn_{10}]_{0.67}\cdot 3en\cdot tol$ (**2**) have been found after one week at room

temperature. Finally after some weeks $[K([2.2.2]crypt)]_5[Co_2@Sn_{17}]$ (**3**) [125] and $[K([2.2.2]crypt])_5[Co_2@Sn_{17}]\cdot en\cdot tol$ (**4**) are obtained, both containing $[Co_2@Sn_{17}]^{5-}$ cluster dimers, which are not present in the starting material. The increased temperature during the crystallization of compound **1** obviously enhances the thermal convection and thus accelerates the crystal growth, probably the presence of uncoordinated K^+ cations in the solution is also promoted, while a reaction time extension leads to compounds containing more oxidized or even dimerized $[Co_x@Sn_9]^{n-}$ clusters. However, independently from any reaction conditions, **2** was obtained from all syntheses as main product or byproduct in different amounts indicating an intrinsic stability or at least a low solubility of this compound. The yields of these reactions are low (calculations based on the molar amount of $K_{4.79}Co_{0.79}Sn_9$), e.g. ~10 % for **1** and **4**, and ~35% for **2** and **3**, and after all reactions elemental tin is found as byproduct in different amounts.

Comparing with the reactions of compound **1** and compound **3**, the less amount of sequestering agent in **1** results in the one potassium per formula being not coordinated by [2.2.2]crypt. The two types of similar intermetalloid cluster $[Co_2@Sn_{17}]^{5-}$ in **3** and **4** were obtained from different ratios of intermetallic precursor and [2.2.2]crypt used in the synthesis. Compound **3** was characterized by EDX with an approximate elemental ratio of K/Co/Sn=5:1.4:17. Compound **2** could also be harvested simultaneously from the synthesis of compound **4**, which EDX shows K/Co/Sn=3.2:1.9:17 for crystals of **4**, and K/Co/Sn≈6:0.8:18.7 for crystals of **2**. The EDX details are shown in ***chapter 6.3***, page 111.

To get insight into the mechanisms of these reactions especially with respect to the amount of filled Sn_9 clusters and to their dimerization, the ^{119}Sn NMR spectroscopic measurements were performed. Nevertheless, after dissolving the precursor in ethylenediamine the ^{119}Sn NMR spectroscopy revealed only a single signal around -1208 ppm indicating empty Sn_9^{4-} clusters with ~10 ppm shift (spectrum see ***chapter 6.1***, page 98).[44,133] From the data in known literature, the solid state ^{119}Sn NMR investigations show significant different results such as the multiple signals between -1040 ppm and -860 ppm for $[Sn_9]^{4-}$ in compound K_4Sn_9, and two broad signals at -689 ppm for $[Co@Sn_9]^{5-}$ and -942 ppm for $[Sn_9]^{4-}$ in $K_{4.79}Co_{0.79}Sn_9$.[180] Possibly signals of filled $Co@Sn_9$ clusters in solutions cannot be observed due to paramagnetism of these ions. Indeed the products contain Co-filled Sn_9 clusters and show paramagnetism, in contrast to the diamagnetic starting compound

$K_{4.79}Co_{0.79}Sn_9$. According to this finding, the soluble $[Co_xSn_y]$ clusters of all new compounds presented here are formally oxidized, compared to the $[CoSn_9]^{5-}$ and unfilled cluster $[Sn_9]^{4-}$ in $K_{4.79}Co_{0.79}Sn_9$.

3.1.2 K[K([2.2.2]crypt)]$_3$[Co$_{0.68}$@Sn$_9$] (1)

Structure Determination

The crystal structure of compound **1** was solved in triclinic $P\bar{1}$ by direct methods. All non-H atoms were refined anisotropically. The positions of hydrogen atoms of the cryptand were geometrically calculated and refined isotropically with a riding model. The detailed crystallographic data of compound **1** are listed in ***chapter 6.2.1***, page 100 in Appendix.

Crystal Structure Description

The K(K[2.2.2]crypt)$_3$[$Co_{0.68}$@Sn_9] (**1**) compound is triclinic, space group $P\bar{1}$, and contains three $[K([2.2.2]crypt)]^+$ cations, one $[Co_{0.68}@Sn_9]^{4-}$ anion and two K atoms at special position resulting in one potassium-atom per cluster bonded with clusters in the crystal lattice (Figure 3.1 and 3.2). In this structure, the $[K([2.2.2]crypt)]^+$ ions and $[Co_{0.68}@Sn_9]^{4-}$ cluster are well-defined and not disordered.

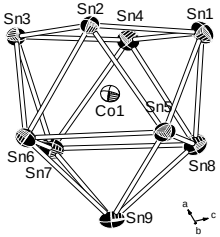

Figure 3.1 Structure of the $[Co@Sn_9]^{4-}$ ion (**1a**). Atoms are drawn with 50 % probability ellipsoids.

The Sn-Sn distance is in the range of 2.9475(4)-3.4352(5) Å in $[Co_{0.68}@Sn_9]^{4-}$ cluster with monocapped square antiprism shape (Figure 3.1), which fits with those of other endohedral clusters. Due to

the insertion of transition metal, the endohedral clusters result in the expansion of Sn-Sn distances from 2.9308(26)-3.3029(27) Å for the empty $[Sn_9]^{4-}$ cluster to 2.9773(6)-3.5893(7) Å for the $[Ni@Sn_9]^{4-}$ cluster and 2.983(1)-3.472(1) Å for the $[Cu@Sn_9]^{3-}$ cluster with C_{4v} symmetry.[79,103,178] The Co-Sn distances are within the range of 2.5531(7)-2.8865(7) Å in cluster **1a**, and some of them are longer than those in original phase in $K_{4.79}Co_{0.79}Sn_9$. The distances between capped Sn atom and centered metal atoms are 2.886(1) Å for **1a**, 2.702(2) Å for $[Co@Sn_9]^{5-}$ (the longest length was chosen), 2.732(1) Å for $[Ni@Sn_9]^{4-}$, 2.770(1) Å for $[Cu@Sn_9]^{3-}$, respectively, which also indicates the size extension of cluster **1a**.

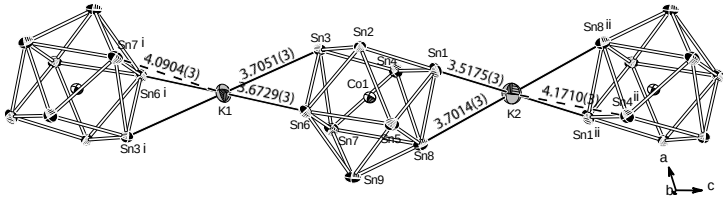

Figure 3.2 The K-Sn bond lengths of the $[K(Co@Sn_9)]^{3-}$ chain in compound **1** (Symmetric codes: (i) -x, -y, -z; (ii) -x, -y, 1-z). Atoms are drawn with 50 % probability ellipsoids.

The infinite chains of K1-(Co@Sn_9)-K2-(Co@Sn_9) spread along the *c* axis through the edge of the unit cell (Figure 3.2 and 3.3), which is isostructural with the unfilled clusters in $[K([2.2.2]crypt)_3[KSn_9]$ and nickel-centered clusters in $K[K([2.2.2]crypt)]_3[Ni@Sn_9]$, and similar to those in $K(K[18\text{-crown-6}])_3[Ni@Sn_9]\cdot 3benzene$.[106,181] The K-Sn bonds in $K[K([2.2.2]crypt)]_3[Ni@Sn_9]$ agree with those in compound **1**, within the range of 3.5073(5)-3.7100(4) Å. The linker lengths in the empty compound $K[K([2.2.2]crypt)]_3[Sn_9]$ extend longer than both metal-centered ones (from 3.5521(27) to 3.7617(24) Å).

Due to the location of inversion centers and the bridged K atoms lying on, the polyatomic anionic clusters could be considered as straight chains. It should be noted that each cluster position shows slight migration with an angle K1-Co-K2 151.6 °, which is 150.5 ° in $K(K[2.2.2]crypt)_3[Ni@Sn_9]$. The distance of K1-K2 in complex **1** shows the length of the chain as the repeating unit of 10.1069(2) Å, which is intermediate between 10.1282(68) Å in the empty Sn_9 compound and 10.0880(6) Å in the Ni@Sn_9 compound. The slight

variation of the chain's length leads to tilted Sn_9 clusters with respect to the K1-K2 vector and to form final zigzag chains.

K1 and K2 atoms locate in the bridging positions between $[Co@Sn_9]^{4-}$ clusters leading to a linear polymer of the composition $^1_\infty[K(Co_{0.68}@Sn_9)]^{3-}$, which are separate from the sequestering agents. The K-Sn distances arrange from 3.5175(3) Å (Sn1-K2) to 3.7051(3) Å (Sn3-K1), while the length of K2-Sn4 and K1-Sn7 seem longer than the above bond deviations [4.1710(3) and 4.0904(3) Å, respectively] (Figure 3.2). Thus, K atoms locate in the center of the bow-tie like connection between four Sn atoms from clusters. The chains are isolated and surrounded by cryptand molecules with potassium atoms. Compound **1** contains three crystallographic independent $(K[2.2.2]crypt)^+$ counter ions (K3, K4, K5), which result in a three-fold negative charge per $[KCo_{0.68}@Sn_9]$ unit, leading to a charge of -3 for this entity.

The electron counts lead to clusters with 22 skeletal electrons. From Wade's rules a *nido* structure in form of a mono-capped square-antiprism with C_{4v} symmetry is expected. This can be satisfied in the $Co@Sn_9$ clusters from the ratio of the diagonal lengths of the open basal square around 1.01 and the dihedral angles 177.6 °, indeed indicating an almost ideal C_{4v} symmetry. More details about structure parameters are shown in table 3.1. The occupation of the cobalt site is around 68%, which indicates a zero charge of Co as one possibility similar to the nickel atom in the analogue $K(K[2.2.2]crypt)_3[Ni^0@Sn_9^{4-}]$.[106] The cobalt atom is slowly oxidized from negative charge to neutral oxidation state. The other possibility is that the Co atom kept at (-1) charge, but the $[Sn_9]^{4-}$ clusters are partly oxidized to $[Sn_9]^{3-}$ to compensate the total negative charge (-4). In both presumptions, either Co(0)-centered cluster or $[Sn_9]^{3-}$ cluster possesses one unpaired electron and the whole compound should reveal paramagnetic property. Unfortunately, the EPR test shows no signal due to the small amount or the non-stability of the crystal.

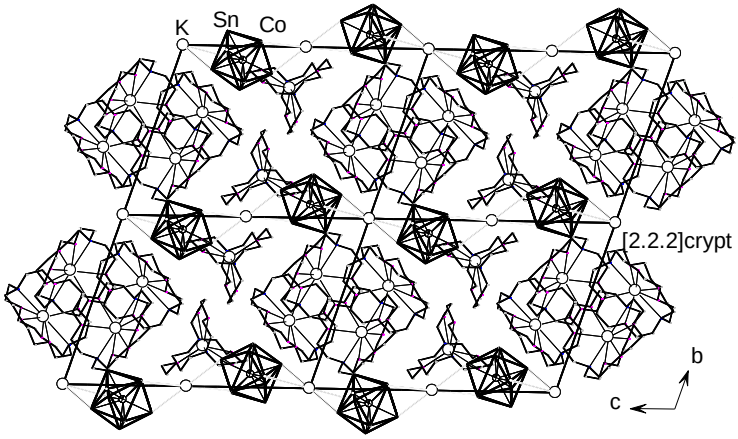

Figure 3.3 Crystal structure packing view of compound **1** along [1 0 0] direction. The hydrogen atoms were omitted for clarity.

Table 3.1 Geometric Parameters of different endohedral Sn_9 Cluster including divided half clusters of dimers.

compound		prism edges[b,c]			dihedral cap to cap fold angle about h °[c]						
	[a]	h_1	h_2	h_3	γ [d]	h/e[e]	α_1	α_2	α_3	d_1/d_2[f]	
$[K([2.2.2]crypt)]_3(KSn_9)$ [181]		1.29	1.03	1	20	1.19	2	29	27	1.02	C_{4v}
$[K([2.2.2]crypt)]_6[Ni@Sn_9]_2$·3en·tol		1.21	1.17	1.02	11	1.13	19	20	34	1.18	~C_{2v}
$K[K(18C6)]_3[Ni@Sn_9]$·3benz [106]		1.26	1.08	1.05	14	1.16	7	27	31	1.09	~C_{4v}
$K[K([2.2.2]crypt)]_3[Ni@Sn_9]$ [106]		1.31	1.12	1.07	16	1.19	6	28	33	1.04	~C_{4v}
$K[K(en)][K(18C6)]_2[Ni@Sn_9]$ ·0.5en		1.31	1.02	1.01	21	1.15	0	30	31	1.01	C_{4v}
$K_{4.79}Co_{0.79}@Sn_9$		1.25	1.17	1.12	8	1.23	14	24	28	1.12	~C_{2v}
$K[K([2.2.2]crypt)]_3[Co@Sn_9]$ (**1**)		1.34	1.04	1.07	21	1.19	2	32	28	1.01	~C_{4v}
$[K([2.2.2]crypt)]_4$ $[Ni_2@GeSn_{16}]$·en [106]	A	1.33	1.33	0.93	26	1.23	16	16	39	1.01/1.01	C_{2v}
	B	1.32	1.32	0.97	23	1.24	16	16	40	1.01/1.01	C_{2v}
$[K([2.2.2]crypt)]_5[Co_2@Sn_{17}]$	A	1.27	1.34	0.99	21	1.24	21	9	37	1.12/1.02	C_v
(**3**)	B	1.31	1.36	0.96	24	1.24	17	8	42	1.06/1.01	C_v
$[K([2.2.2]crypt)]_5[Co_2@Sn_{17}]$· en·tol	A	1.32	0.97	1.35	24	1.24	16	10	42	1.04/1.00	~C_{2v}
(**4**)	B	1.31	1.32	0.98	22	1.23	15	15	39	1.06/1.05	C_{2v}

a) A and B denote different half of dimer cluster $M_2@Sn_{17}$. b) Relative prism heights, scaled to the value 3.194 Å, the shortest height in $[K([2.2.2]crypt)]_6([Sn_9][Sn_9])$·1.5en·0.5tol. [74] c) The best monocapped square antiprism is chosen. If the structure is close to D_{3h} symmetry the longest height is considered as a diagonal in the C_{4v} symmetric cluster. d) γ shows the dihedral angle between the triangular bases. e) *h* and *e* are the mean values of the prism heights and the triangular edges, respectively. f) The half of dimer clusters often show two open faces with two values of diagonal ratio d_1/d_2.

3.1.3 $[K([2.2.2]crypt)]_6[Sn_9]_{1.21}[Co@Sn_9]_{0.17}[Co@Sn_{10}]_{0.62}\cdot 3en\cdot tol$ (2)

Structure Determination

The crystal structure of compound **2** was solved in the monoclinic space group $P2_1/c$ (No. 14) by direct methods. All non-H atoms were refined anisotropically. The positions of the hydrogen atoms of cryptand, toluene and ethylenediamine molecules were geometrically calculated and refined isotropically with a riding model. Data and structure refinement parameters of compound **2** are listed in ***chapter 6.2.2***, page 101. The composition of compound **2** is determined by the resulting single crystal structure analysis and confirmed by means of EDX in ***chapter 6.3***, page 102. The EDX analysis shows the ratio of K/Co/Sn to be around the theoretical results of 6:0.8:18.7.

Crystal Structure Description

The crystal structure of $[K([2.2.2]crypt)]_6[Sn_9]_{1.21}[Co@Sn_9]_{0.17}[Co@Sn_{10}]_{0.62}\cdot 3en\cdot tol$ (**2**) contains two crystallographically independent cluster anions in the asymmetric unit, with six $[K([2.2.2]crypt)]^+$ cations compensating the charges. Both clusters are highly disordered, so the affected atoms split positions are introduced and the range of Sn-Sn bonds in the clusters is broader than that normally formed in ideal clusters due to the heavy distortion of the polyhedra. The complicated structure model of both clusters can be built with different ratios of $[Sn_9]$, $[Co@Sn_9]$ and $[Co@Sn_{10}]$ subunits. For the clarity of further description, the two clusters are noted as cluster **2a** and **2b**. Cluster **2a** can be divided to four subunits: **2aA**, **2aB**, **2aC** and **2aD**; cluster **2b** can be composed by three subunits: **2bA**, **2bB** and **2bC**.

The cluster **2a** splits to four sub-clusters with different occupancies: 39% of cluster **2aA** $[Co_x@Sn_9]^{3-}$, 15% of cluster **2aB** $[Co_y@Sn_9]^{3-}$, 17% of cluster **2aC** $[Co@Sn_{10}]^{3-}$ and 29% of cluster **2aD** $[Co@Sn_{10}]^{3-}$. In this model of cluster **2a**, the positions of atoms Sn1, Sn2, Sn3, Sn4 and Sn5 are fixed with 100% of occupation, while other tin atoms are

splitting to more than one position, shown in Figure 3.4 and Table 3.2 of the views of a whole cluster and four subunits at the same locations. Considering the six charge-balancing cations with two clusters, each cluster can be speculated to have a negative charge of -3. Combining all the preconditions of Co(-1) in precursor $K_{4.79}Co_{0.79}Sn_9$ as well as the formation of $[Sn_{10}]^{2-}$ and $[Sn_9]^{n-}$ (n = 2, 3, 4), the clusters can be supposed to be composed of three types of anions $[Sn_9]^{3-}$, $[Co(-1)@Sn_9]^{3-}$ and $[Co(-1)@Sn_{10}]^{3-}$. The exact cobalt content of cluster **2a** is 51%, however the distribution to the four sub-clusters is unknown.

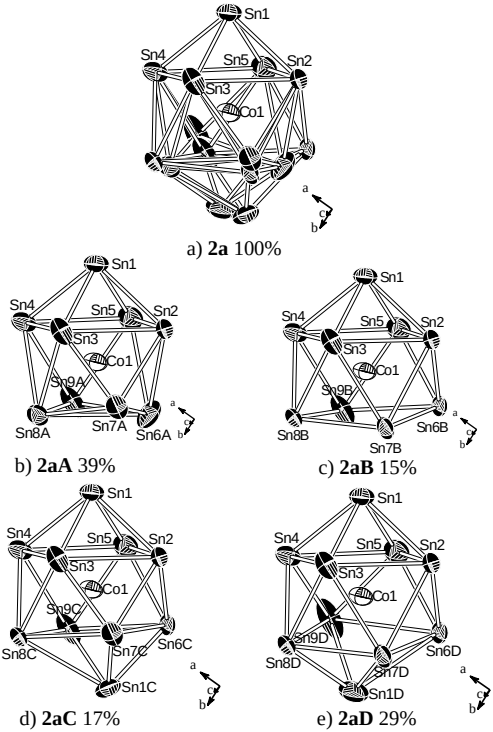

a) **2a** 100%

b) **2aA** 39%

c) **2aB** 15%

d) **2aC** 17%

e) **2aD** 29%

Figure 3.4 Cluster **2a** (a) and the four individual split sub-structures (b-e) at the same position. Anisotropic displacement ellipsoids are shown at 50% probability level.

Table 3.2 The distribution of clusters and split sub-clusters as well as the probable content of cobalt in compound **2**.

Cluster	Percentage(%)	Co (%)	the shortest Co-Sn bond length (Å)
2a	100	51	
2aA	39	x	Co1-Sn6A 2.277(4)
2aB	15	5-x	Co1-Sn7B 2.406(4)
2aC	17	17	Co1-Sn5 2.492(3)
2aD	29	29	Co1-Sn5 2.492(3)
2b	100	28	
2bA	84	12	Co2-Sn17 2.322(5)
2bB	9	9	Co2-Sn11 2.721(5)
2bC	7	7	Co2-Sn36 2.534(17)

Table 3.3 Structure Parameters of the three $[Sn_9]$ clusters in compound **2**.

cluster	prism edges[a, b]					dihedral cap to cap fold angle about h (°)[b]				
	h_1	h_2	h_3	γ(°)[c]	h/e[d]	α_1	α_2	α_3	d_1/d_2[e]	
2aA	1.01	1.06	1.08	4	1.07	21	29	15	1.33	~ D_{3h}
2aB	1.02	0.98	1.19	14	1.07	21	29	11	1.25	C_{2v}
2bA	1.02	1.00	1.06	4	1.05	18	23	17	1.40	~ D_{3h}

(a) Relative prism heights, scaled to the value 3.194 Å, the shortest height in $[K([2.2.2]crypt)]_6[Sn_9]_2 \cdot 1.5en \cdot 0.5tol$.[74] (b) The best monocapped square antiprism is chosen. If the structure is close to D_{3h} symmetry the longest height is considered as a diagonal in the C_{4v} symmetric cluster. **2aA**: h_1 Sn2-Sn3, h_2 Sn5-Sn4, h_3 Sn6A-Sn8A; **2aB**: h_1 Sn2-Sn5, h_2 Sn3-Sn4, h_3 Sn7B-Sn9B; 2bA: h_1 Sn13-Sn14, h_2 Sn17-Sn18, h_3 Sn15-Sn19. (c) γ shows the dihedral angle between the triangular bases. (d) h and e are the mean values of the prism heights and the triangular edges, respectively. (e) The chosen basal squares are Sn6A-Sn7A-Sn8A-Sn9A in **2aA**, Sn6B-Sn7B-Sn8B-Sn9B in **2aB**, Sn11-Sn15-Sn12-Sn19 in **2bA**, respectively. d_1 and d_2 refer to diagonal distances of the basal squares.

In cluster **2aA** $[Co_x@Sn_9]^{3-}$, the Sn-Sn contacts range between 2.773(3) [Sn6A-Sn9A] and 3.370(1) Å [Sn4-Sn5]. The cage of cluster **2aA** adopts a slightly distorted D_{3h} symmetry with two relatively elongated prism heights of central trigonal prism, the corresponding geometry parameters are shown in Table 3.3. The possible Co-Sn bond length in **2aA** are between 2.277(4) [Sn6A-Co1] and 2.938(2) Å [Sn1-Co1]. From the unrealistically short Sn-Co bond lengths in **2aA** can be deduced, that, this cluster is not filled with an endohedral Co atom, and x≈0. The polyhedron **2aB** displays a distorted C_{2v} symmetry with Sn-Sn bond range of 2.825(2) [Sn5-Sn6B] - 3.370(1) Å [Sn4-Sn5]

and Co-Sn bond range of 2.406(4) [Co1-Sn7B] - 2.938(2) Å [Sn1-Co1]. The reasonable Sn-Co bond lengths suggest the cluster **2aB** to be partly cobalt centered with probable content of 5 percentages. Cluster **2aB** possesses relatively long diagonal distances with a ratio of d_1/d_2 1.25 [Sn6B-Sn8B: 4.762(1) Å; Sn7B-Sn9B: 3.813(1) Å], which indicates a gross distortion of the monocapped square antiprism structure.

Table 3.4 Selective bond lengths and angles of the four [Sn_{10}] clusters in compound **2**.

Cluster	**2aC**	**2aD**	**2bB**	**2bC** [e]
E-E (Å)	2.754(1)-3.746(1)	2.719(7)-3.574(1)	2.850(1)-3.898(1)	2.772(1)-3.830(1)
$M_{central}$-E (Å) [a]	2.444(3)-3.026(4)	2.406(4)-2.958(4)	2.336(5)-2.800(5)	2.533(6)-3.036(16)
$M_{central}$-E_{cap} (Å) [b]	2.938(2), 3.026(4)	2.938(1), 2.958(1)	2.847(5), 3.119(10)	
E_{cap}-E_{square} (Å)	2.754(1)-3.135(1)	2.719(7)-3.040(1)	2.850(1)-3.002(10)	
E_{square}-E_{square} (Å) [c]	3.049(1)-3.746(1)	2.970(1)-3.574(1)	2.926(1)-3.898(1)	
$E_{antiprism}$-$E_{antiprism}$ (Å) [d]	2.787(3)-3.080(2)	2.825(2)-3.205(4)	2.849(1)-3.194(1)	
E_{cap}-$M_{central}$-E_{cap} (°)	166	167	153	
Torsion angle of Square (°)	1, 1	1, 1	1, 3	
Dihedral angle of Squares (°)	5	9	10	

(a) $M_{central}$: centering Co atom; (b) E_{cap}: the capping Sn atom; (c) E_{square}: the Sn atom of two basal squares of antiprism in [Sn_{10}] clusters; (d) $E_{antiprism}$: the Sn atom of antiprism in [Sn_{10}] clusters; (e) **2bC** shows the 10-membered cage without clearly observed antiprism or capping Sn atoms.

The Co-capsuled 10-vertices cluster **2aC** shows a deviant bicapped square antiprism structure, which results in two types of skeleton Sn atoms: capping Sn atoms (Sn1 and Sn1C, noted as Sn_{cap}) and Sn atoms of the antiprism (noted as Sn_{ap}). Due to the peculiar positions of Sn7C and Sn1C, the Sn-Sn distances extend from 2.754(1)- 3.755(1) Å. The contacts between Sn-Sn atoms can be noted as three types: i) type 1:

Sn_{cap}- Sn_{ap} range between 2.754(1)-3.135(1) Å; ii) type 2: the Sn_{ap}-Sn_{ap} side lengths of two basal squares in the antiprism are significantly longer than former bonds, within 3.049(1)-3.370(1) Å except the extremely long bond 3.755(1) Å [Sn6C-Sn7C]; iii) type 3: the bond lengths between the basal squares in the antiprism are in accordance with those of Sn_{ap}-Sn_{ap}, in range of 2.787(3)-3.080(2) Å. The two basal square planes (Sn2-Sn3-Sn4-Sn5 with torsion angles of 1 ° and Sn6C-Sn7C-Sn8C-Sn9C with 1 °) are almost parallel to each other with a dihedral angle 5 °. The connections between the centering Co1 and two Sn_{cap} have distances of 2.938(2) Å [Sn1-Co1] and 3.026(4) Å [Sn1C-Co1]. The distances between Sn_{ap}-Co1 range from 2.444(3) Å [Sn9C-Co1] to 2.799(4) Å [Sn7C-Co1]. The atoms Sn1, Co1 and Sn1C form a bending central axis of the polyhedron with an angle of 166 °.

In cluster **2aD**, due to the angle of Sn1-Co1-Sn1D (167 °), the whole structure seems to bend to atom Sn9D. The two square flats (Sn2-Sn3-Sn4-Sn5 and Sn6D-Sn7D-Sn8D-Sn9D) both with torsion angles of 1 °, form a larger dihedral angle of 9 °than that of cluster **2aC**. Thus, although similar as the cluster **2aC**, **2aD** displays an obviously more twisted bicapped square antiprism because of the special location of Sn9D. The Sn-Sn distances range in 2.719(7) [Sn1D-Sn9D] -3.574(1) Å [Sn6D-Sn9D]. The three aforementioned kinds of bond lengths are around 2.719(7) [Sn1D-Sn9D] - 3.040(1) Å [Sn1D-Sn6D] for type 1, 2.970(1) [Sn7D-Sn8D] - 3.574(1) Å [Sn6D-Sn9D] for type 2, and 2.825(2) [Sn5-Sn6D] -3.205(4) Å [Sn3-Sn7D] for type 3, respectively. The Co-Sn distances are between 2.406(4) [Sn7D-Co1] and 2.958(4) Å [Sn1D-Co1].

The cluster **2b** splits into one partly endohedrally filled $[Co@Sn_9]$ and two different splitting $[Co@Sn_{10}]$ subunits: 84% for $[Co_z@Sn_9]^{3-}$ (cluster **2bA**), 9% for $[Co@Sn_{10}]^{3-}$ (cluster **2bB**), 7% with $[Co@Sn_{10}]^{3-}$ (cluster **2bC**). The exact cobalt content of cluster **2b** is 28%, thus the whole 84 percentages for cluster **2bA** can be divided into 12% $[Co@Sn_9]^{3-}$ and 72% unfilled $[Sn_9]^{3-}$, and $z \approx 0.12$. The locations of atoms Sn11 and Sn12 are fixed without splitting, as shown in Figure 3.5.

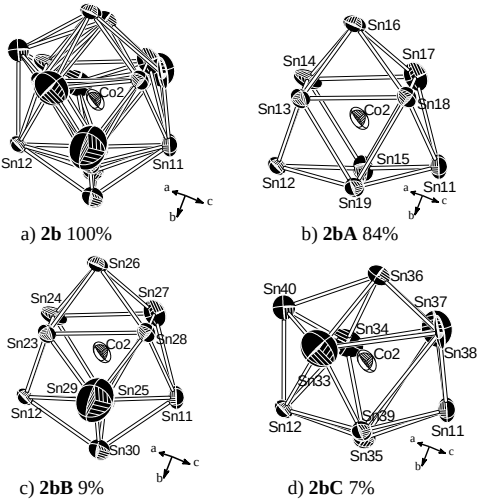

Figure 3.5 Cluster **2b** (a) and three individual split sub-structures (b-d) at the same location. Anisotropic displacement ellipsoids are shown at 50% probability level.

Cluster **2bA**, as the main substructure of cluster **2b**, reveals a tricapped trigonal prism with one elongated prism height 3.381(1) Å [Sn15-Sn19]. Besides, the Sn-Sn bond lengths agree with those in **2aA** and other known [Sn_9] clusters, within the range of 2.914(1) [Sn11-Sn19] and 3.260(2) Å [Sn13-Sn14]. The Co-Sn distances are between 2.322(5) [Sn17-Co2] and 2.847(5) Å [Sn16-Co2]. The occupation of cobalt in **2bA** seems a minor with 12 percentages.

The two capped Sn atoms (Sn26 and Sn30) and the central Co2 atom of cluster **2bB** form an angle of 153 °, and the planar antiprism square phase (Sn23-Sn24-Sn27-Sn28 with a torsion angle 1 °) tilt to the other planar antiprism square phase (Sn11-Sn25-Sn12-Sn29 with a torsion angle 3 °) by a dihedral angle of 10 °. The distributions of three types of Sn-Sn contacts range between 2.850(1) and 3.002(10) Å for type 1 [the shortest: Sn29-Sn30, the longest: Sn12-Sn30], 2.926(1) - 3.898(1) Å for type 2 [the shortest: Sn11-Sn25, the longest: Sn12-Sn29], 2.849(1)-3.194(1) Å for type 3 [the shortest: Sn28-Sn29, the longest: Sn25-Sn27], respectively. The connections between Co2 and the two

capping Sn atoms are 2.847(5) Å [Sn26-Co2] and 3.119(10) Å [Sn30-Co2], which are remarkably longer than the bond lengths of Co-Sn_{ap} [2.336(5)-2.800(5) Å, the shortest: Sn25-Co2, the longest: Sn12-Co2] except the abnormal long bond [Sn29-Co2: 3.408(1) Å]. The entity of cluster **2bB** exhibits a cage with a distorted bicapped square antiprism structure.

Polyhedron **2bC** shows the most significant distortion of the 10-membered cage without clearly observed antiprism or capping Sn atoms. The Co-Sn contacts range between 2.533(6)-3.036(16) Å [Sn39-Co2, Sn38-Co2]. The Sn-Sn connections lie in 2.772(1)-3.830(1) Å [Sn33-Sn39, Sn35-Sn37]. The distances of Co-Sn and Sn-Sn generally fit with those of other 10-membered cages in this compound.

The three nine-skeleton atoms clusters $[Co_x@Sn_9]^{3-}$ **2aA**, **2aB** and **2bA** show different deviations from the ideal D_{3h}-symmetry, which approximately fit with the Wade electron counting rules. In the above clusters, $[Sn_9]$ cages adopt a negative charge between -2 and -3, depending on the content of cobalt (-1). The entire clusters present unambiguous change with -3. The other four endohedral $[Co(-1)@Sn_{10}]^{3-}$ anions (**2aC**, **2aD**, **2bB** and **2bC**) can be regarded as the 10-vertex $[Sn_{10}]^{2-}$ with distorted bicapped square antiprism centered by a Co atom. When the charge -3 for the whole cluster and -1 for central cobalt are taken to consideration, and the Sn atoms contribute two electrons to cluster bonding, thus result in a 22 skeleton electron with a *closo*-geometry. The endohedral cluster $[Co(-1)@Sn_{10}]^{3-}$ features an isoelectronic structure to clusters $[Pb_{10}]^{2-}$ and $[Ni@Pb_{10}]^{2-}$. The reasonable thermal ellipsoids and the high disorder in these clusters lead to a pseudo-D_{4d} symmetry, but not a similar pentagonal prismatic D_{5h} symmetry in $[Co@Ge_{10}]^{3-}$ and $[Fe@Ge_{10}]^{3-}$ anions.

The cluster arrangements in the crystal structure display as hexagonal layer packing along the *c* axis, shown in Figure 3.6.

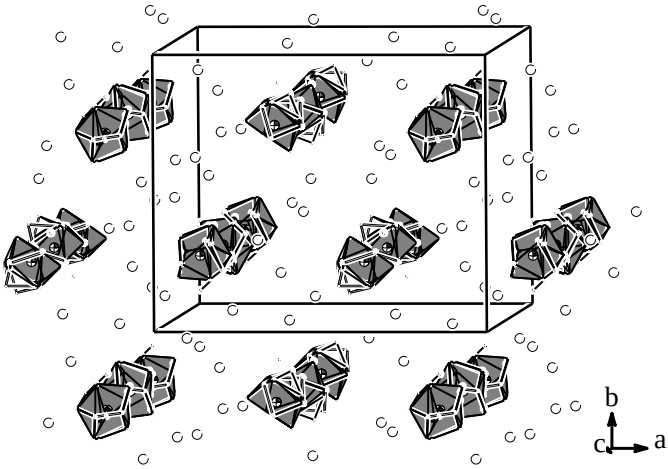

Figure 3.6 View of cluster packing in compound **2** along the *c* axis. All cryptand and solvent molecules are omitted for clarity. K: white spheres, Co: white and black octant ellipsoids, Sn polyhedra: grey.

3.1.4 $[K([2.2.2]crypt)]_5[Co_2@Sn_{17}]$ (3) and $[K([2.2.2]crypt)]_5[Co_2@Sn_{17}]\cdot en\cdot tol$ (4)

Structure Determination

From both lack block crystals of compound **3** $[K([2.2.2]crypt)]_5[Co_2@Sn_{17}]$ and compound **4** $[K([2.2.2]crypt)]_5[Co_2@Sn_{17}]\cdot en\cdot tol$, the crystal structures were solved in monoclinic $P2_1/n$ (No. 14) and $P2_1/n$ (No. 14) by direct methods, respectively. All non-H-atoms were refined anisotropically. The positions of the hydrogen atoms of cryptand, toluene and ethylenediamine molecules were geometrically calculated and refined isotropically with a riding model. The difference Fourier map of compound **3** showed many peaks of very low electronic density due to an extensive disorder of the ethylenediamine molecules in the structure. Thus, the contributions from disordered guest molecules were

subtracted by using the SQUEEZE subroutine of the PLATON software suite.[182,183]

Data and structure refinement parameters of compound **3** and **4** are listed in ***chapter 6.2.3*** and ***chapter 6.2.4***, page 102-103. The EDX results are shown in appendix ***chapter 6.3***, page 111.

Crystal Structure Description

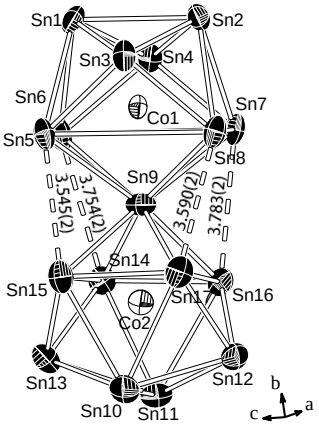

Figure 3.7 Structure of the $[Co_2@Sn_{17}]^{5-}$ anion in compound **3**. Atoms are drawn with 50 % probability ellipsoids.

The $[K([2.2.2]crypt)]_5[Co_2@Sn_{17}]$ (**3**) salt was crystallized and structurally characterized in the monoclinic space group $P2_1/c$, (a=15.2473(2) Å, b=33.4895(5) Å, and c=30.9531(5) Å, β=110.1660(10) °, V=14836.5(4) Å^3, Z=4). The asymmetric unit contains one cluster $[Co_2@Sn_{17}]$ surprisingly devoid of disorder, and five $[K([2.2.2]crypt)]^+$ cations balancing the charge. The dimer $[Co_2@Sn_{17}]^{5-}$ cluster shown in Figure 3.7, can be defined by two almost identical $[Co@Sn_9]$ cages ($Co1@Sn_9$, $Co2@Sn_9$) fused at one vertex (atom Sn9) during the partly oxidation process.

In cluster **3a**, the Sn-Sn distances spread in a broad range of 2.945(2) [Sn4-Sn8]-4.300(2) Å [Sn6-Sn7]. The two Co atoms are encapsulated at the center of each $[Sn_9]$ cage which can be regarded to a tricapped

trigonal prism with two elongated prism heights. The four longer prism heights are 4.204(2) [Sn5-Sn8], 4.300(2) [Sn6-Sn7], 4.175(2) [Sn14-Sn15], and 4.224(2) Å [Sn16-Sn17], respectively. The relatively elongated contacts of Sn-Sn atoms are formed owing to the existence of four quite planar rectangular squares [Sn3-Sn6-Sn9-Sn7 with a torsion angle of 7 °, Sn4-Sn5-Sn9-Sn8 with 11 °, Sn9-Sn14-Sn13-Sn15 with 11 °, Sn9-Sn16-Sn12-Sn17 with 11 °]. These four square faces condensed at the vertex of atom Sn9. The shorter prism heights show the distances of 3.088(2) [Sn1-Sn2] and 3.139(2) [Sn10-Sn11] for cages $Co1@Sn_9$ and $Co2@Sn_9$, respectively. The Sn-Sn bond lengths with a range of 2.945(2)-3247(2) Å, match well with those of other known Sn_9 clusters.[55] The shared atom Sn9 seems to be located at the center of a square antiprism formed by eight other Sn atoms. The two basal square faces in the above antiprism (Sn5-Sn6-Sn7-Sn8, Sn14-Sn15-Sn16-Sn17) are nearly parallel to each other with a dihedral angle of 3 °. The closest Sn-Sn distances between the two cages ($Co1@Sn_9$, $Co2@Sn_9$) are 3.545(2) [Sn5-Sn14], 3.754(2) [Sn6-Sn15], 3.783(2)[Sn7-Sn16], and 3.590(2) Å [Sn8-Sn17], respectively. The distances between the vertex Sn and the cluster centering Co atoms of 2.383(2) Å [Co1-Sn9] and 2.391(3) Å [Co2-Sn9] are significantly shorter than all other Co-Sn bonds with a range of 2.646(3)-2.713(2) Å for [$Co1@Sn_9$] and 2.631(3)-2.749(23) Å for [$Co2@Sn_9$], and also dramatically shorter than the distance between the capping Sn and interstitial Co of 2.886(1) Å in compound **1**. The angle of Co1-Sn9-Co2 (176 °) shows the central axis deviating only slightly from linearity. The two $Co@Sn_9$ cluster units are rotated to each other with an angle of about 83 ° around the central axis (based on the dihedral angle of Sn1-Sn2-Sn9 and Sn9-Sn10-Sn11).

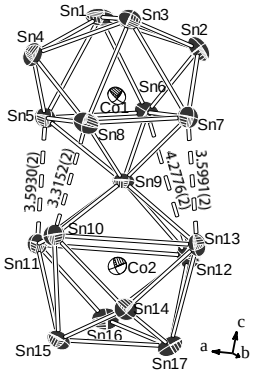

Figure 3.8 Structure of the $[Co_2@Sn_{17}]^{5-}$ anions in compound **4**. Atoms are drawn with 50 % probability ellipsoids.

The crystal structure of $[K([2.2.2]crypt)]_5[Co_2@Sn_{17}]\cdot en\cdot tol$ (**4**) was refined in space group monoclinic, $P2_1/n$, (a=17.9334(7) Å, b=25.3186(11) Å, and c=32.3075(15) Å, β=93.057(4) °, V=14648.3(11) Å^3, Z=4). The obvious difference between the unit cells of compounds **3** and **4** results from not only the solvent molecules but also the structure of clusters and their three-dimensional packing. Due to the presence of five $[K([2.2.2]crypt)]^+$ cations, the cluster **4a** features fivefold negative charge.

Although cluster **4a** has the same formula as cluster **3a** $[Co_2@Sn_{17}]^{5-}$, both consisting of two fused $[Co@Sn_9]$ cages sharing one common vertex Sn atom (Figure 3.8), the structures of these two polyhdera show perceptible differences. In cluster **4a**, the two $[Co@Sn_9]$ subunits can also be considered as derivatives of a tricapped trigonal prism with two elongated prism heights. These elongated Sn-Sn distances [4.186(1) Å (Sn5-Sn8), 4.319(1) Å (Sn6-Sn7), 4.282 (1) Å (Sn11-Sn12), and 4.047(1) Å (Sn10-Sn13)] in cluster **4a**, fit well with those of cluster **3a**. The four elongated heights belong to four approximately rectangular faces (Sn2-Sn7-Sn9-Sn6 with a torsion angle of 6 °, Sn4-Sn5-Sn9-Sn8 with 13 °, Sn9-Sn11-Sn16-Sn12 with 6 °, Sn9-Sn10-Sn14-Sn13 with 15 °). The shorter prism heights of Sn1-Sn3 [3.059(1) Å] and Sn15-Sn17 [3.157(1) Å] match with the other Sn-Sn bond lengths with a range of 2.953(1)-3.271(1) Å. The vertex atom Sn9 occupies the

central position of a rectangular antiprism formed by the surrounding eight Sn atoms. The rectangular faces of the antiprism are tilt to each other due to one significantly short bond Sn8-Sn10 of 3.315(1) Å. The comparison of the two antiprisms is shown in Figure 3.9: in cluster **3a** the two shortest heights are located at the same side of the antiprism adopting a "*cis*" conformation, while for cluster **4a** the "*trans*" setting with one quite short and one very long height is realized.

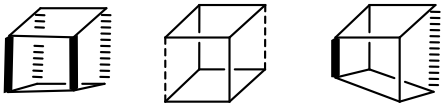

cis- ***trans-***

Figure 3.9 Schematic views of rectangular antiprism in cluster **3a** and **4a**.

The connections between the vertex Sn9 and the centered Co atoms of cluster **4a** [2.406(1) Å for Co1-Sn9, 2.406(1) Å for Co2-Sn9] are slightly longer than those of cluster **3a**. The other Co-Sn bond lengths expand from 2.653(1) to 2.721(1) Å for [Co1@Sn_9] and from 2.618(1) Å [Sn11-Co2] to 2.769 Å [Sn14-Co2] for [Co2@Sn_9]. The larger variation of the bond lengths in **4a** leads to more tilted subunits of the dimer cluster with respect to the Co1-Co2 vector as it is the case in the anion **3a**. This can be visualized by the Co1-Sn9-Co2 bond angles: the angle Co1-Sn9-Co2 in cluster **4a** of 166 °is smaller than that of 176 °in cluster **3a**, which indicates the formation of a more bend dimer cluster around Sn9. The two Co@Sn_9 cluster units of **4a** are rotated to each other with an angle of about 81 °around the central axis (based on the dihedral angle of Sn1-Sn3-Sn9 and Sn9-Sn15-Sn17).

Both **3a** and **4a** anions are isostructural to the $[Ni_2@Sn_{17}]^{4-}$ and $[Ni_2@GeSn_{16}]^{4-}$ anions.[106,108] The latter two compounds were synthesized by dissolving K_4Sn_9/"$K_4Ge_{4.5}Sn_{4.5}$" with $[Ni(cod)]_2$ in ethylenediamine solution. However, these four compounds represent different lattice parameters and apparently different packing.

Accompanying with the different spatial configuration of two $[Co_2@Sn_{17}]^{5-}$ anions, the compensating alkali metal cations localize and pack in different way. It is worth to be noted, that from [1 0 1] projection potassium atoms in compound **4** aggregate to form

honeycomb-like channels with the [Co_2@Sn_{17}] clusters residing in the center (Figure 3.10). Comparing to **4**, potassium atoms in **3** disperse evenly in the unit cell (Figure 3.11a and c). Along the *b* axis, it is easy to notice that clusters in compound **3** display layers with potassium atoms slantingly stippled between clusters (Figure 3.11b).

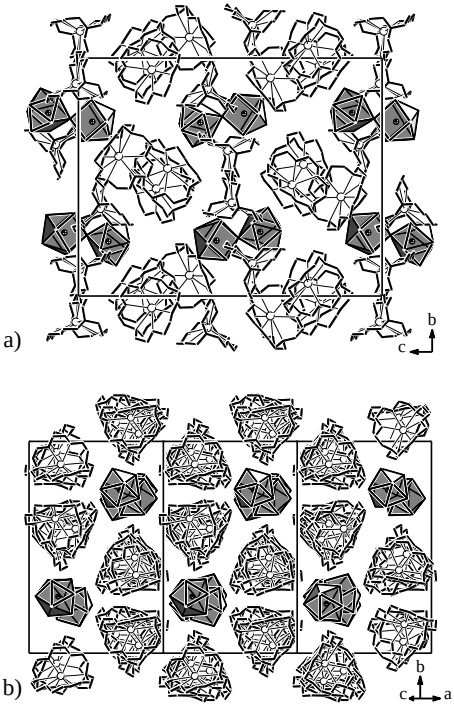

Figure 3.10 Crystal structure of compound **4** view along (a) [1 0 0] and (b) [1 0 1] direction. The hydrogen atoms and solvent molecules were omitted for clarity; K atoms are drawn as white spheres, [Co_2@Sn_{17}] clusters as grey polyhedra.

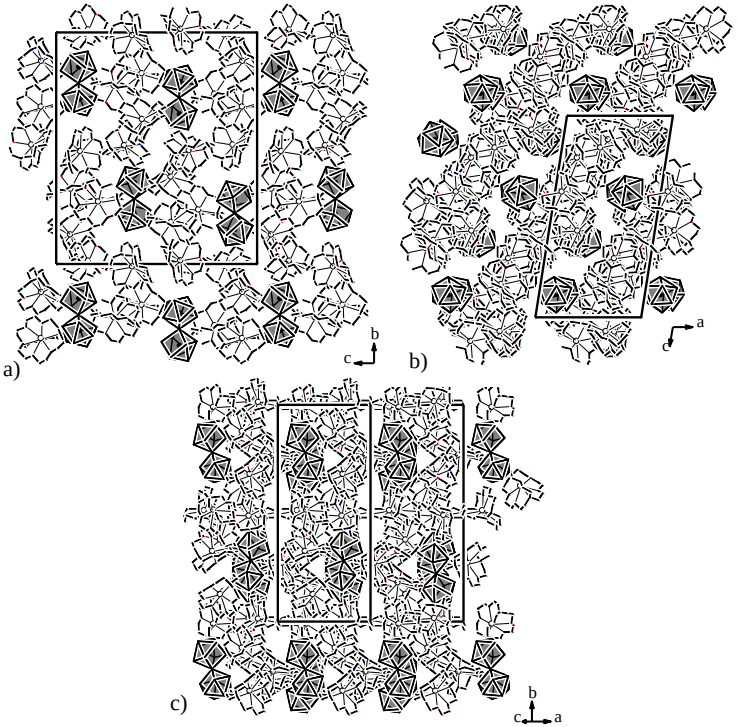

Figure 3.11 Arrangement of the structure building units in compound **3**, space group setting analogically to **4** in $P2_1/n$ (different from ***chapter 3.1.4***, page 34). View along (a) [1 0 0], (b) [0 1 0] and (c) [1 0 1] direction. The hydrogen atoms were omitted for clarity; K atoms are drawn as white spheres, $[Co_2@Sn_{17}]$ clusters as grey polyhedra.

3.1.5 EPR Spectra

As indicated by the fivefold negative charge, the $[Co_2@Sn_{17}]^{5-}$ cluster possesses an unpaired electron, which should cause paramagnetism. From the Schlenk tube of reaction, a large crystal of compound **3** with a side length of about one millimeter was freshly put into an EPR tube inside the glovebox. The EPR measurements were

performed at different temperatures of 293 K and 153 K. The EPR spectrum and the simulated spectrum for 153 K are shown in Figure 3.12. The g-value at room temperature was determined relative to a Mn standard with $g = 1.981$. For the spectrum at low temperature, the signal shape fits best with a simulation assuming a diluted spin system with the two g tensors, $g_{\parallel} = 1.914$, $g_{\perp} = 2.066$, which confirms the axial symmetry of the paramagnetic species.

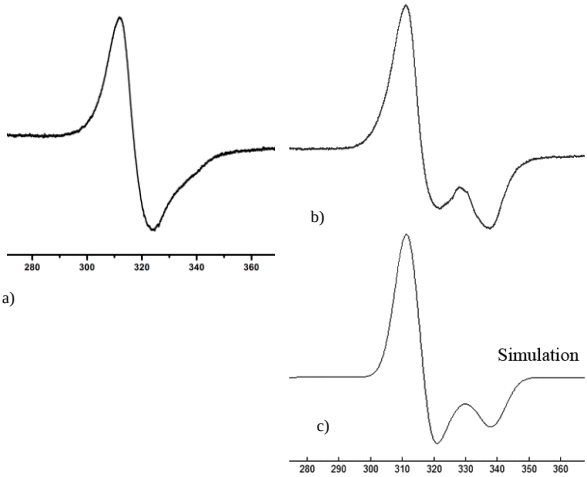

Figure 3.12 EPR spectra of crystals of compound **3** (a) at 293 K and (b) at 153 K and (c) the simulation of the spectrum at 153K was performed with two different g tensors ($g_{\parallel} = 1.914$, $g_{\perp} = 2.066$).

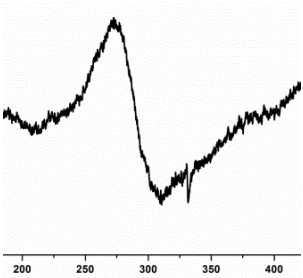

Figure 3.13 EPR spectrum of crystals of compound **4** at 103 K (without Mn standard). (The sharp signal is from the quartz EPR tube.)

Although compound **4** also contains a $[Co_2@Sn_{17}]^{5-}$ cluster with an unpaired electron, no EPR signal was detectable above a temperature of 103 K, where a weak signal with $g = 2.291$ appeared (Figure 3.13). This might be affected by the twisted dimer cluster almost losing the axial symmetry.

3.2 Endohedral Rhodium-Centered Tetrelatomic Clusters

As mentioned in ***chapter 1.1***, page 1, Rh-Sn bimetallic shows great advantages in selective catalytic hydrogenation reactions. The increasing number of the formation of Rh-Sn binary or ternary phase have been established through solid state synthesis approaches, such as $RhSn_2$, $RhSn_3$, $RhSn_4$, $Li_xRh_3Sn_{7-x}$, $R_5Rh_4Sn_{10}$ (R = Ce, Pr, Nd), $RRhSn_3$ (R = Ce, Pr), $Yb_3Rh_4Sn_{13}$, *etc*.[184-190] To our knowledge, rare stannides in related Rh-Sn systems have been found in solution chemistry. To investigate the reactivity of the Rh-Sn compounds, an intermetallic compound with the nominal composition of "K_3RhSn_6" was synthesized following the procedure in ***chapter 5.3.1***, page 91. The low crystallinity cannot reveal the composition of this intermetalloid, while the products of the solution reactions evidence the existence of RhSn phases.

3.2.1 $[K([2.2.2]crypt)]_6[Sn_9]_{1.53}[Rh@Sn_{10}]_{0.47}\cdot 3en\cdot tol$ (5)

Synthesis and Characterization

Crystals of compound **5** were achieved from a red-brown mixture of an ethylenediamine solution of an intermetallic phase with the nominal composition of "K_3RhSn_6" and cryptand. Toluene solvent was layered on the filtrated solution (synthesis details see ***chapter 5.3.2***, page 93). Few pieces of black plate crystals formed among the solid residue with a crystallographically determined composition $[K([2.2.2]crypt)]_6[Sn_9]_{1.53}[Rh@Sn_{10}]_{0.47}\cdot 3en\cdot tol$. Attempts to crystallize $[Rh@Sn_n]^{3-}$ using alternative sequestering reagents and/or from

different solvent mixtures were unsuccessful.

The crystal structure of compound **5** was solved by direct methods and refined in the monoclinic space group $P2_1/c$ (No. 14). All non-H atoms were refined anisotropically. The positions of the hydrogen atoms of cryptand, toluene and ethylenediamine molecules were geometrically calculated and refined isotropically with a riding model. Data and structure refinement parameters of compound **5** are listed in ***chapter 6.2.5***, page 104. The EDX analysis shows the ratio of K/Rh/Sn to be around 2:0.5:9.5.

Crystal Structure Description

$[K([2.2.2]crypt)]_6[Sn_9]_{1.53}[Rh@Sn_{10}]_{0.47}\cdot 3en\cdot tol$ (**5**) crystallizes in space group $P2_1/c$ and reveals two cluster anions in the asymmetric unit alongside six charge-balancing $[K([2.2.2]crypt)]^+$ cations. Both independent clusters are highly disordered and composed with different ratios of $[Sn_9]$ and $[Rh@Sn_{10}]$ substructures. For further discussion, the two disordered clusters in compound **5** are noted as cluster **5a** and **5b**. Cluster **5a** split to four subunits: **5aA**, **5aB**, **5aC** and **5aD**; Cluster **5b** split to three subunits: **5bA**, **5bB** and **5bC**.

Best refinement results are obtained using a structure model, in which the cluster **5a** is composed by four sub-clusters with different occupations (Table 3.5): 46% with $[Sn_9]^{3-}$ (cluster **5aA**), 24% with $[Sn_9]^{3-}$ (cluster **5aB**), 20% with $[Rh1@Sn_{10}]^{3-}$ (cluster **5aC**), and 10% with $[Rh1@Sn_{10}]^{3-}$ (cluster **5aD**). In these clusters, atoms Sn1, Sn2 and Sn4 are fully occupied with the same positions in all clusters, while other atoms are splitting to different positions. The Figure 3.14 exhibits the views of whole model **5a** and four splitting sub-clusters along the same direction.

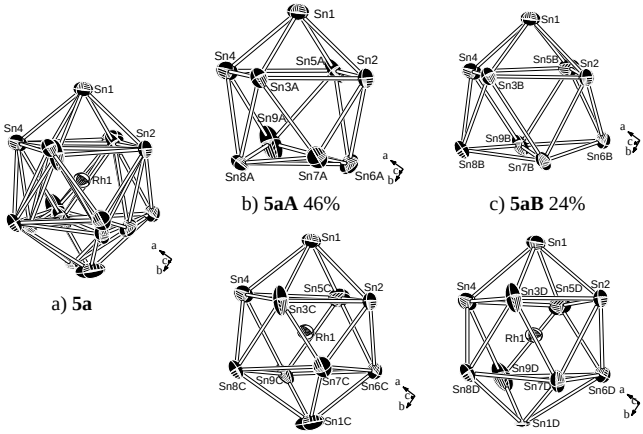

a) **5a**

b) **5aA** 46%

c) **5aB** 24%

d) **5aC** 20%

e) **5aD** 10%

Figure 3.14 Cluster **5a** and four individual splitting sub-structures at the same position. Anisotropic displacement ellipsoids are shown at 50% probability level.

Table 3.5 The distribution of clusters and split sub-clusters as well as the probable content of rhodium in compound **5**.

Cluster	Percentage(%)	Rh (%)
5a	100	30
5aA	46	0
5aB	24	0
5aC	20	20
5aD	10	10
5b	100	17
5bA	83	0
5bB	8	8
5bC	9	9

Table 3.6 Geometric Parameters of three unfilled Sn_9 Cluster in compound **5**.

compound	prism edges[a) c)]					dihedral cap to cap fold angle about h[f) c)]				
	e[b)]	h_1	h_2	h_3	γ[d)]	h/e[e)]	α_1	α_2	α_3	d_1/d_2[f)]	
5aA	21	1.05	1.04	1.04	1	1.08	17	18	21	1.44	~ D_{3h}
5aB	21	1.04	0.98	1.13	9	1.04	13	20	30	1.33	C_{2v}
5bA	21	1.05	1.02	1.00	3	1.06	16	18	21	1.42	~ D_{3h}

(a) Relative prism heights, scaled to the value 3.194 Å, the shortest height in $[K([2.2.2]crypt)]_6([Sn_9][Sn_9])\cdot 1.5en\cdot 0.5tol$.[74] (b) The number of skeleton electron. (c) The best monocapped square antiprism is chosen. If the structure is close to D_{3h} symmetry the longest height is considered as a diagonal in the C_{4v} symmetric cluster. (d) γ shows the dihedral angle between the triangular bases. (e) *h* and *e* are the mean values of the prism heights and the triangular edges, respectively. (f) The chosen basal squares are Sn1-Sn4-Sn9A-Sn5A in **5aA**, Sn6B-Sn7B-Sn8B-Sn9B in **5aB**, Sn11-Sn15-Sn12-Sn19 in **5bA**, respectively. d_1 and d_2 refer to diagonal distances of the basal squares.

Table 3.7 Selective bond lengths and angles of the four $[Sn_{10}]$ clusters in compound **5**.

Cluster	**5aC**	**5aD**	**5bB**	**5bC**[e]
E-E (Å)	2.585(1)-3.740(1)	2.332(1)-3.406(1)	2.653(1)-3.730(1)	2.638(1)-3.566(1)
$M_{central}$-E (Å)[a]	2.387(1)-2.986(1)	2.360(1)-2.986(1)	2.352(1)-2.957(1)	2.336(1)-2.987(1)
$M_{central}$-E_{cap} (Å)[b]	2.960(1), 2.986(1)	2.903(1), 2.986(1)	2.953(1), 2.957(1)	2.612(1), 2.987(1)
E_{cap}-E_{square} (Å)	2.868(1)-3.038(1)	2.660(1)-3.092(1)	2.688(1)-3.020(1)	2.638(1)-3.047(1)
E_{square}-E_{square} (Å)[c]	3.042(1)-3.317(1)	2.972(1)-3.318(1)	2.952(1)-3.484(1)	3.256(1)-3.566(1)
$E_{antiprism}$-$E_{antiprism}$ (Å)[d]	2.912(1)-3.065(1)	2.912(1)-3.127(1)	2.840(1)-3.020(1)	2.694(1)-3.285(1)
E_{cap}-$M_{central}$-E_{cap} (°)	173	167	162	172
Torsion angle of Square (°)	1, 2	2, 8	1, 1	0, 4
Dihedral angle of Squares (°)	6	5	11	2

(a) $M_{central}$: centering Rh atom; (b) E_{cap}: the capping Sn atom; (c) E_{square}: the Sn atom of two basal squares of antiprism in [Sn10] clusters; (d) Eantiprism: the Sn atom of antiprism in [Sn10] clusters; (e) **5bC** shows the 10-membered cage with the central axis (Sn11-Rh2-Sn40) in different direction compared to that in cluster **5bB** (Sn26-Rh2-Sn30)

In unfilled cluster **5aA**, the Sn-Sn bond lengths range in 2.915(1) Å

[Sn3A-Sn7A] - 3.364(1) Å [Sn6A-Sn8A]. The whole polyhedron **5aA** adopts nearly ideal D_{3h} symmetry with three elongated heights, the relative structure parameters are shown in Table 3.6. The Sn-Sn distances of cluster **5aB** vary between 2.912(1) Å [Sn5B-Sn6B] and 3.318(1) Å [Sn5B-Sn2]. The cage **5aB** shows a distorted C_{2v} geometry with one elongated prism height [Sn7B-Sn9B] of 3.622(1) Å.

In the metal-filled 10-memembered cluster **5aC**, the Sn-Sn distances lie in 2.585(1) Å [Sn3C-Sn7C] and 3.740(1) Å [Sn6C-Sn7C], shown in Table 3.7. The longest and shortest bonds are formed because of the splitting position of Sn7C. The skeleton tin atoms can be divided to two types: capped Sn atoms [Sn1 and Sn1C, noted as Sn_{cap}] and other eight Sn atoms of the antiprism [noted as Sn_{ap}], which results in three types of Sn-Sn distance: i) Type 1, distances of Sn_{cap}- Sn_{ap} localize in 2.868(1)-3.038(1) Å; ii) Type 2, the edge lengths of two basal squares in the antiprism are longer than former bonds, within 3.042(1)-3.317(1) Å; iii) Type 3, the connection bonds between the basal in the antiprism agree with bonds of type I, around 2.912(1)-3.065(1) Å. The two basal square faces (Sn2-Sn3C-Sn4-Sn5C and Sn6C-Sn7C-Sn8C-Sn9C) are nearly two planes with torsion angles of 2 ° and 1 °, respectively. These two squares are almost parallel with a dihedral angle 6 °. The centered Rh1 connects with two Sn_{cap} with 2.960(1) Å and 2.986(1) Å. The distances between Rh1-Sn_{ap} range from 2.387(1) Å to 2.787(1) Å. The angle of Sn1-Rh1-Sn1C is 173 °, which indicates a slightly twisty central axis of the polyhedron. Thus, the cluster **5aC** shows a distorted bicapped square antiprism cage.

In cluster **5aD**, the Sn-Sn distances range in 2.332(1) Å [Sn1D-Sn9D] and 3.406(1) Å [Sn6D-Sn9D], due to unique position of Sn9D in the structure. Type 1 bond lengths ranges in **5aD** are broader than those in cluster **5aC**, around 2.660(1)-3.092(1) Å [Sn1D-Sn7D, Sn1D-Sn9D]. Type 2 bond lengths are within 2.972(1)-3.318(1) Å [Sn6D-Sn7D, Sn2-Sn5D]. Type 3 bond distances localize between 2.912(1) and 3.127(1) Å [Sn2-Sn6D, Sn2-Sn7D]. The two base planes (Sn2-Sn3D-Sn4-Sn5D and Sn6D-Sn7D-Sn8D-Sn9D) with torsion angles of 2 ° and 8 °, displays a dihedral angle of 5 °. The bond length of Rh1-Sn1D is 2.903(1) Å and the distances of Rh1-Sn_{ap} in cluster **5aD** reveals in the regions of 2.360(1)-2.718(1) Å. The angle of Sn1-Rh1-Sn1D is less than that of cluster **5aC** 167 °, which results in a more distorted bicapped square antiprism geometry.

The cluster **5b** site adopts one splitting [Sn_9] cluster and two splitting

[Rh@Sn_{10}] clusters: 83% with $[Sn_9]^{3-}$ (cluster **5bA**), 8% with $[Rh2@Sn_{10}]^{3-}$ (cluster **5bB**), 9% with $[Rh2@Sn_{10}]^{3-}$ (cluster **5bC**). The positions of atoms Sn11 and Sn12 are the same in all clusters without splitting, shown in Figure 3.15. The main part **5bA** of the cluster shows an almost D_{3h}-symmetric cage with Sn-Sn bonds range in 2.923(1) [Sn11-Sn19] to 3.362(1) Å [Sn15-Sn19], which is similar to those in cluster **5aA**.

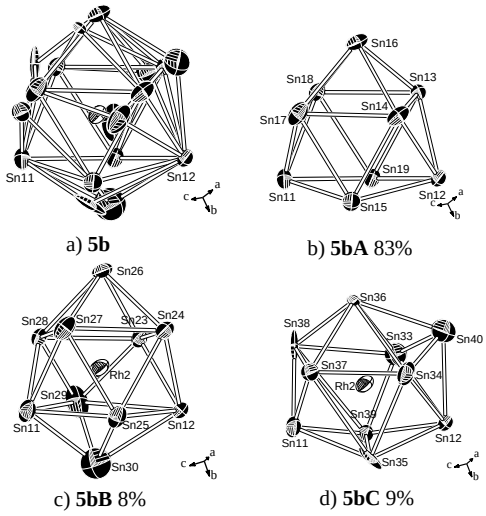

a) **5b** b) **5bA** 83%

c) **5bB** 8% d) **5bC** 9%

Figure 3.15 Cluster **5b** and three individual splitting sub-structures at the same position. Anisotropic displacement ellipsoids are shown at 50% probability level.

In the cluster **5bB**, the location of atom Sn29 affects the Sn-Sn bond lengths within the range of 2.653(1) [Sn28-Sn29]-3.730(1) Å [Sn12-Sn29]. Type 1 bond lengths are around 2.688(1) [Sn29-Sn30]-3.020(1) Å [Sn12-Sn30], type 2 bond lengths vary between 2.952(1) [Sn12-Sn25] and 3.484(1) Å [Sn11-Sn29], and type 3 bonds range in 2.840(1) [Sn25-Sn30] and 3.020(1) Å [Sn12-Sn30]. The dihedral angle of two plane squares (Sn23-Sn24-Sn27-Sn28 and Sn12-Sn25-11-Sn29 with both torsion angles 1 °) is 11 °. The lengths of Rh2-Sn_{cap} (Sn26, Sn30) and Rh2-Sn_{ap} bonds range between 2.953(1)-2.957(1) Å and 2.352(1)-2.820(1) Å, respectively. The angle

of Sn26-Rh2-Sn30 is 162 °. Cluster **5bB** shows a similar distortion as the 10-vertices deltahedral cage above.

The central axis (Sn11-Rh2-Sn40) of cluster **5bC** shows in different direction compared to that in cluster **5bB** (Sn26-Rh2-Sn30), with an angle between the axis of 172 °. Mainly due to the position of atom Sn38, the cluster shows an expansion structure with Sn-Sn bonds lengths from 2.774(1) Å [Sn34-Sn40] to 3.566(1) Å [Sn38-Sn39]. The types 1-3 bonds lengths are in the range of 2.638(1)-3.047(1) Å, 3.256(1)-3.566(1) Å, and 2.694(1)-3.285(1) Å, respectively. The Rh2-Sn_{ap} distances are between 2.336(1) [Rh2-Sn39] and 2.867(1) Å [Rh2-Sn35]. The shortest Rh-Sn_{cap} bond is 2.612(1) Å [Rh2-Sn_{cap}], while the other Rh2-Sn40 is 2.987(1) Å. The two square faces (Sn12-Sn33-Sn36-Sn34 and Sn35-Sn37-Sn38-Sn39) whose torsion angles are 0 ° and 4 °, are nearly parallel to each other with a small dihedral angle of 2 °.

In above endohedrally metal-filled clusters **5aC**, **5aD**, **5bB** and **5bC**, some bond lengths were observed unrealistically short (i.e., 2.332(1) Å [Sn1D-Sn9D]), which might result from the imperfect structure models built for these significantly complicated disorder situation.

The three unfilled clusters $[Sn_9]^{3-}$ **5aA**, **5aB** and **5bA** show almost similar structures with approximately D_{3h}-symmetry. The four endohedral $[Rh(-1)@Sn_{10}]^{3-}$ anions can be understood as a 10-vertex $[Sn_{10}]^{2-}$ with distorted bicapped square antiprism centered by a Rh atom. If the -3 charge of the whole cluster and Rh(-1) are taken into consideration, and the Sn atoms donate two electrons to the cluster skeleton bonding, thus result in a 22 electron with a *closo* geometry. The endohedral clusters $[Rh(-1)@Sn_{10}]^{3-}$ are isoelectronic to clusters $[Pb_{10}]^{2-}$ and $[Ni(0)@Pb_{10}]^{2-}$.[107] The reasonable thermal ellipsoids and the disorder for the clusters give rise to clusters with pseudo-D_{4d} symmetry, but certainly not to a pentagonal prismatic D_{5h} symmetry as observed in $[Co@Ge_{10}]^{3-}$ and $[Fe@Ge_{10}]^{3-}$ anions.[123,124] If compared to the contact of the capped tin and centered metal atoms with Sn-Co (2.70 Å) in $K_{4.79}Co_{0.79}Sn_9$,[125] Sn-Fe (2.81 Å) in $[Fe@Sn_{10}]^{3-}$ [122] and Sn-Ni (2.73 Å) in $[Ni@Sn_9]^{3-}$,[106] the two axial Sn-Rh distances are elongated with a mean value of 2.91 Å.

Parallel to the crystallographic *b* and *c* axes, the clusters are arranged in double layers of clusters centered by Rh1 and Rh2 (shown in Figure 3.16a with different colors). Along the *c* axis the clusters show a distorted primitive hexagonal packing, shown in Figure 3.16b.

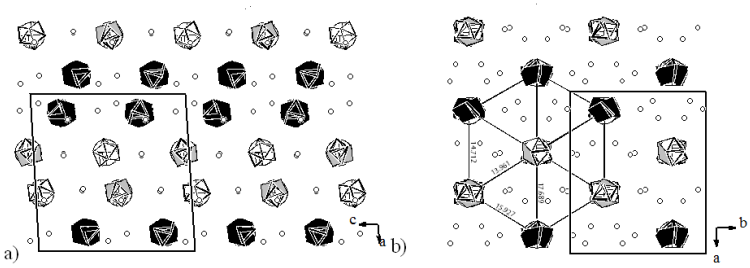

Figure 3.16 Crystal packing in the crystal structure of compound **5**, view (a) along the *b* axis, (b) along the *c* axis. The C/H/N/O atoms were omitted for clarity. The clusters around Rh1 are shown as grey polyhedral, the clusters around Rh2 are drawn in black, K atoms are shown as white dots.

3.2.2 EPR Spectra

Both the tricapped trigonal prism and the bicapped square antiprism exhibited by **5** are remarkable unique for a ligand-free clusters. Electron paramagnetic resonance (EPR) measurements confirm the paramagnetic character of this compound. While the starting alloy K_3RhSn_6 gives no EPR signal, the EPR spectrum of a frozen crude solution measured at 153 K all show a strong resonance with two experimental *g* values, 1.926 and 2.04, as expected for an axially symmetric species, in Figure 3.17a. The paramagnetic character of the cluster anion and is presumably similar to the signals of dmf solution of $[K([2.2.2]crypt)]_3[Sn_9]$ at 77 K ($g_1 = 2.03$, $g_2 = 2.02$, $g_3 = 2.00$),[71] which fits well with a simulation assuming a diluted spin system with axially anisotropic *g* tensors ($g_{\parallel} = 1.926$, $g_{\perp} = 2.048$). The spectrum of the solid compound **5**, performed on one single piece of a crystal of **5**, shows a rather weak signal with a g-value of 2.042, as seen in Figure 3.17c, which seems different from the signals of the crystal sample of $[K([2.2.2]crypt)]_3[Sn_9]$ at 77 K (g_1 = 2.01, g_2 = 1.99, g_3 = 1.94). Although $[Sn_9]^{3-}$ clusters as the main splitting part of clusters in compound **5**, the paramagnetic property of compound **5** is significantly

different from the metal-unfilled compound $[K([2.2.2]crypt)]_3[Sn_9]$, which indicates that the novel clusters with metal insertion were formed in compound **5**.

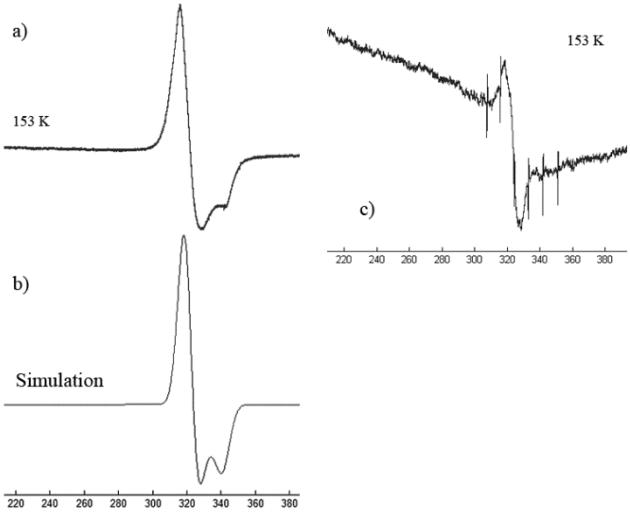

Figure 3.17 EPR spectra of (a) crude reaction solution and (b) simulation, (c) the one piece of crystal of compound **5** at 153 K (both with Mn standard). The simulation of the spectrum was performed with two different *g* tensors ($g_{\parallel}$ = 1.926, $g_{\perp}$ = 2.048).

3.3 Endohedral Iridium-Centered Clusters

Stannides of the late transition metals from Ir occur in various compositions and structures, such as Ir_5Sn_7, $IrSn_4$, $LiIrSn_4$, $Li_xIr_3Sn_{7-x}$, $Mg_xIr_3Sn_{7-x}$ (x=0-1.67), *etc*.[186,191-196] These intermetallic compounds were generally found when the solid synthesis reaction was carried out in tin-rich melts with tin applying as solvent and reactant. Lately, a novel endohedral stannaspherene $[Ir@Sn_{12}]^{3-}$ in $[K([2.2.2]crypt)]_3[Ir@Sn_{12}]\cdot en\cdot tol$ was synthesized, starting with K_4Sn_9 and $[IrCl(cod)]_2$ in ethylenediamine, and via another capped cluster anion $[Sn_9Ir(cod)]^{3-}$ as an intermediate product.[126] These findings intrigue us to synthesize a solid sample with the nominal composition

"Rb_3IrSn_{12}" (***chapter 5.3.1***, page 91). Assumed from the neat solid the Ir-filled clusters are already preformed. Due to low crystallinity, it is not possible to clarify. Therefore, the solution experiments were performed and indirectly proved the existence of [Ir@Sn_{12}] clusters in the solid phase.

3.3.1 [Rb([2.2.2]crypt)]$_3$[Ir@Sn_{12}]·en·2tol (6)

Synthesis and Characterization

Compound **6** was obtained from an orange-brown solution of a intermetallic phase with the nominal composition "Rb_3IrSn_{12}" and [2.2.2]crypt in ethylenediamine. Few pieces of black block crystals formed among the solid residue with the crystallographic determined composition [Rb([2.2.2]crypt)]$_3$[Ir@Sn_{12}]·en·2tol (synthesis details see ***chapter 5.3.2***, page 93). The crystalline salt is extremely air- and moisture-sensitive.

The crystal structure of compound **6** was solved by direct methods and the structure refinement was carried out in the monoclinic space group *C2/c* (No. 15). All non-H atoms are refined anisotropically. One of the two clusters displays rotational disorder. The atoms (Sn1, Sn3, Sn5 and Sn6) are disordered and the atoms on splitting positions on two atomic sites each show elongated ellipsoids. The ethylenediamine and toluene molecules were refined with isotropic displacement parameters due to the disorder. The positions of the hydrogen atoms of cryptand, toluene and ethylenediamine molecules were geometrically calculated and refined isotropically with a riding model. Data and structure refinement parameters of compound **6** are listed in ***chapter 6.2.6***, page 105.

Crystal Structure Description

The [Rb([2.2.2]crypt)]$_3$[Ir@Sn_{12}]·en·2tol salt is monoclinic and shows a high degree of disorder. The asymmetric unit contains two half clusters: the cluster **6a** (Sn1 to Sn6) consisting of atoms, which, after splitting into two positions, still show relatively elongated ellipsoids; while cluster **6b** (Sn7 to Sn12) is devoid of disorder, shown in Figure

3.18. The whole structure is an analogue of reported $[K([2.2.2]crypt)]_3[Ir@Sn_{12}]\cdot en\cdot tol$, which was synthesized from K_4Sn_9 with $[IrCl(cod)]_2$ step-by-step in solution. Both kinds of approaches for synthesis of $[Ir@Sn_{12}]^{3-}$ does not provide very reproducible and high yields, thus no more further analysis can be done for potential properties.

$[Rb([2.2.2]crypt)]_3[Ir@Sn_{12}]\cdot en\cdot 2tol$ reveals the isotopic same space group within standard deviation same lattice parameters as $[K([2.2.2]crypt)]_3[Ir@Sn_{12}]\cdot en\cdot tol$. Interestingly, $[Ir@Sn_{12}]$ clusters also show one ordered and one disordered as the analogue. The details about the crystallographic data comparison of both compounds shows in ***chapter 6.2.6***, page 105.

In cluster **6a**, the atoms Sn2 and Sn4 are not split. The Sn-Sn bonds lengths in cluster **6aA** and **6aB** range between 2.975(9)-3.149(7) Å and 2.775(17)-3.258(18) Å with mean values of 3.081 Å and 3.006 Å, respectively, which are all in the range found for $[Sn_9]^{3-}$ and $[Sn_9]^{4-}$.[72,181] The Ir-Sn contacts in both clusters are in the ranges of 2.891(1)-3.9114(2) Å and 2.849(13)-2.8984(1) Å with average lengths of 2.924 and 2.862 Å, respectively. The R/d ratios of the icosahedral model of the two clusters are 0.949 and 0.952, which are slightly distorted from the ideal model of 0.951.[45,64]

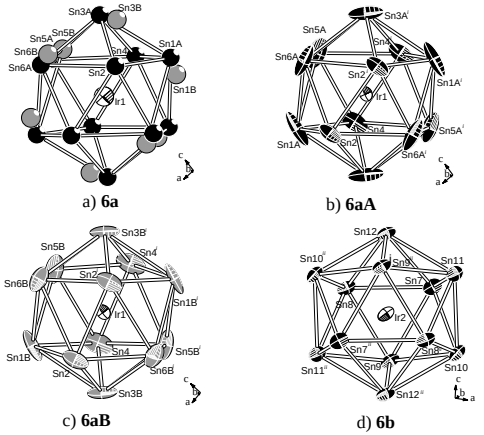

Figure 3.18 ORTEP drawing of the $[Ir@Sn_{12}]^{3-}$ anions in compound **6**: (a) **6a**, (b) **6aA**, (c) **6aB**, (d) **6b**. Atoms are drawn with 50 % probability ellipsoids. (Symmetric codes: (i) -x, y, 0.5-z; (ii) -x, -y, -z.)

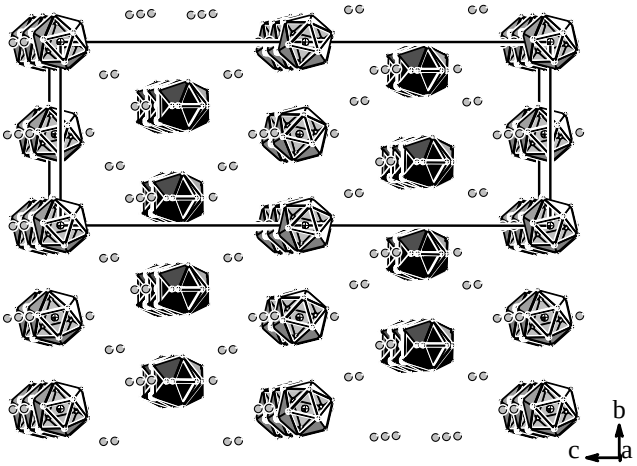

Figure 3.19 The arrangement of layer packing perpendicular to *c* axis in compound **6**. Clusters **6a** shown as black polyhedra, and clusters **6b** drawn in grey.

The structure of cluster **6b** corresponds to a typical icosahedral cage. The Sn-Sn distances along the edges of the cage range from 3.0215(11) to 3.0957(11) Å [Sn7-Sn12, Sn9-Sn12^{ii}, (ii) -x, -y, -z] with a mean value of 3.0700 Å, which is close to those reported nona-stannide clusters.[72,181] The Ir-Sn distances are in a very narrow range of 2.9098(8) to 2.9392(7) Å [Ir2-Sn9, Ir2-Sn8] with an average value of 2.9180 Å. The R/d ratio for $[Ir@Sn_{12}]^{3-}$ in **6b** is 0.950 and deviates slightly from the value in regular model.

Both the $[Ir@Sn_{12}]^{3-}$ clusters are 12-vertex 26 electron polyhedra with nearly ideal *closo* icosahedral structures as expected from the Wade-Mingos electron counting rules. According to this rules, the Sn atoms contribute two electrons to cluster bonding, and Ir atom donates one electron to the -3 charge of the cluster, that give a 26 skeleton electron (2n+2) cluster with a *closo* geometry. The 30 Sn-Sn bonds and 12 Sn-Ir bonds in **6** match the reported values of Sn-Sn bonds (3.065 Å) and Sn-Ir bonds (2.922 Å) in $[K([2.2.2]crypt)]_3[Ir@Sn_{12}]\cdot en\cdot tol$, which are both slightly shorter than the calculated interatomic distances of

3.144 Å Sn-Sn and 2.990 Å Sn-Ir in $[Ir@Sn_{12}]^{3-}$.[126] The metal-filling of the icosahedral cluster seems to have little effect on the stannaspherene if taking into account the simulated unfilled cluster $[Sn_{12}]^{2-}$ with Sn-Sn bond lengths of 3.125 Å. The metal-encapsulated cluster enhances the condensed cage unit with the contacts between the core and skeleton atoms.

Regarding the clusters arrangement, **6a** and **6b** form layers perpendicular to the *c* axis, respectively, shown in Figure 3.19.

3.4 Heteroatomic Sb/Sn Nona-atomic Polyanions

As introduced in ***chapter 1.4***, the heteropolyatomic deltahedral clusters of main group elements generally originate from two synthetic routes: i) to mix the pure phase precursor with the organic ligand of main group elements in solution. For instance, Sevov and coworkers reported $[(EGe_8)\text{-}(Ge_8E)]^{4-}$ (*E* = Sb, Bi) and $[Ge_7Sb_2]^{2-}$ through the reactions of Ge_9^{4-} with EPh_3 (*E* = Sb, Bi) at elevated temperatures or with sonication.[156] ii) to melt mixed elements stoichiometrically in solid state. However, only one case of the endohedral main-group clusters has been presented till now. The $[Ni@TlSn_9]^{3-}$ cluster is isoelectronic to $[Pb_{10}]^{2-}$ clusters through two-step synthetic approach: Sn_9^{4-} ions mixed with $Ni(cod)_2$ to form an intermediate cluster $[Ni@Sn_9]^{4-}$, which further reacted with TlCp to form *closo*-species $[Ni@TlSn_9]^{3-}$. To investigate the reactivity of the pre-existing endohedral cluster $[Co@Sn_9]^{5-}$ with other main group elements, the reactions of $K_{4.79}Co_{0.79}Sn_9$ and EPh_3 (*E* = As, Sb, Bi) were explored in various conditions. Finally, a novel heteroatomic compound was formed with charge of -2. The similar reaction was applied to Rb_4Sn_9 and another new species was found later.

3.4.1 Endohedrally Metal-centered Compound $[K([2.2.2]crypt)]_2[Co_x@Sn_{7-x}Sb_{2+x}]$ x≈0.58 (7)

Synthesis and Characterization

Compound **7** was obtained from a brown solution of the precursor $K_{4.79}Co_{0.79}Sn_9$ and $SbPh_3$ in presence of [2.2.2]crypt in ethylenediamine. The toluene solution was layered on the filtrate for diffusion to crystalize the compounds (more synthetic details see ***chapter 5.3.3***, page 95). Two pieces of black block crystals formed among solid residue on the bottom of the Schlenk tube, with a composition of $[K([2.2.2]crypt)]_2[Co_x@Sn_{7-x}Sb_{2+x}]$ x≈0.58 determined by single crystal X-ray diffraction.

The structure of compound **7** was solved by direct methods and refined in the monoclinic space group *C2/c* (No. 15). Due to the difference of one electron between the elements, it was not possible to distinguish Sb/Sn atoms by X-ray diffraction, and all the Sb atoms were refined as Sn atoms. However, the EDX analysis shows the presence of Co, Sb, Sn atoms in this compound, shown in Table 3.8. All non-H atoms are refined anisotropically. The positions of the hydrogen atoms of cryptand were geometrically calculated and refined isotropically with the riding model. Data and structure refinement parameters of Compound **7** are listed in the table of ***chapter 6.2.7***, page 106.

Table 3.8 EDX-results of crystal samples in compound **7**.

test	K (%)	Co (%)	Sn (%)	Sb (%)
A	14(±3)	5(±2)	57(±7)	23(±4)
B	15(±3)	5(±2)	59(±6)	21(±3)
C	13(±3)	4(±2)	59(±7)	29(±4)
D	11(±3)	4(±3)	58(±8)	27(±5)
theoretical value of $K_2Co_{0.5}Sb_{2.5}Sn_{6.5}$	17(2/11.5)	4(0.5/11.5)	57(6.5/11.5)	22(2.5/11.5)

Crystal Structure Description

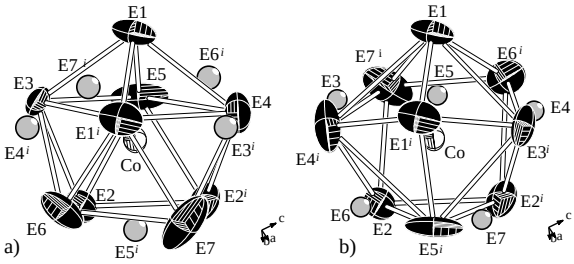

Figure 3.20 Two splitting structure of the $[Co_{0.58}@E_9]^{2-}$ (E = Sb/Sn) anions in compound **7**. Atoms are drawn with 50 % probability ellipsoids. Sn atoms stand for mixed Sn/Sb atoms. (Symmetric code: (i) 1-x, y, 0.5-z.)

Compound **7** crystallizes in the monoclinic space group *C2/c*. The asymmetric unit of **7** comprises one nine-member cage with partly cobalt-insertion and two [2.2.2]cryptand sequestered K cations to balance the charge of the whole system. The compound was formed through the oxidation of $[Co@Sn_9]^{5-}$ in solution with the formation of residue and tin mirror. The only two small pieces of crystals feature highly sensitive out of the mother liquid and a poor yield, thus no further analysis to take.

For the convenience of further discussion, E is used to represent Sn and Sb doped atomic species. The disordered $[Co@E_9]^{2-}$ anion could be split to two nearly identical clusters with sharing E1 and E2 atoms and to form C_{4v}-symmetry with distortion from the *nido*-polyhedra, shown in Figure 3.20. The mean values of $M_{centered}$-E bond lengths are 2.563 Å in cluster **7a** with the range from 2.389 to 2.724 Å, which are slightly shorter than those of Co-Sn bonds in the original cage $[Co@Sn_9]^{5-}$ (2.56-2.66 Å) in $K_{4.79}Co_{0.79}Sn_9$, the derivative $[Co@Sn_9]^{4-}$ cage (2.55-2.89 Å) in compound **1** and the dimer cage $[Co_2@Sn_{17}]^{5-}$ (2.63-2.72 Å) in compound **3**. The E-E contact along the capped square face E1^i-E3-E4-E5 (E1 as the cap vertical, from 2.8159(1) Å for E1-E3 to 3.0818(2) Å for E1-E4 in cluster **7a**) with average bonds length 2.95 Å are longer than a typical tin single bond (2.80 Å in α-Sn) or Sb-Sb bonds in ligand-free Zintl ions (i.e., Sb_7^{3-}, Sb_{11}^{3-}).[197,198] The range of

E-E distances is significantly broader in Table 3.9, 2.816(3)-3.576(1) Å, because of the presence of both 4- and 5-connected vertices and cluster disorder. The average Sn/Sb-Sn/Sb distances (3.03 Å in cluster **7a**) agree with the similar mean value of doping bond length for Sn/Bi-Sn/Bi (2.870-3.014 Å in $[La@Sn_7Bi_7]^{4-}$,[160] 2.948-3.018 Å in $[(Sn_6Ge_2Bi)_2]^{4-}$ [158] and 2.949 Å in $[Sn_2Bi_2]^{2-}$).[199] The open basal plane of the disordered E_9 cage is almost planar with torsion angles of 10.99 °. The ratio of the diagonal lengths of open basal plane E2-E2^{i}-E7-E6 is 1.09 for cluster **7a** with mono-capped square antiprism geometry shown in Table 3.10. The doped cluster **7a** displays a structural analogue of the empty pure $[Sn_9]^{4-}$ polyanion, and more condensed shape than pure phases $[Co@Sn_9]^{5-}$ and $[Co@Sn_9]^{4-}$.

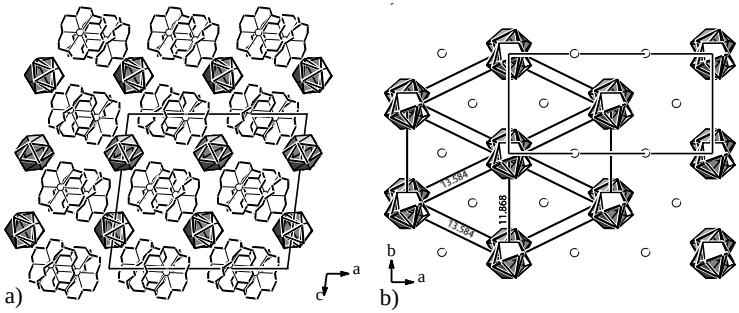

Figure 3.21 (a) The arrangement of layer packing along *b* axis and (b) the hexagonal packing along *c* axis in compound **7** (distances in Å). [2.2.2]crypt molecules omitted for clarity, E_9 clusters as polyhedra, potassium atoms white, Sn/Sb atoms black).

According to the crystallographic data, two $[K([2.2.2]crypt)]^{+}$ cations ensure the polyanion with charge of 2-. Meanwhile, the cluster $[Sn_7Sb_2]^{2-}$ is isoelectronic to $[Sn_9]^{4-}$ anions based on the Wades' rule. Thus, the C_{4v} symmetry is expected occurring to cluster **7**. Considering the charge of cobalt, it remains the same -1 in cluster **7** as that in precursor $K_{4.79}Co_{0.79}Sn_9$, which makes the cluster formula speculated to be $[Co_x@Sn_{7-x}Sb_{2+x}]^{2-}$. According to the experiment results, the refinement of the crystal indicates the occupation of cobalt atom with 58%. Therefore, due to the charge of -2, the ratio of Sn and Sb must be (7-x)/(2+x) in accordance with the Co content, which can be supported

by the results of EDX. The EDX analysis prove the ratios between Sn and Sb to be around (6.61-6.18)/(2.39-2.82). Finally, the formula of the cluster can be deduced as $[Co(-1)_x@Sn_{7-x}Sb_{2+x}]^{2-}$ with x≈0.58.

The $[Co_{0.58}@E_9]^{2-}$ polyanions are arranged as hexagonal layers packing in the *ab* plane, which are separated by layers of $[K([2.2.2]crypt)]^+$ cations. The distances between the centering cobalt atoms of adjacent clusters of compound **7** are in the range from 11.868 to 13.584 Å, shown as Figure 3.21.

Table 3.9 Selected bonds length (Å) in cluster **7a**. (Symmetric code: (i) 1-x, y, 0.5-z)

E1-Co 2.555(2)	E1-E3 3.2040(2)	E2-E7^i 2.866(3)	E6-E7 2.907(3)
E2-Co 2.572(2)	E1-E1^i 2.929 (2)	E2-E2^i 2.921(2)	E2-E3 3.095(4)
E3-Co 2.453(3)	E1-E6^i 2.818(2)	E2-E6 2.921(2)	E3-E6 2.943(3)
E4-Co 2.552(4)	E1-E5 2.983(2)	E2-E4^i 2.930(4)	E3-E5 3.210(4)
E5-Co 2.3885(19)	E1-E7^i 3.053(3)	E2-E5 2.989(2)	E4-E7 3.010(5)
E6-Co 2.7239(16)	E1-E4 3.082(4)	E2-E5^i 3.021(2)	E1-E3^i 3.2040(2)
E7-Co 2.700(2)	E1-E4^i 3.3626(1)	E4^i-E5^i 3.5755(2)	

Table 3.10 Selected structural parameters for the heteroatomic cluster **7a**.

Compound	prism edges [a, b]					dihedral cap to cap fold angle about *h* ( ) [b]				
	h_1	h_2	h_3	γ( )[c]	h/e[d]	α_1	α_2	α_3	d_1/d_2[e]	
cluster **7a**	1.00	1.05	1.34	24	1.17	12	38	37	1.09	~C_{2v}
cluster **7b**	1.00	1.22	1.12	13	1.14	11	31	31	1.09	~C_{2v}

(a) The shortest height (h_1, E_1-E_3) is the relative prism heights, 3.2040(2) Å. (b) The best monocapped square antiprism is chosen. If the structure is close to D_{3h} symmetry the longest height is considered as a diagonal in the C_{4v} symmetric cluster. (c) γ shows the dihedral angle between the triangular bases. (d) *h* and *e* are the mean values of the prism heights and the triangular edges, respectively. (e) The chosen basal squares are Sn2^i-Sn2-Sn6-Sn7 in **7a**, and Sn2-Sn2^i-Sn6^i-Sn7^i in **7b**, respectively. d_1 and d_2 refer to diagonal distances of the basal squares.

3.4.2 $[Rb([2.2.2]crypt)]_2[Sb_xSn_{9-x}]\cdot 3tol\cdot 2en$ x≈2 (8)

Synthesis and Characterization

Red hexagonal plate crystals of compound $[Rb([2.2.2]crypt)]_2[Sb_xSn_{9-x}]\cdot 3tol\cdot 2en$ x≈2 (**8**) are made from a stoichiometric mixture of Rb_4Sn_9 and $SbPh_3$ in the presence of cryptand in ethylenediamine (synthesis procedure see ***chapter 5.3.3***, page 95).

Table 3.11 EDX-results of crystal samples in compound **8**.

test	Rb (%)	Sn (%)	Sb (%)
A	24(±3)	57(±5)	19(±3)
B	25(±3)	55(±5)	20(±3)
C	32(±3)	49(±5)	19(±3)
D	28(±3)	54(±5)	18(±3)
E	30(±3)	51(±5)	18(±3)
F	32(±4)	50(±5)	18(±3)
theoretical value of $Rb_2Sb_2Sn_7$	18(2/11)	64(7/11)	18(2/11)
theoretical value of $Rb_2Sb_3Sn_6$	18(2/11)	55(6/11)	27(3/11)

Crystals of compound **8** were indexed in the hexagonal system; the structure was solved by direct methods and refined in space group $P6_3/m$ (No. 176). All non-H atoms were refined with anisotropic thermal displace parameters. After the structure refinement it is not possible to distinguish between the elements Sn and Sb for the $[E_9]^{2-}$ cluster atoms from structural parameters. Therefore the cluster atoms were assigned and refined as Sn atoms, although EDX (Table 3.11) and mass spectroscopy, and structural considerations unequivocally identify them as Sb/Sn mixed atoms. The location of the hydrogen atoms of cryptand and solvent molecules are geometrically calculated and refined isotropically with the riding model. Data and structure refinement parameters of compound **8** are listed in the table of ***chapter 6.2.8***, page 107.

Crystal Structure Description

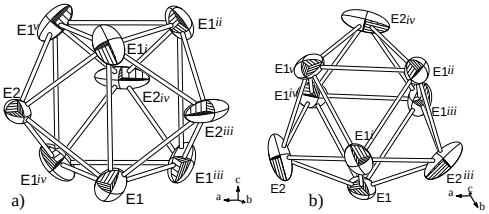

Figure 3.22 ORTEP drawing of the $[Sn_{9-x}Sb_x]^{2-}$ anions in compound **8**. Atoms are drawn with 50 % probability ellipsoids. (Symmetric codes: (i) x, y, 0.5-z; (ii) -y, x-y, 0.5-z; (iii) -y, x-y, z; (iv) -x+y, -x, z. (v) –x+y, -x, 0.5-z)

Table 3.12 Selected bonds length (Å) in cluster **8a**.

E1-E1^{i} 3.456(1)	E1-E2^{i} 2.873(1)	E1-E1^{iii} 3.022(1)
E1-E2^{iii} 2.925(1)	E1-E2 2.873 (1)	E1-E1^{iv} 3.022(1)

(i) x, y, 0.5-z; (ii) -y, x-y, 0.5-z; (iii) -y, x-y, z; (iv) -x+y, -x, z.

Compound **8** crystallizes hexagonally in space group $P6_3/m$. All entities of the crystal structure, one $[Rb([2.2.2]crypt)]^+$ complex, one $[Sb_xSn_{9-x}]^{2-}$ cluster surprisingly devoid of disorder (Figure 3.22), one toluene and one ethylenediamine molecule in the asymmetric unit, are situated at symmetry axes, and therefore show threefold molecular symmetry. Because the solvent molecules do not contain this high molecular symmetry, the toluene and the ethylenediamine molecules are rotationally disordered.

The D_{3h} symmetry cluster is formed by two individual atoms E1 and E2 (E = Sn/Sb). Due to the crystallographic symmetry (C_3-axis and mirror plane), the E1 site forms a trigonal prism with E2 located at the mirror plane forming the caps, shown in Figure 3.22. Thus, the shape of the $[E_9]$ cluster in compound **8** can be described as tricapped trigonal prism, with ideal D_{3h} symmetry with equal elongated prism heights of 3.457(1) Å. The bond lengths of skeletal Sn/Sb atoms range between 2.873(1)-3.456(1) Å (Table 3.12), which generally agree with the distance of Sn-Sn bonds in $[Sn_9]^{3-}$ in D_{3h} symmetry.[72] Deviations of the D_{3h} symmetry cannot be detected due to the high site symmetry given

by space group symmetry. Nevertheless, such deviations seem to be probably due to residual electron density found close the Sn atoms after the structure refinement.

Because of one electron difference between the elements, it is difficult to distinguish between Sn and Sb by X-ray diffraction, and it was not possible in the present structure determination. EDX measurement and mass spectrometry have been taken to identify these elements, the discussion of mass spectrometry details in ***chapter 3.4.4***, page 63. According to EDX measurements, the ratio of tin and antimony is around 7:2 (Table 3.11), which fits well with $[Sn_{9-x}Sb_x]^{(4-x)-}$ with C_{4v}-symmetry.

The $[Rb([2.2.2]crypt)]^+$ and ethylenediamine molecules generate layer A, E_9 clusters and toluene molecules form layer B, and these two layers are alternate piled arrange in direction of *c* axis, as shown in Figure 3.23.

To date, the ligand-free monomeric species E_n ($n \geq 9$) with formal charge of 2- include $[Si_9]^{2-}$,[69] $[Ge_9]^{2-}$,[68,200] $[Ge_{10}]^{2-}$,[201] $[Pb_{10}]^{2-}$,[76,107,202] $[Ni@Pb_{10}]^{2-}$,[107] $[M@Pb_{12}]^{2-}$(M = Ni, Pd, Pt)[76,203]. $[Pb_{12}]^{2-}$[76] can be detected by X-ray diffraction. Besides, oligomers with charge 2- per cluster are well documented for $[Ge_9{=}Ge_9{=}Ge_9]^{6-}$, $[Ge_9{=}Ge_9{=}Ge_9{=}Ge_9]^{8-}$, $_\infty\{[Ge_9]\}^{2-}$ with intercluster bonding to reduce the charge. The charges are reduced to 2- due to partially substitute tin atoms with one more nucleus antimony atoms in compound **7**-**8**. According to Wade's rules, despite their formal charge of 2-, the nine-atom clusters in these formations should remain *nido*-species with 22 skeletal electrons and would exhibit Sn_9^{4-} when monomeric. Cluster **7a** adopts approximately aforementioned symmetry, which is consistent with the known cluster $[Ge_7Sb_2]^{2-}$,[156] due to the ratio of Sn/Sb less than 7/2 as well as the occupation and the charge of cobalt atom. However, the *closo*-cluster of compound **8** shows exception of the structure rules. Interestingly, the pseudo three-fold symmetry of **8** may be caused by the rotational disorder, which also occurs to another mixed species $[Pb_7Bi_2]^{2-}$.[171] The compound **8** containing $[Sn_{9-x}Sb_x]^{2-}$ ($x \approx 2$) anion with D_{3h}-symmetry shows remarkable different packing from other known structures of $[Ge_9]^{2-}$ cluster with D_{3h}-symmetry and $[Si_9]^{2-}$ cluster with almost C_{4v}-symmetry.[63, 69] To our knowledge, the clusters $[Sn_{9-x}Sb_x]^{2-}$ ($x \approx 2$) in $[Rb([2.2.2]crypt)]_2[Sb_xSn_{9-x}]\cdot 3tol\cdot 2en$ and $[Sn_7Sb_2]^{2-}$ in $[K([2.2.2]crypt)]_2[Co_x@Sn_{7-x}Sb_{2+x}]$ ($x \approx 0.58$) are first cases of $[E_9]^{2-}$ with atom Sn involved.

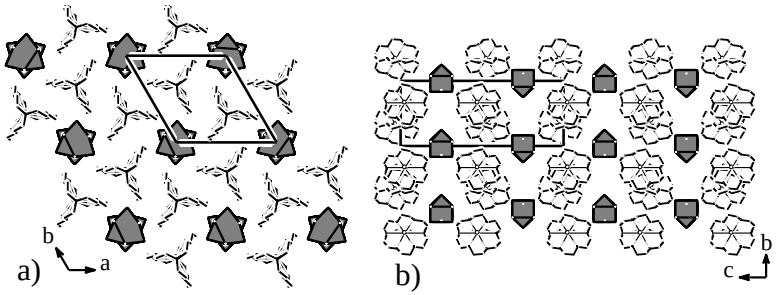

Figure 3.23 Crystal structure of compound **8** (a) the hexagonal layers view along *c* axis, (b) the arrangement view along the *b* axis.

3.4.3 Raman Spectrum of Compound 8

Due to air and moisture sensitive, black crystals of compound **8** were sealed in a silica tube to investigate the vibrational behavior via Raman spectroscopy. For comparison, the characteristic vibrations of $[Sn_9]$ species for Rb_4Sn_9 solid sample and $Rb[Rb([2.2.2]crypt)]_3[Sn_9]$ crystals were also spectroscopically determined.

Their measured Raman spectra of Rb_4Sn_9 exhibit minor shift and nearly similar as the known spectra of K_4Sn_9 and Cs_4Sn_9,[47] with characteristic frequencies of about 147 cm^{-1}. To contrast to the bare $[Sn_9]^{4-}$ cluster and cations with/without sequestering reagents, $Rb[Rb([2.2.2]crypt)]_3[Sn_9]$ crystals were synthesized, which showed the fundamental peak at around 149 cm^{-1} with a slight shift from that of Rb_4Sn_9. The simple vibrational patterns with a very intense breathing mode at ca. 153 cm^{-1} in compound **8**, agrees with identification sonde 151-154 cm^{-1} ($[Sn_9]$), whose position is independent from the nature of the counter ions and environment.[47] $[E_9]^{4-}$ cluster can be expected with 20 Raman-active modes with the C_{4v} symmetry: $\Gamma_{vib} = 4\ A_1 + 3\ B_1 + 3\ B_2 + 5\ E$.[47] The other feature pattern of the spectra is the lack of bands, which means that only very few active modes are clearly detectable due to the missing by the accidental coincidence with relatively wavenumber regions and the low Raman intensities. Thus, the Raman spectrum of compound **8** fits well into the series of the known $[Sn_9]$ in A_4E_9 and $A_{12}E_{17}$ phase as well as the same organic ligands sequestered species $Rb[Rb([2.2.2]crypt)]_3[Sn_9]$, exhibiting extremely strong

breathing mode at 153 cm^{-1} (n_2, A_1) for the symmetric intracluster vibrations. The other broad bands at 101 and 105 cm^{-1} are not single fundamentals. Further studies of $[E_9]^{n-}$ spectra is still undergoing.

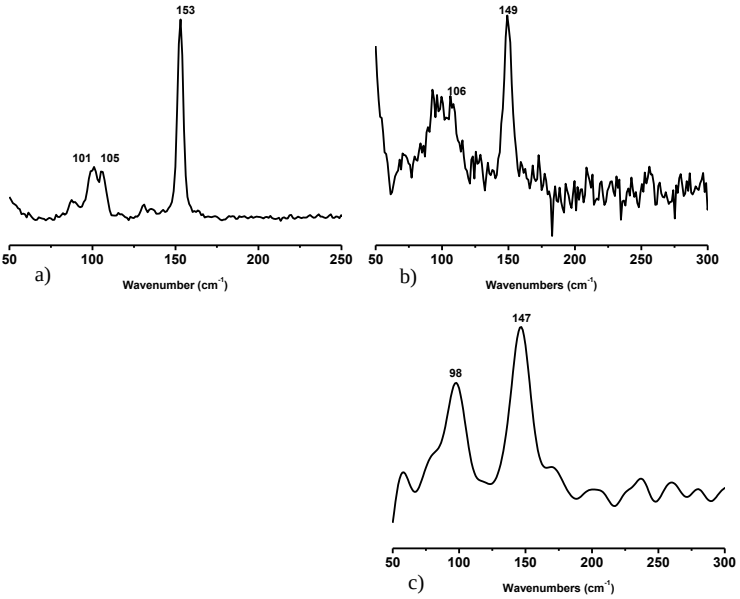

Figure 3.24 Raman spectra of cluster $[E_9]^{2-}$ (E = Sb/Sn) in crystal samples of (a) compound **8** and $[Sn_9]^{4-}$ clusters in solid crystal samples of (b) $Rb[Rb([2.2.2]crypt)]_3[Sn_9]$ and (c) Rb_4Sn_9. In the spectra, wavenumbers (cm^{-1}) are plotted vs. arbitrary Raman intensities.

3.4.4 Mass Spectra of Compound 8

The ESI mass spectrum (negative ion mode) of dissolving the crystals of compound **8** in ethylenediamine shows distinctive mass envelopes associated with the combination of $[Sn_7Sb_2]^{1-}$, $[Sn_6Sb_3]^{1-}$ and $[Sn_5Sb_4]^{1-}$ ions (Figure 3.25) It is common to observe the oxidized parent ion to Zintl ions. Due to the small mass differences, it is difficult to distinguish the distributions. However, it is still obvious that $[Sn_7Sb_2]^{1-}$ match the shifts better.

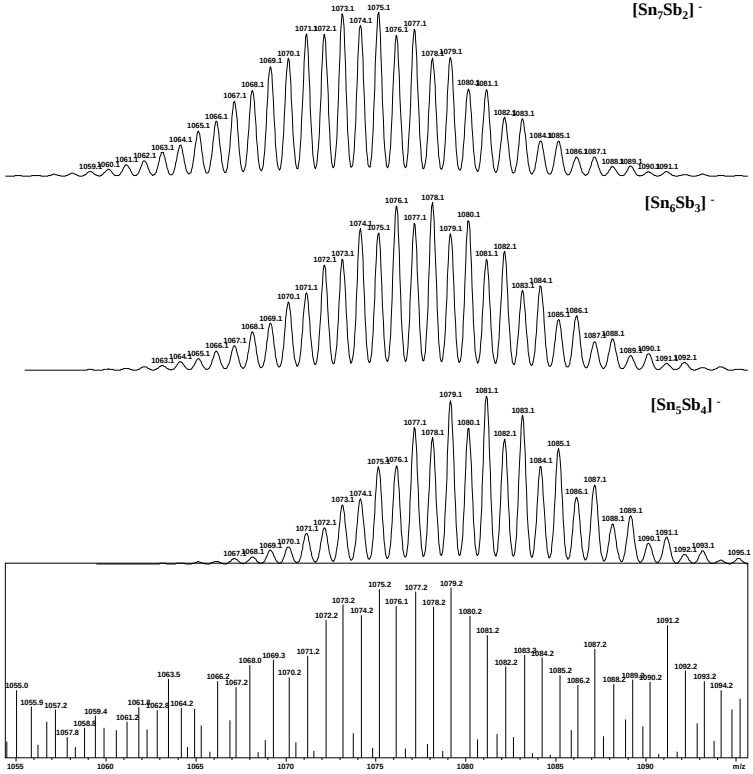

Figure 3.25 Negative ion mode ESI mass spectrum of $[Rb([2.2.2]crypt)]_2[Sb_xSn_{9-x}]\cdot 3tol\cdot 2en$ ($x\approx 2$) crystals dissolving in en. The upper three show the simulated patterns $[Sn_7Sb_2]^{1-}$, $[Sn_6Sb_3]^{1-}$ and $[Sn_6Sb_3]^{1-}$ ions, the below one with lines mode show the combination pattern of oxidized ions above.

3.5 Tetrel-atomic Polyanions and Organometallic Compounds

3.5.1 $[K(18\text{-crown-6})en_2][K(18\text{-crown-6})]_3[Ge_9(CH{=}CH_2)]_2{\cdot}2en$ (9)

As known, $[K(18\text{-crown-6})]_2[Ge_9(CH{=}CH_2)_2]{\cdot}en$ can be harvested by K_4Ge_9 and BTMSA in ethylenediamine and toluene. Recently, the reaction of $[H_2C{=}HC\text{-}Ge_9\text{-}CH{=}CH_2]^{2-}$ shows the capability to be reduced to $[Ge_9]^{4-}$ in liquid ammonia with the presence of the element K. This finding indicates the cleavage of the Ge-C bonding and a probable intermediate $[Ge_9\text{-}CH{=}CH_2]^{3-}$ or radical $[{\cdot}Ge_9\text{-}CH{=}CH_2]^{2-}$. The intermediate radical $[{\cdot}Ge_9\text{-}CH{=}CH_2]^{2-}$ exhibits two possible routes to form the final product: i) further reduced to the $[Ge_9]^{4-}$ clusters; ii) conjunct with another intermediate radical to form a dimer cage $[H_2C{=}HC\text{-}Ge_9\text{-}Ge_9\text{-}CH{=}CH_2]^{4-}$. Thus, speculated as the similar function as element K, a series of experiments applying K_4Ge_9, K_4Sn_9, K_4Pb_9, and $K_{4.79}Co_{0.79}Sn_9$ as reducers were explored to $[K(18\text{-crown-6})]_2[Ge_9(CH{=}CH_2)_2]{\cdot}en$, respectively. However, all these attempts were unsuccessful except for $K_{4.79}Co_{0.79}Sn_9$.

Synthesis and Characterization

Compound **9** has been obtained from an orange-brown solution of the Zintl phase $K_{4.79}Co_{0.79}Sn_9$ and pure bright orange crystals $[K(18\text{-crown-6})]_2[Ge_9(CH{=}CH_2)_2]{\cdot}en$ in ethylenediamine, shown in Figure 3.26. The toluene solution and overdosed 18-crown-6 were layered on the filtrate after sonication. Thin deep brown brick-like crystals formed among solid residue, with a composition of $[K(18\text{-crown-6})en_2][K(18\text{-crown-6})]_3[Ge_9(CH{=}CH_2)]_2{\cdot}2en$ (**9**) determined by single crystal X-ray diffraction (synthesis procedure see ***chapter 5.3.4***, page 96). There is no direct evidence to prove the exact function of intermetallic compound $K_{4.79}Co_{0.79}Sn_9$ in this reaction. The formation of the vinylated Ge_9 dimer obtained under special reaction conditions, and the reasons remains unknown.[129]

The structure of compound **9** was solved and refined in the triclinic space group $P\overline{1}$ by direct methods. All non H atoms are refined anisotropically. The positions of the hydrogen atoms of vinyl groups, crown ether and ethylenediamine molecules were geometrically calculated and refined isotropically with a riding model. Data and structure refinement parameters of compound **9** are listed in Table of ***chapter 6.2.9***, page 108. The EDX analysis shows only K and Ge, but no Co and Sn as heavier elements.

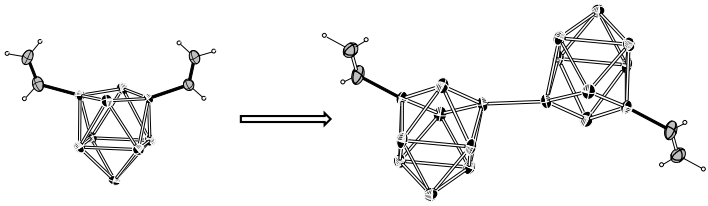

Figure 3.26 The synthesis process of compound **9**.

Crystal Structure Description

Compound **9** obtained from ethylenediamine crystallize in the triclinic space group $P\overline{1}$. The asymmetric unit of **9** contains one divinylated dimer of [Ge_9] cages, two K atoms (K1, K2) sequestered by 18-crown-6 which are bridged by two ethylenediamine molecules, and another [K(18-crown-6)] unit (K3) coordinated with another two ethylenediamine molecules. Atoms K2 and K3 are situated on special crystallographic positions and thus two of the crown ether molecules contain crystallographic inversion symmetry. The same is valid for the $[Ge_9(CH{=}CH_2)]_2$ dimer occupying the corners of the unit cell.

The intracluster Ge-Ge bond length of **9a** lie in a range of 2.500(1)-2.932(1) Å (Figure 3.27), with an average distance 2.643 Å, which are in accordance with those investigated in other Ge_9 clusters with 20-22 skeletal electrons.[24] The details of Ge-Ge bond lengths are shown in Table 3.13.

The mono-capped square antiprism Ge_9 unit of **9a** displays a distorted *nido* Ge_9-Wade polyhedron in which the distortion can be described by the ratio between the two diagonal lengths in the basal plane, which is d_2/d_1=1.27 [d_2(Ge2-Ge4)=3.991(1) Å and d_1(Ge1-Ge3) = 3.159(1) Å]. The dihedral angles (Ge1-Ge2-Ge3-Ge4 in **9a**) of the

open rectangular faces of 4 °show an obvious deviation from 180 °of an ideal model. Three different elongated heights [h_1(Ge5-Ge8)=2.694(1) Å, h_2(Ge6-Ge7)=2.731(1) Å, h_3(Ge1-Ge3)=3.159(1) Å] point to a C_s symmetrical polyhedron between *nido* and *closo*-type, although C_{2v} symmetry is commonly investigated for Ge_9 clusters, shown in Figure 3.28 and Table 3.14.

Table 3.13 Selected bonds length (Å) in cluster **9a**. (Symmetric code: (i) -x, -y, -z)

Ge1-C1 1.956(7)	Ge2-Ge7 2.658(1)	Ge4-Ge5 2.657(1)	Ge6-Ge7 2.731(1)
Ge1-Ge4 2.499(1)	Ge2-Ge6 2.678(1)	Ge4-Ge5 2.657(1)	Ge7-Ge9 2.576(1)
Ge1-Ge2 2.529 (1)	Ge3-Ge4 2.557(1)	Ge5-Ge9 2.588(1)	Ge7-Ge8 2.863 (1)
Ge1-Ge6 2.593(1)	Ge3-Ge8 2.631(1)	Ge5-Ge8 2.694(1)	Ge8-Ge9 2.605(1)
Ge1-Ge5 2.596 (1)	Ge3-Ge7 2.648(1)	Ge5-Ge6 2.932(1)	Ge3-Ge3^{i} 2.507(2)
Ge2-Ge3 2.596(1)	Ge4-Ge8 2.645(1)	Ge6-Ge9 2.571(1)	

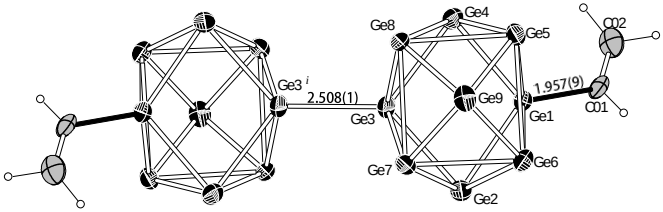

Figure 3.27 Dimeric anions **9a** with selected bond lengths. Heavy atoms are shown with 50% occupation probability. Carbon atoms are shown in grey, Ge atoms in black. Hydrogen atoms are omitted for clarity. (i) -x, -y, -z.

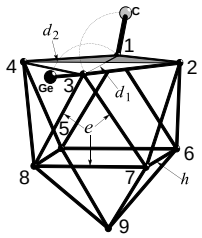

Figure 3.28 Schematic cluster of the structural parameters for the description of the cluster symmetry. Details are shown in Table 3.14.

Table 3.14 Selected structural parameters for the cluster in **9a**.

	h_2 [Å]	h_1/ h_2	h_3/ h_2	d_2/ d_1[a]	α[b][°]	ω_1, [c][°]	ω_2	$d_{Ge\text{-}C}$[Å]	$d_{C=C}$[Å]
9a	2.694(1)	1.01	1.17	1.26	4	156,173		1.957(9)	1.296(12)

[a] h_1, $h2$ and h_3 stand for the distances of Ge5-Ge8, Ge6-Ge7 and Ge1-Ge3. d_1 and d_2 identify Ge_1-Ge_3 and Ge2-Ge4, respectively. [b] Dihedral angle at the open basal plane: angle between the triangular faces Ge1-Ge3-Ge4 and Ge1-Ge3-Ge2. [c] Out-of plane angle: ω_1 represents angle C_{vinyl}-Ge1-Ge3, ω_2 represents angle Ge1-Ge3-$Ge3^{i}_{cluster\ B}$. (Symmetric code: (i) -x, -y, -z.)

The distance between Ge atoms of the Ge_9 cluster and the C-atoms of the vinyl group is 1.957(9) Å. It is very typical for the Ge-C(sp^2) bond length in these species of clusters (1.954-1.992 Å in $[Ge_9(CHCH_2)_2]^{2-}$, 2.05 Å in $[Ge_9(CHCH_2)]^{3-}$, 1.929 Å in $[Ge_9(CHCH\text{-}Fc)_2]^{2-}$),[97,100,103] which agrees with the range of 1.91-2.04 Å of other distances between Ge and sp^2-hybridized carbon atoms based on entries of the Cambridge Structural Database.[204] The length of the double bond C01-C02 (1.295(9) Å) is close to such bonds between sp^2-hybridized carbon atoms (mean distance of 1.33 Å). The dihedral angle between the vinyl group and the square phase of Ge_9 shows 58 ° and the torsion angle of C02-C01-Ge1-Ge3 is 44 ° in **9a**, which are significantly different from the corresponding angles 77 ° and 86 ° for the analogue $[H_2C{=}HC\text{-}Ge_9\text{-}Ge_9\text{-}CH{=}CH_2]^{4-}$ cluster in the crystal form of $[K([2.2.2]crypt)]_4[Ge_9(CH{=}CH_2)]_2{\cdot}en$.[129]

Similar as $[Ge_9\text{-}Ge_9]^{6-}$ anions, two vinyl group connect to the two open rectangular face of Ge_9 polyhedron through addition reaction, which occurs to reduce the charge to -4. The Ge_9 cages of the anions $[H_2C{=}HC\text{-}Ge_9\text{-}Ge_9\text{-}CH{=}CH_2]^{4-}$ (**9a**, Figure 3.27) form distorted *nido*-polyhedra in accordance with Wade rules. The functionalized dimer **9a** is interconnected by means of a single covalent bond with 2.508(1) Å bond length, and matches well with other Ge-Ge inter-cluster bonds in the known dimers $[Ge_9\text{-}Ge_9]^{6-}$ (2.488(2) Å),[80,205] $[SbGe_8\text{-}Ge_8Sb]^{4-}$ (2.487(2) Å),[156] $[BiGe_8\text{-}Ge_8Bi]^{4-}$ (2.569(3) Å),[156] $[BiSn_6Ge_2\text{-}Ge_2Sn_6Bi]^{4-}$ (2.494(2) Å),[158] $[Ph_2Sb\text{-}Ge_9\text{-}Ge_9\text{-}SbPh_2]^{4-}$ (2.482(2) Å),[89] $[^tBu\text{-}Ge_9\text{-}Ge_9\text{-}^tBu]^{4-}$ (2.528(1) Å)[96]. More comparisons about other Ge-Ge distances can be found in Table 3.15.

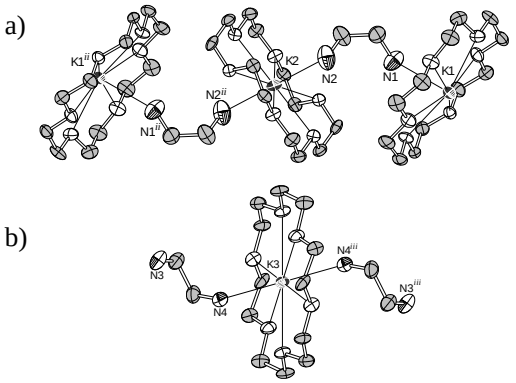

Figure 3.29 The chains of $\{[K(18\text{-crown-}6)]_3 \bullet 2en\}^{3+}$ cation and complex $[K(18\text{-crown-}6)en_2]^+$. Carbon atoms are shown in grey, and oxygen atoms in white. Hydrogen atoms are omitted for clarity. (Symmetric codes: (ii) 1-x, 1-y, -z; (iii) 1-x, 1-y, 1-z.)

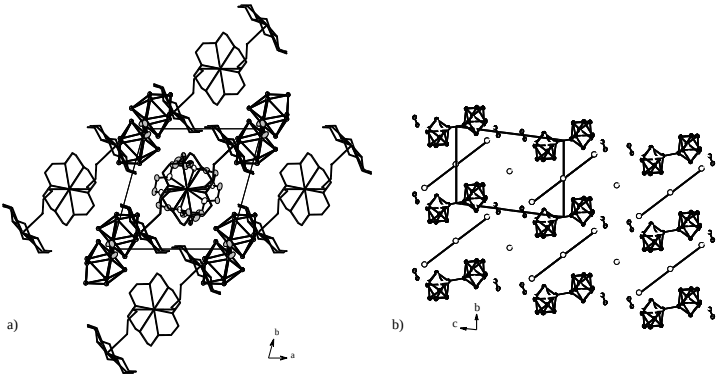

Figure 3.30 Crystal packing and low-dimensional arrangements of compound **9** (a) along *c* axis:$[K(18\text{-crown-}6)en_2]^+$ cation is located in the center of the unit cell. $\{[K(18\text{-crown-}6)]_3 \bullet 2en\}^{3+}$ cations are shown in wires/sticks model for differentiation. (b) along *a* axis: all the organic ligands coordinating with potassium atoms are omited for clarity. $\{[K(18\text{-crown-}6)]_3 \bullet 2en\}^{3+}$ cation show as three potassium atoms (white dots) bonding.

It is worth noting that the short chain I of $\{[K(18\text{-crown-6})]_3 \bullet 2en\}^{3+}$ cation (K1, K2) are composed by the coordination capablity of potassium with N-donor (enthylenediamine) and O-donor (crown ether) ligands shown in Figure 3.29. K3 atom locates exactly the center of the unit cell, coordinating with one crown ether and two ethylenediamine (shorten as en) molecules to build another shorter chain II. In both chains, en molecules adopt "*cis*" conformations due to the possiblitity to coordinate two potassium atoms. The distance of K1 and Ge1 shows the shortest contact between K and cluster of 4.257(2) Å, which is relatively longer than others.[24,55,129]

Along the *c* axis, the dimer clusters locate in a layer and the potassium atoms localize in another layer as shown in Figure 3.30. If considering $\{[Ge_9(CHCH_2)]_2\}^{4-}$ anions as a node and the anions occupying the corners of the unit cell, the whole three dimension arrangement of $\{[Ge_9(CHCH_2)]_2\}^{4-}$ clusters possess a standard α-Po topology network.

Table 3.15 Ge-Ge bonds length of some known Ge_9 clusters in selective compounds.

Clusters	Compounds	Intercluster Bond Length (Å)	Intracluster Bond Length (Å)	ref.
Dimer	**9**	2.508	2.499-2.863	
$[R\text{-}Ge_9\text{-}Ge_9\text{-}R]^{4-}$	$[K([2.2.2]crypt)]_4[Ge_9(CHCH_2)]_2\cdot en$	2.504	2.514-2.895	129
	$[K([2.2.2]crypt)]_4[^tBu\text{-}Ge_9\text{-}Ge_9\text{-}^tBu]\cdot 7en$	2.528	2.568-2.904	96
	$[K([2.2.2]crypt)]_4[Ph_2Sb\text{-}Ge_9\text{-}Ge_9\text{-}SbPh_2]\cdot 2.5en$	2.482	2.556-2.815	89
	$[K([2.2.2]crypt)]_4[Ph_3Sn\text{-}Ge_9\text{-}Ge_9\text{-}SnPh_3]\cdot 2en$	2.481	2.540-2.868	206
$[Ge_9\text{-}Ge_9]^{6-}$	$Cs_4[K([2.2.2]crypt)]_2[Ge_9\text{-}Ge_9]\cdot 6en$	2.488	2.525-2.778	80
	$M_6[(Ge_9\text{-}Ge_9)](DMF)_{12}$ (M = K, Rb)	2.420/2.471 (K) 2.464/2.467 (Rb)	2.488-2.887 (K) 2.508-2.885 (Rb)	207
Trimer	$[Rb([2.2.2]crypt)]_6[Ge_9{=}Ge_9{=}Ge_9]\cdot 3en$	2.579-2.601	2.523-3.085	57
$[Ge_9{=}Ge_9{=}Ge_9]^{6-}$	$[K(18\text{-crown-}6)]_6[Ge_9{=}Ge_9{=}Ge_9]\cdot 3en$	2.581-2.640	2.493-3.011	83
Tetramer	$[Rb(18\text{-crown-}6)]_8[Ge_9{=}Ge_9{=}Ge_9{=}Ge_9]\cdot 2en$	2.548-2.673	2.517-2.747	58
$[Ge_9{=}Ge_9{=}Ge_9{=}Ge_9]^{8-}$	$[K(18\text{-crown-}6)]_8[Ge_9{=}Ge_9{=}Ge_9{=}Ge_9]\cdot 8en$	2.554-2.752	2.486-3.025	84
Polymer $_\infty$**$[\text{-}(Ge_9)\text{-}]^{2-}$**	$[K(18\text{-crown-}6)]_2[\text{-}(Ge_9)\text{-}]$	2.486	2.552-2.864	81

3.5.2 Raman Spectrum of Compound 9

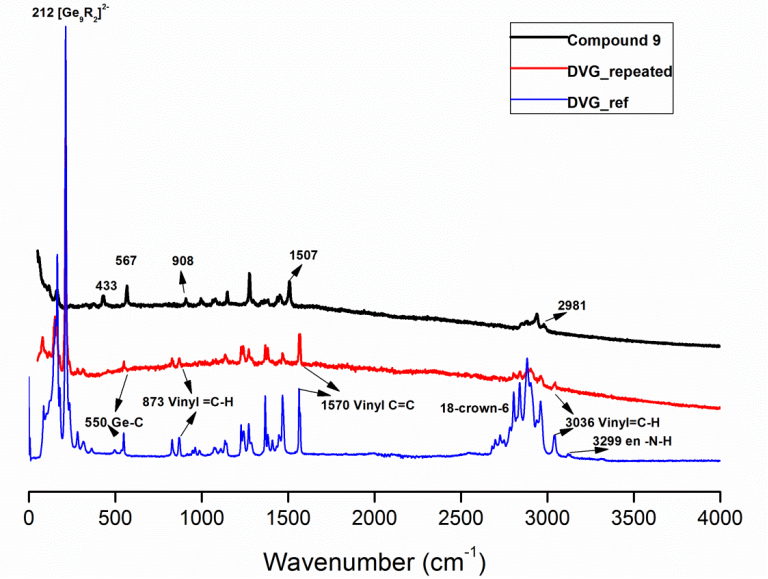

Figure 3.31 Raman spectrum of organic fragments of compound **9** and the starting materials (divinyl-germanium compound $[K(18\text{-crown-6})]_2[Ge_9(CH{=}CH_2)_2]\cdot en$, abbreviated to DVG) in experimental repetition and in literature[129].

Crystals of the compound **9** was characterized by a Raman spectrometer. The vibrational spectra of compound **9** at room temperatue are shown in Figure 3.31 and Figure 3.32 In Table 3.16, the main vibration frequencies are summarized. In the 2800-3000 cm^{-1} region, the fluctruate band corresponds to (-C-H) stretching mode of 18-crown-6 coordinating with K ions.[208-210] The low frequency 433 cm^{-1} can be recognized as the (C=C) vinyl-bending mode, and vibrational band at 908 cm^{-1} can be assighed to ($=CH_2$) wag, though the other identifatcation bands for vinyl group at around 1600 cm^{-1} despear due to the intensity. The intensity of band at 567 cm^{-1} belongs to υ(Ge-C)

modes in cluser **9a**. The assignments of the characteristic vibrations of the bound to a Ge atom vinyl group almost conform the Ge-C vibration of vibrational frequencies in alkyl germanides.[129,211-213] The weak peaks of ethylenediamin dispear because of the relatively low intensity. The shife of vibration pattern in organic fragement between the divinylated mono-[Ge_9] cluster compound [K(18-crown-6)]$_2$[Ge_9($CH=CH_2$)$_2$]·en and compound **9** [K(18-crown-6)en$_2$][K(18-crown-6)]$_3$[(CH_2=CH)$_2$$Ge_9$-$Ge_9$($CH=CH_2$)]· 2en, indicates the changes of bonds length and different coordination environments of potassium. [129]

Table 3.16 Observed Raman wavenumbers and vibrational assignments of compound **9**.

Raman wavenumbers (cm^{-1})	Assignment	Vibration type
164	Ge_9-Cluster	
216	dimer Cluster	
291	dimer Cluster	
433	Vinyl group	C=C
567	Ge-C bind	
908	Vinyl group	=C-H Deformation
995	18-crown-6	-C-O Valence
1073	18-crown-6	
1147	18-crown-6	-C-O-C Valence
1277	18-crown-6	
1372	18-crown-6	
1454	18-crown-6	
1507	18-crown-6	
2853	18-crown-6	-C-H Valence
2884	18-crown-6	-CH_2 Valence
2938	18-crown-6	-C-H Valence
2981	18-crown-6	-CH_2 Valence

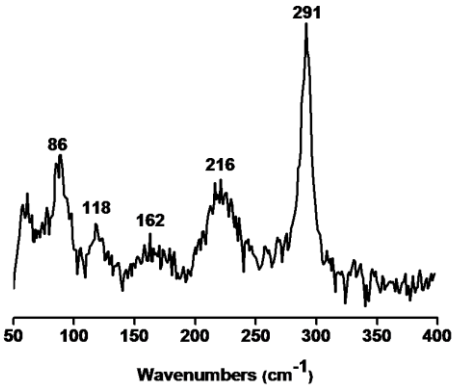

Figure 3.32 Raman spectrum in the range of the Ge_9 cluster modes of compound **9**.

In Raman spectrum, the vibration bands of germanium phases or materials are commonly observed at the region of 200-300 cm^{-1}, such as 275 cm^{-1} for α-Ge,[214] 225, 265, 280 cm^{-1} for allo-Ge,[215] 290 cm^{-1} for hexagonal germanium (germanene),[216,217] The distinction in vibrational spectroscopy between monomer and oligomer [Ge_9] species has been investegated by Somer *et al*.[218,219] The breathing mode at *ca.* 220 cm^{-1} can be recognized as identification sonde of $[Ge_9]^{4-}$ anions.[47] In compound **9**, the spectra reveal in wave regions relevant for inter- and intra- cluster "breathing vibration" with two separate frequency groups, at 291 cm^{-1} (inter)/216 cm^{-1} (intra). Comparing to cmopounds $K_6[Ge_9\text{-}Ge_9]\cdot 12dmf$ and $[K(18\text{-crown-}6)]_2[\text{-}(Ge_9)\text{-}]$, the identifications of these two vibrations (200-300 cm^{-1}) occur in the regions at 270 cm^{-1}(inter)/220 cm^{-1} (intra) and 269 cm^{-1}(inter)/200 cm^{-1} (intra), respectively.[220] The vibration of functional dimer [R-Ge_9-Ge_9-R] with a shift of 20 cm^{-1} can be speculated due to the differences of Ge-Ge *exo*-bond length and effect of organic groups and cluster geometry. It should be noted that the bands of cluster and organic groups can be detected separately with relatively high intensity. After 104 trials, it remained unsuccessful to observe both parts at the same experiment with unclear reason. Further work is planned, but not within the scope of this study.

3.5.3 $[K(18\text{-crown-}6)]_2[K([2.2.2]crypt)][KSn_9]\cdot 1.5en$ (10)

To attempt to produce the endohedral cluster through the classic solution route, the mixtures of the intermetallic phase K_4Sn_9 and the organometallic compound $[Co(anthracene)_2][K(18\text{-crown-}6)(THF)_2]\cdot THF$ were dissolved in ethylenediamine with the presence of cryptand. The reaction products show no existence of metal-filled endohedral clusters, nevertheless, another two kinds of crystals have been obtained.

Synthesis and Characterization

The crystals of $[K(18\text{-crown-}6)]_2[K([2.2.2]crypt)][KSn_9]\cdot 1.5en$ (**10**) were isolated from a solution of K_4Sn_9 with $[Co(anthracene)_2][K(18\text{-crown-}6)(THF)_2]\cdot THF$ (**11**) as well as cryptand in ethylenediamine and characterized by single crystal X-ray diffraction (synthesis procedure see ***chapter 5.3.4***, page 96). Single-crystal X-ray structure determinations confirm that two types of crystals coexist in this reaction and both types contain four potassium ions per each Sn_9 polyanion with different sequestering reagents: the known compound $[K([2.2.2]crypt)]_3[KSn_9]$ [181] and additionally $[K(18\text{-crown-}6)]_2[K([2.2.2]crypt)][KSn_9]\cdot 1.5en$ (**10**). The structure of compound **10** was solved and refined in the triclinic space group $P\bar{1}$ by direct methods. All non H atoms are refined anisotropically. The positions of the hydrogen atoms of cryptand, crown ether and ethylenediamine molecules were geometrically calculated and refined isotropically with a riding model. Data and structure refinement parameters of compound **10** are listed in the table of ***chapter 6.2.10***, page 109.

Crystal Structure Description

Applying the experimental procedure introduced, the reaction of K_4Sn_9 and compound $[K(18\text{-crown-}6)(THF)_2][Co(anthracene)_2]\cdot(THF)$ with [2.2.2]crypt formed two types of crystals: $[K([2.2.2]crypt)]_3[KSn_9]$ [181] and compound **10** $[K(18\text{-crown-}6)]_2[K([2.2.2]crypt)][KSn_9]\cdot 1.5en$.

The composition of four K atoms per polyanion indicates each Sn_9 cluster with a fourfold negative charge. Similar to the known structure of $[K([2.2.2]crypt)]_3[KSn_9]$, compound **10** possesses an infinite chain composed by Sn_9 and bridging naked K atoms. In compound **10**, the potassium atoms show three types of coordination environment, shown in Figure 3.33 and Figure 3.34b: i) K atoms (K1) as linker between Sn_9 clusters, that are not further coordinated to other molecules; ii) K atoms (K2) sequestered by [2.2.2]crypt; and iii) K atoms (K3 and K4) coordinating with 18-crown-6 and in contact with the cluster. Due to distinct function of sequestering reagents, K atoms together with the linked clusters are separated by organic molecules to form linear chains that partly have contacts with further K atoms. Compound **10** displays a unique one-dimensional substructure $^1_\infty[(K_3Sn_9)^{1-}]$, which is different from the non-charged chain $^1_\infty[(K_4Sn_9)^0]$ in $[K([18]crown\text{-}6)]_3[KSn_9]\cdot en$ [221] and from $^1_\infty[(KSn_9)^{3-}]$ in $[K([2.2.2]crypt)]_3[KSn_9]$ containing three K atoms without any direct contact with anions.

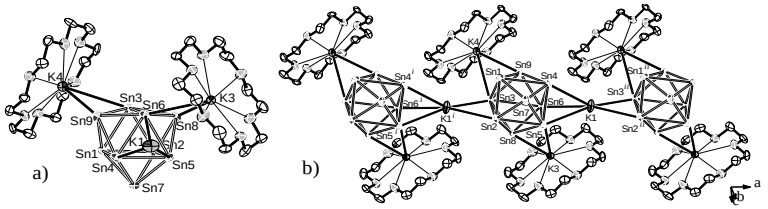

Figure 3.33 Details of the crystal structure and the coordination environment of K1, K3, K4 in compound **10**. The displacement parameters of all the atoms are shown with 50% probability ellipsoids. H atoms were omitted for clarity. (Symmetric codes: (i) -1+x, y, z; (ii) 1+x, y, z.)

In **10**, two K atoms (K3, K4) of [K(18-crown-6)] units are directly bound to the Sn_9 polyhedra with K-Sn distances in the range of 3.561 to 3.891 Å, shown Figure X. If considering the two slightly longer contacts in **10** (K4-Sn1 4.385(1) and K3-Sn5 4.276(1) Å) as interactions, the K atoms coordinate to polyanions with η^3-form. Comparing to the bridging K1 atoms, the K1-Sn distances are slightly longer in the range of 3.584 to 3.992 Å with η^2- and η^3-form (excluding the elongation bond K1-Sn1 4.305 Å), which are all in accordance with the values observed in the Zintl phase KSn. The K2 atoms of

[K([2.2.2]crypt)] units possess obviously larger distances to the nearest tin atoms of the polyanions (>7.67 Å). The weak intermolecular interactions between the H atoms of the crown ether and atoms Sn1, Sn3, Sn9 with the Sn-H distance range of 3.12-3.20 Å, support the final supramolecular structure assembly.

The polyhedron of the anion **10a** displays a distinct symmetry from normal known Sn_9^{4-} anions (Table 3.14). According to the classification of the structures of E_9 polyhedra, type A and B can be divided by the following criteria in Figure 1.1 in ***chapter 1.2.2***, page 4: An ideal tricapped trigonal prism A (*closo*-type) with equal prism heights *h* and edge lengths *e* possesses an *h*/*e* ratio of 1.0 and also three equal dihedral angles α, and the dihedral angle γ between two basal faces of prism equals zero. The monocapped square antiprism B (*nido*-type) possesses a noncapped face with two diagonals of equal length *d*. Based on Wade-Mingos' electron counting rules for bonding, $[Sn_9]^{4-}$ anions can be predicted to exhibit the *nido*-type as the anions in compounds $[K([2.2.2]crypt)]_3[KSn_9]$ [181] and $[Na([2.2.2]crypt)]_4[Sn_9]$ [41] with C_{4v} symmetry. Due to one electron deficient, $[Sn_9]^{3-}$ ions possess structures between the two types A and B. The hypothetical $[Sn_9]^{2-}$ cluster is expected to form a *closo* polyhedron. The distortions derived from type A correspond to an elongated trigonal prism with increased *h*/*e* ratios, as shown in Table 3.14. $[Sn_9]^{4-}$ anions in **10** do not show C_{4v} symmetry but distorted variants deduced from type A, affect with two more electrons on the orbital occupation. The anions can be described approximately with D_{3h} symmetry and tricapped trigonal prisms with one prism height about 10% elongation than others, which is similar to the structure of $[K(18\text{-crown-}6)]_3[KSn_9]$ and different from that of $[K([2.2.2]crypt)]_3[KSn_9]$ (Table 3.17). All heights of the prism are elongated which reflects the fact that the LUMO of a hypothetical $[Sn_9]^{2-}$ is anti-bonding along the prism height. The structure assembly of compound **10** indicates the possibility of different effects of polyethyleneoxides and cyclic crown ethers to the structures of polyanions.

Table 3.17 Geometric Parameters of $[Sn_9]^{4-}$ Cluster in related compounds.

Compound [a]	h_1, h_2, h_3 [b]	h/e [c]	γ[°] [d]	α[°] [e]	d_1/d_2 [f]	
[K([2.2.2]crypt)][K(18-crown-6)]$_2$[KSn_9] **10**	1.08, 1.05, 1.14	1.15	6	14, 20, 22	1.25	~ D_{3h}
[K([2.2.2]crypt)]$_6$[Sn_9·Sn_9] [74]	1.10, 1.02, 1.00	1.08	6	13, 19, 23	1.45	~ D_{3h}
[K([2.2.2]crypt)]$_3$[Sn_9] [222]	1.01, 1.02, 1.05	1.07	3	15, 18, 19	1.43	~ D_{3h}
[K([2.2.2]crypt)] $_3$[KSn_9] [181]	1.29, 1.03, 1.00	1.19	20	2, 28, 29	1.02	~C_{4v}
[Na([2.2.2]crypt)]$_4$[Sn_9] [41]	1.32, 1.04, 1.01	1.19	22	3,29, 30	1.02	~C_{4v}
[K(18-crown-6)]$_3$[KSn_9] [221]	1.17, 1.06, 1.05	1.15	8	13, 22, 24	1.21	~ D_{3h}
[K(18-crown-6)]$_4$[Sn_9] [221]	1.11, 1.08, 1.04	1.14	4	15, 17, 22	1.32	~ D_{3h}

[a] Formulae without solvent molecules. [b] Relative prism heights, scaled to the value 3.194 Å, the shortest height in [K([2.2.2]crypt)]$_6$([Sn_9][Sn_9])·1.5en·0.5tol.[74] Heights h_1-h_3 correspond to the distances Sn1-Sn4, Sn2-Sn5, and Sn3-Sn6, respectively. [c] h and e are the mean values of the prism heights and the triangular edges, respectively. [d] the dihedral angle between the triangular bases (triangles Sn1-Sn2-Sn3 and Sn4-Sn5-Sn6).[e] Dihedral angles Sn3-Sn6-Sn8-Sn9, Sn1-Sn4-Sn7-Sn9, Sn2-Sn5-Sn7-Sn8. [f] The best monocapped square antiprism is chosen. If the structure is close to D_{3h} symmetry the longest height is considered as a diagonal in the C_{4v} symmetric cluster. d_1 and d_2 refer to distances Sn8-Sn9 and Sn3-Sn6.

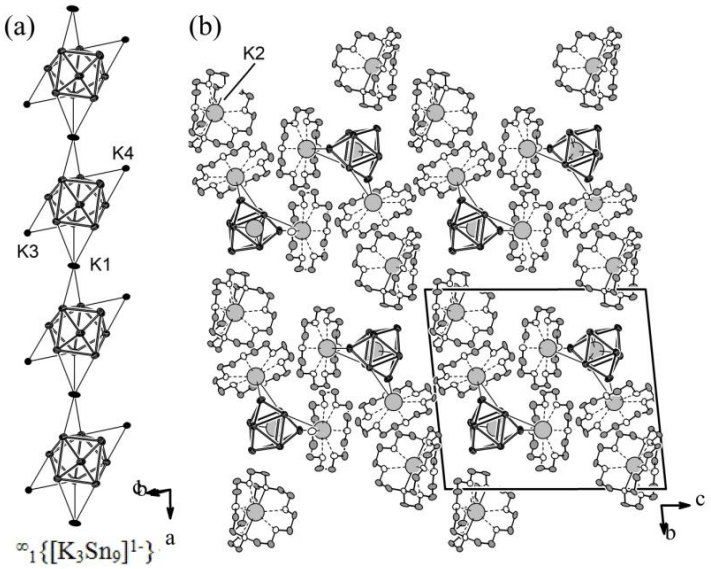

Figure 3.34 (a) A one-dimensional $^{1}_{\infty}[(K_3Sn_9)^{1-}]$ chain parallel to the *a* axis. (b) Relative arrangement of ions and molecules as viewed along the *a* axis. Atom symbols: K, large and grey circles; Sn, black circles; C and N/O, small white and grey circles. The H atoms and solvent molecules were omitted for clarity.

3.5.4 [K(18-crown-6)(THF)$_2$][Co(anthracene)$_2$]·THF (11)

Organometallic compounds with transition metals in a low oxidation state are important precursors for the formation of intermetalloid clusters from Zintl anions.[56] Transition metal complexes with polycyclic aromatic hydrocarbons as ligands can serve as storable, but reactive sources of low-valent metal atoms or even anions.[223] Within this group of compounds, anthracene has been found as a prominent, sometimes favoured ligand,[224,225] which can act as a η^2,[226] η^4, and η^6,[224,227] in its monohydrogenated form even as a η^5 [228] ligand. Regarding the entries of the Cambridge Structural

Database,[229] it is interesting that homoleptic anthracene complexes have been obtained exclusively with η^4 coordination of the transition metals Ti, Zr, Hf,[230] Nb,[231] Ta,[232] Fe,[233] and Co.[234]

As aforementioned, the organometallic compounds are commonly used to react with unfilled Zintl clusters in the synthesis route for achieving the novel endohedral clusters. Thus, this compound was synthesized in order to obtain some Co-filled Zintl anions by this classic method, unfortunately which was not successful yet.

Synthesis and Characterization

The compound **11** was obtained via reduction of $CoBr_2$ by potassium anthracene in THF. Although the reaction conditions were very similar to those described by Brennessel, Young & Ellis[234] (synthesis details see ***chapter 5.3.5***, page 97), the compound was found to crystallize including an additional solvent molecule (Figure 3.34), and thus forms a new crystal structure. The structure of compound **11** was solved and refined by direct methods. All non H atoms are refined anisotropically. The positions of the hydrogen atoms of anthracene, the crown ether and THF molecules were geometrically calculated and refined isotropically with a riding model. Data and structure refinement parameters of Compound **11** are listed in ***chapter 6.2.11***, page 110.

Crystal Structure Description

Different from the literature, the crystals are indexed with the orthorhombic space group $P2_12_12_1$ instead of $P1$ as published before.[234] Besides these differences, the structural entities, which are present in both compounds, show almost the same shape (Figure 3. 35 and Figure 3.36).

The Co atom is sandwiched by two anthracene molecules in 1,2,3,4-η coordination, respectively, with a slight tilt of 10.2% for the two planes formed by the respective coordinating atoms C1-C4. The $[C_6]$ rings, which are directly bond to the Co atom, are in eclipsed position, but the main molecule axes form an angle of about 65%. The anthracene molecules are folded at an axis running through the C1 and C4 atoms, the angles between the planes formed by C1, C2, C3, and

C4 and by C1, and C4-C14 are almost identical (29.18% and 28.99% for both molecules).

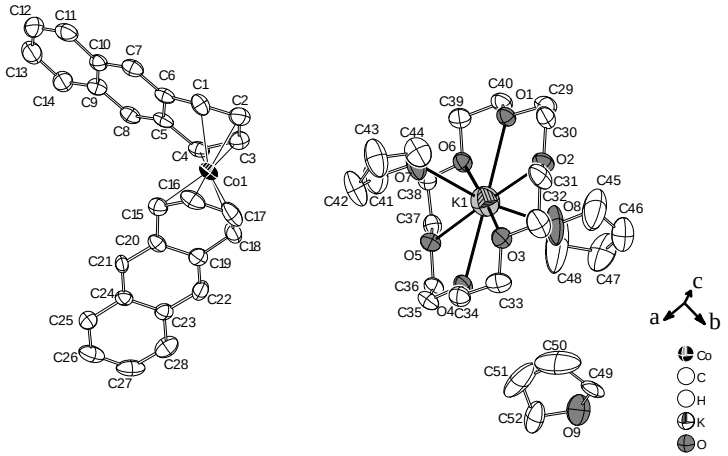

Figure 3.35 Asymmetric unit of compound **11**. Displacement ellipsoids are drawn at the 50% probability level, H atoms and atoms of the disordered atoms of the free THF molecule are omitted for clarity.

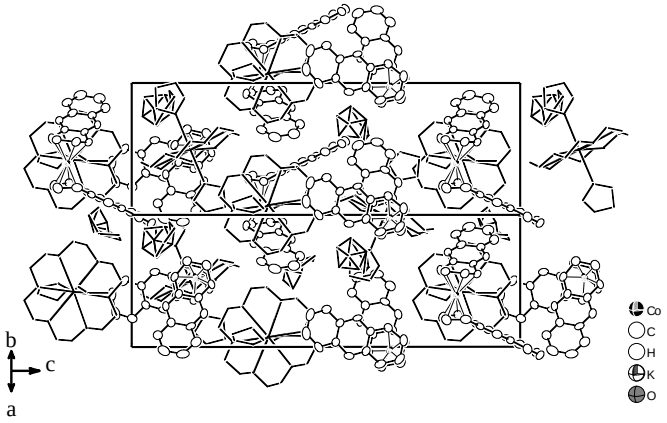

Figure 3.36 Unit cell of compound **11**, view along [$\bar{1}$ $\bar{1}$ 0].

4 Summary and Outlook

The reactions described in **chapter 3.1** between $K_{4.79}Co_{0.79}Sn_9$ and [2.2.2]crypt produce four different compounds as the effects of time, temperature or other reaction conditions.[140,141] Four types of novel Zintl clusters $[Co@Sn_9]^{4-}$, $[Co@Sn_9]^{3-}$, $[Co@Sn_{10}]^{3-}$, and $[Co_2@Sn_{17}]^{5-}$ isomers were isolated from four reactions aforementioned, which adopt different structures in four distinct compounds $K[K([2.2.2]crypt)]_3[Co_{0.68}@Sn_9]$ (**1**), $[K([2.2.2]crypt)]_6[Sn_9]_{1.21}[Co@Sn_9]_{0.17}[Co@Sn_{10}]_{0.62}\cdot 3en\cdot tol$ (**2**), $[K([2.2.2]crypt)]_5[Co_2@Sn_{17}]$ (**3**) and $[K([2.2.2]crypt)]_5[Co_2@Sn_{17}]\cdot en\cdot tol$ (**4**), respectively. All the final products of cobalt-filled clusters display oxidative somehow, either the clusters coupling or variety of oxidation state, which result in the variations of magnetism in products. To contrast to the diamagnetic precursor $K_{4.79}Co_{0.79}Sn_9$, the paramagnetic properties of compound **3** and **4** have been investigated by electron paramagnetic resonance analysis (EPR).

The Rh-centered cluster $[Rh@Sn_{10}]^{3-}$ was isolated from $[K([2.2.2]crypt)]_6[Sn_9]_{1.52}[Rh@Sn_{10}]_{0.48}\cdot 3en\cdot tol$ (**5**), which presented in **chapter 3.2**. This compound was synthesized from another intermetallic compound with a nominal composition of "K_3RhSn_6". According to electron paramagnetic resonance spectrum, although $[Sn_9]^{3-}$ clusters as the main splitting part of clusters in compound **5**, the paramagnetic property of compound **5** is significantly different from the metal-unfilled compound $[K([2.2.2]crypt)]_3[Sn_9]$, which indicates that the novel clusters with metal insertion were formed in this compound.

The extraction of the ternary phase with a nominal composition of "Rb_3IrSn_{12}" in ethylenediamine directly lead to an Ir-capsuled cluster in **$[Rb([2.2.2]crypt)]_3[Ir@Sn_{12}]\cdot en\cdot 2tol$** (**6**). Its analogue $[Ir@Sn_{12}]^{3-}$ cluster in $[K([2.2.2]crypt)]_3[Ir@Sn_{12}]\cdot en\cdot tol$ was achieved before by a two-step synthesis in solution from Sn_9^{4-} ions, which is discussed in

chapter 3.3.

Based on systematically studies about the formation of above anions, it is worthy to be noticed that the size of interstitial metal atoms has a notable impact on the polyhedral shape of the clusters. Due to the small size of cobalt atom, the insertion can occur to varieties of 9- or 10-membered clusters with fully or partly occupation. Whereas rhodium atom goes into the similar shape of 10-membered clusters as cobalt species, the proportion of centered rhodium decreases dramatically. Further, none but 12-membered polyhedra can be achieved till now, which can comprise the large size of iridium atoms.

In **chapter 3.4**, $[K([2.2.2]crypt)]_2[Co_x@Sn_{7-x}Sb_{2+x}]$ ($x\approx0.58$) (**7**) is the first *exo*-substituted endohedral compound obtained directly by the extraction of endohedral filled clusters in the intermetallic compound $K_{4.79}Co_{0.79}Sn_9$ and $SbPh_3$ in ethylenediamine. The products from the reaction of $[Sn_9]^{4-}$ and $SbPh_3$ illustrate the first oxidative case of $[E_9]^{2-}$ cluster (E=Sb/Sn) with atom Sn involved in compound $[Rb([2.2.2]crypt)]_2[Sn_{9-x}Sb_x]\cdot3tol\cdot2en$ ($x\approx2$) (**8**), which have been examined by mass spectrum. The Sb atom *exo*-substituent changes the oxidation state of the isolated clusters but not the skeletal electrons. The investigation of Raman spectrum for $[E_9]^{2-}$ (E = Sn/Sb) clusters shows similar characteristic frequencies at around 153 cm^{-1} as those of $[Sn_9]^{4-}$ clusters in Rb_4Sn_9 and $Rb[Rb([2.2.2]crypt)]_3[Sn_9]$ species, which indicates that $[E_9]^{2-}$ (E = Sn/Sb) clusters is isoelectronic to $[Sn_9]^{4-}$ essentially. Moreover, it provides synthetic information regarding the formation of the novel heteroatomic clusters.**Chapter 3.5** describes a novel bisvinylated dimeric $[Ge_9]$ cluster in the form of crystals of $[K(18\text{-crown-}6)en_2][K(18\text{-crown-}6)]_3[(CH_2CH)Ge_9Ge_9(CHCH_2)]\cdot2en$ (**9**) in terms of Raman spectroscopy, whose breathing vibrations show two separate frequency groups at 291 cm^{-1} $_{(inter\text{-}cluster)}$/216 cm^{-1} $_{(intra\text{-}cluster)}$. An organometallic compound $[K(18\text{-crown-}6)(THF)_2][Co(anthracene)_2](THF)$ (**11**) was synthesized to react with $[Sn_9]^{4-}$ ions to contribute Co-filled clusters with the presence of [2.2.2]crypt though the classic solution synthesis. However, no endohedrally metal-filled clusters but one $[Sn_9]^{4-}$ cluster with mixed sequestering reagents was found in the crystals of $[K(18\text{-crown-}6)]_2[K([2.2.2]crypt)][KSn_9]\cdot1.5en$ (**10**).

The series of novel endohedral polyanions with Group 9 metal-filled have been isolated based on trials under different reaction conditions,

and further characterized and analyzed. Employing the mechanism of chemical conversion synthesis in the reaction of Zintl ions, these clusters were obtained from directly extraction the corresponding solutions of the intermetallic compound precursors with different nominal compositions, which were synthesized by solid state reactions. This synthetic approach can result in diversity of novel cluster structures under the influence of solvent, sequestering agent, reaction temperature *etc*. These products are members of the increasing number of ligand-free and intermetallic group 14 clusters. Their formation and dynamic properties reveal the atomistic processes to build and rebind the structures. Solvothermo technique and normal diffusion applied in the reactions from single source precursors CoSn alloys to form variant CoSn alloys, which present the significant impact of reaction conditions on structures. The alternative changed Co-Sn and Rh-Sn phases provide insight into the potential applications in electronic batteries and catalytic synthesis.

5 Experimental Section

5.1 General Experimental Methods

5.1.1 Inert Gas Technique

All precursors and all products are highly sensitive towards air and moisture. Therefore, all the storage, weight and handling of materials during the reactions were carried out under an argon atmosphere using standard glove box and Schlenk techniques. The glove boxes (Labmaster MB 200B, Company *MBraun*, H_2O < 0.1 ppm; O_2 < 0.1 ppm) were operated with argon 4.8 (*Westphalen*, purity: 99.998 Vol.-%), which was permanently recycled via circulation over a copper catalyst and mole sieve. Forming gas (*Westphalen*, 95% nitrogen, 5% hydrogen) was used to frequently regenerate the catalyst itself. All reactions in solution were carried out at Schlenk lines with argon 4.8 (*Westphalen*, purity: 99.998 Vol.-%), which was piped through a drying unit prior to use (BTS catalyst, molecular sieve 4 Å and additionally Silica Gel Orange 2 - 5 mm and P_4O_{10}). A two-way-cock system was applied to either fill the reaction vessels with argon or evacuate them with an oil rotary vane pump. Standard Schlenk tubes (10 mL - 25 mL), were kept at 120 ℃ in an oven and heated at 550 ℃ under dynamic vacuum and afterwards filled with argon for three times before using as reaction vessels. Ground joints were thereby lubricated with Lithelen high vacuum grease (*Leypold Vakuum*). All Schlenk tubes were sealed with septa/glass stoppers and parafilms®/clamps during the reaction and for long term crystallization. The solvent was injected to the Schlenk tubes by syringes (*B Braun*). The transfer of solution was carried out with Teflon tubes. The filtration processes at Schlenk lines were done with Teflon tubes and cannula stuffed with filter paper and glass wool. The filtration

processes inside the glovebox were performed with Pasteur pipettes stuffed with glass wool.

5.1.2 Solvothermal Technique and Preparation of Glass Ampoules

Solvothermal technique can be applied widely in materials chemistry as a specific approach for novel materials synthesis or new processes for shaping material. The solvothermal reaction can be affect by different factors: the physical and chemical property of the solvent, the nature of the precursors and experimental conditions. Here, ethylenediamine and toluene were chosen as general reaction solvents.

The small glass tubes (length: 25 cm) were cut from adequate glass tubes (diameter: 10 mm, wall thickness: 1 mm, length: 1 m). The shorten glass tubes were sealed at one bottom and joint with a standard ground-glass stoppered bottle neck (NS 14.5) at another side by a flame gun with oxygen (*Westphalen*, purity: 99.9991 Vol.-%) and natural gas (Gas system in lab), and consequently melt to a prolonged tube (length: ~35 cm). Inside the glovebox, the solid Zintl phase precursor was dissolved in ethylenediamine in presence of sequestering agent, then filtered to the aforementioned tube and layered with toluene. The tube with a glass stopper and a clamp was transferred outside the glovebox to connect with Schlenk line. The mixed solution were frozen by liquid nitrogen and then kept under dynamic vacuum. The glass tube was sealed at both ends as an airtight container (length: ~15cm) by the flame gun. The sealed ampoule was placed in the oven at different temperatures for further reactions.

5.1.3 Preparation of Nb Ampoules

Thermal treatment of all solid state synthesis reactions was carried out in Nb ampoules. For instance, the small Nb cylinders (length: 5 cm) were manually cut from adequate Nb tubes (diameter: 10 mm, wall thickness: 0.5 mm). The cylinders were squeezed at one bottom and subsequently arc melted using an arc furnace MAM 1 (*Edmund*

Bühler) inside a glove box. The arc furnace system possesses a movable tungsten electrode and a water-cooled copper block, which was enclosed inside a small chamber and connected with a vacuum pump. During the welding process, which comes up with more than 1000 ℃, the ampoules were cooled inside the small chamber by vacuum and argon flow. The ampoules were cleaned by sonication in acetone and acetic acid and dried in the oven at 120 ℃. The corresponding elements or precursors were filled into the ampoules inside a glove box, and then the second side of the ampoule was sealed by squeeze and arc melting as described above.

5.1.4 Apparatus for General Solid State Synthesis

The solid state synthesis for the Zintl phases with transition metal was carried out inside the Nb ampoules placed into fused silica tubes, which were evacuated and filled with argon for three times to prevent the oxidation of the ampoule material during the thermal treatment.

Generally, the solid state synthesis for A_4E_9 (A = K, Rb; E = Ge, Sn) phases was carried out inside stainless still autoclaves under argon, which was filled with reactants inside the glovebox. And the autoclave was placed into a corundum tube connecting with a rubber balloon, which was evacuated and filled with argon for three times and finally filled with argon to prevent the permeation of the air and water steam during the thermal reaction.

The fused silica tubes or corundum tubes were placed inside the tube furnace (Loba 1200-40-600 of the company *HTM Reetz GmbH*, inner diameter 45 mm, length 300 mm, T_{max} 1200 ℃). The oven consisted of a continuous heating zone without active cooling. The temperature was programmed and controlled by a special temperature regulator of the company *Eurotherm Deutschland GmbH*.

5.1.5 Chemicals and Materials

[2.2.2]crypt was dried under vacuum for 10 hours, 18-crown-6 was sublimated under dynamic vacuum at a temperature of 83 ℃ and subsequently dried under vacuum, then kept inside a glove box. All

alkali metals (K-Rb) were stored inside the glove box. Table 5.1 describes the commercially available chemicals used in this work. THF and toluene were dried by using a solvent purification system of the company *MBraun* (MB SPS).

Table 5.1 Description of reagents used in this work.

Name	Manufacturer	Shape	Purity	Storage
Germanium	Chempur	Pieces	99.999 %	Glove Box
Tin	Chempur	Bowls	99.999 %	Glove Box
Potassium	Lab inventory	Ampoule	Liquated	Glove Box
Rubidium	Lab inventory	Ampoule	Liquated	Glove Box
Cobalt	Alfa Aesar	Pieces	99.9+%	Lab
Iridium	Chempur	Powder	99.9%	Lab
Rhodium	Chempur	Granules	99.9%	Lab
THF	Merck	Liquid	Desiccation in PSP	Lab
DMF	Merck	Liquid	Storage over CaH_2 freshly distilled	Lab
Ethylenediamine	Merck	Liquid	Storage over CaH_2 freshly distilled	Lab
Bis(trimethyl-silyl)acetylene	Merck	Liquid	For synthesis	Lab
Diethyl ether	Lab inventory	Liquid	Desiccation in PSP	Lab
Toluene	Lab inventory	Liquid	Desiccation in PSP	Lab
Hexane	Merck	Liquid	Desiccation in PSP	Lab
$CoBr_2$, anhydrous	Sigma-Aldrich	Beads	99.99%	Glove Box
$SbPh_3$	Sigma-Aldrich	Powder	Desiccation in vacuo	Lab
Anthracene	Merck	Powder	Desiccation in vacuo	Lab
[2.2.2]crypt	Merck	Powder	Desiccation in vacuo	Lab
18-crown-6	Merck	Powder	Sublimated	Lab

5.2 Methods for Characterization

5.2.1 Single Crystal X-ray Diffraction

The single crystal X-ray diffraction method was used for crystal structure determination of the products. The measurements were performed on an Xcalibur 3 (*Oxford Diffractions*) or an APEX 2 (*Bruker*) diffractometer (Mo-$K_{\alpha 1}$ radiation, λ = 0.71073 Å, graphite monochromator, 40 mA, 50 kV). Both diffractometers were equipped with a Charge Coupled Device detector (CCD). Glass capillaries were used to fix the crystal sample. During the measurement a nitrogen flow were blown onto the sample to keep it cool and under inert gas condition by a Cryrostat Cryojet Controller of *Oxford Cryosystems*. The program *XPREP* was used for space group determination and unit cell determination.[235] The structure solution and refinements were performed by the program *SHELXS-97* with Direct Methods and full-matrix least-squares calculations against F^2.[191,236]

5.2.2 X-ray Powder Diffraction

The composition and purity of the solid phases were determined by powder X-ray diffraction. The sample was ground to fine powder in an agate mortar and mixed with diamond powder inside the glove box, and then filled into a glass capillary (*Hilgenberg*, diameter: 0.3 mm, wall thickness: 0.01 mm). Subsequently the capillary was sealed above the filling level, melted by a tungsten wire and covered with wax.

The powder diagrams were collected on STADIP II diffractometers (STOE Darmstadt, Cu-$K_{\alpha 1}$ radiation, λ = 1.54056 Å, Ge-monochromator, 30 mA, 50 kV) equipped with a linear position sensitive detector (L-PSD) with $2\theta_{eff} \sim 40°$, or with an imaging plate sensitive detector (IP-PSD) with 2θ range of 0-140°. Debye-Scherer geometry was used for capillaries or transmission geometry for flatbed sample holder. The measured patterns can be compared with the patterns calculated from single crystal data to examine the purity of the phases. The data processing of the measured patterns and calculations of the theoretical patterns were performed with the STOE program

package *WinXPow*.[186]

5.2.3 Energy Dispersive X-ray Analysis (EDX)

The EDX analysis was carried out to investigate the chemical composition of the products and any other solid residues. The analysis was performed with scanning electron microscope *JEOL* 5900LV spectrometer operating at 20 kV and equipped with an INCA energy dispersive X-raymicroanalysis system (*Oxford Instruments*). The products were directly placed on the sample holder in glove box for sample preparing and were transferred to the spectrometer with small glass vessels.

5.2.4 Mass Spectroscopy

Mass spectroscopy was performed on a HCT Series electrospray ion trap mass spectrometer (ESI ionization) by *Bruker Daltonik GmbH* in the negative ion mode with the m/z range 50-3000, spray shield voltage -3.5 kV, dry gas flow 5.0 L/min, dry temperature 125 ℃, capillary voltage -4 kV, lens voltage -5 V and -60 V. The data collection and the spectrum were shown by software Compass 1.3 for esquire/HCT, and the spectrum simulation were processed by software DataAnalysis Version 4.0 SP 5 by *Bruker Daltonik GmbH*.

5.2.5 Electron Paramagnetic Resonance (EPR)

EPR spectroscopic investigations were performed by *JEOL* JES-FA 200 spectrometer at X-band frequency ($\nu \sim 9$GHz, modulation 0.4 mT) on liquid and solid samples at ambient temperature and at 153/103 K. The crude reacting mixture solution was filtered into a fused silica EPR tube under inert gas atmosphere as liquid sample. The solid samples were directly filled into fused silica EPR tube inside a glove box with the resulting crystals. *g* values were calculated in relation to signals of the Mn standards.

5.2.6 Raman Spectroscopy

The FT-Raman measurements were performed on powdered amples sealed in pyrex tubes (diameter: 7 mm) with a Raman microscopy spectrometer (LabRAM HR, HORIBA Scientific, Japan) (He-Ne Laser, 633 nm, 14 mW).

5.2.7 Nuclear Magnetic Resonance (NMR) Measurement

NMR measurement as a convenient and fast method can determine the reaction process and the structure of the product. The tests were measured with a 400 MHz *JEOL* spectrometer and a *Bruker* AMX 400. The samples were prepared in glove box and covered with tight cap and parafilms. Me_4Si and Me_4Sn in C_6D_6 (0 ppm) were used as standards for calibrations of ^{1}H and ^{119}Sn NMR, respectively. The processing of the spectra was performed using software MestreNova.

5.3 Synthesis

5.3.1 Solid State Synthesis for the Synthesis of Precursors

5.3.1.1 Synthesis of K_4Ge_9, K_4Sn_9 and Rb_4Sn_9 Phases

A_4E_9 (A = K, Rb; E = Ge, Sn) phases were synthesized by reduction of the elements from group 14 with alkali metals. Stoichiometric amounts (K:E = 4:9) of the elements were fused at high temperature and then cooled down to room temperature. A 10% excess of K was used to compensate the loss of alkali metal at high temperatures. The reaction led to the formation of single crystals of the K_4E_9 phases.

The reactions were carried out in a stainless steel autoclave and a corundum tube, both filled with argon atmosphere. Heating rate, reaction temperature, reaction time as well as cooling rate were

programmed. After cooling down to room temperature, the products were collected in glove box and ground to fine powders. Powder X-ray diffraction measurements were carried out to determine the purity of the products. The reaction conditions are summarized in Table 5.2.

Table 5.2 Reaction conditions of the synthesis of A_4E_9 (A = K, Rb; E = Ge, Sn) phases.

Phase	Amount of A (g)	Amount of E (g)	Heating rate (℃ / min)	Reaction Temperature (℃)	Cooling rate (℃ / hour)
K_4Ge_9	0.8	3.01	3	650 for 20h	1
K_4Sn_9	0.8	4.92	3	550 for 20h	1
Rb_4Sn_9	1.1	3.13	3	550 for 20h	1

5.3.1.2 Synthesis of $K_{4.79}Co_{0.79}Sn_9$ Phase [125]

An alloy of the nominal composition "CoSn" was synthesized by arc melting of the elements. The resulting regulus, which contained a mixture of phases such as CoSn, Co_3Sn_2, $CoSn_2$, and Sn, was further homogenized in an agate mortar. Then Sn and K pieces were mixed with "CoSn" according to an atomic ratio of K/Co/Sn 5:1.2:9, loaded in a niobium crucible, which was welded-sealed on both sides under argon, jacketed in a fused silica Schlenk tube, and evacuated to prevent oxidation of the crucibles at high temperatures. The sample was first heated in a tube-resistant furnace to 1000 ℃ and held at that temperature for 8 h. Next, the temperature was lowered at a rate of 6 ℃ h^{-1} to 550 ℃, held at that temperature for 24 h, and finally quenched under air. This procedure yielded good-quality single crystals of $K_{5-x}Co_{1-x}Sn_9$.

5.3.1.3 Solids with Nominal Compositions of "Rb_3IrSn_{12}" and "K_3RhSn_6" [237]

"**Rb_3IrSn_{12}**": First, the Ir powder was pressed to the pellet and arc-melted with the pieces of Sn to the binary Ir–Sn precursor in ratio Ir:Sn = 1:12. The regulus was turned upside down and melted three times to ensure homogenization. Then, the pieces of Rb were mixed with the as prepared Ir–Sn alloy and sealed in a niobium ampoule

(overall ratio Rb:Ir:Sn = 3:1:12). The ampoule was placed in a silica tube which was evacuated, sealed, and inserted in a vertical resistance tube furnace. The sample was heated to 1000 ℃ at a rate of 3 ℃ min^{-1}, held at this temperature for 8 hours, and then slowly cooled to 550 ℃ at a rate of 0.1 ℃ min^{-1}, held at this temperature for 24 h and finally quenched by switching off the oven to room temperature. An air-sensitive crystalline dark silver lustrous product was obtained from the reaction.

"**K_3RhSn_6**": An alloy of the nominal composition Rh:Sn = 1:2 was synthesized by arc melting of the elements. Then pieces of Sn and K were mixed with the powdered Rh-Sn precursor according to an atomic ratio of K:Rh:Sn = 3:1:6. The ampoule was placed in a silica tube which was evacuated, sealed, and inserted in a vertical resistance tube furnace. The sample was heated to 950 ℃ at a rate of 3 ℃ min^{-1}, held at this temperature for 8 hours, and then slowly cooled to 300 ℃ at a rate of 0.1 ℃ min^{-1} and finally quenched by switching off the oven to room temperature. An air-sensitive crystalline dark silver lustrous product was obtained from the reaction.

5.3.2 Synthesis of Metal-centered Clusters in Solutions

5.3.2.1 Synthesis of Co-centered Compounds 1-4

$K[K([2.2.2]crypt)]_3[Co_{0.68}@Sn_9]$ (1). $K_{5-x}Co_{1-x}Sn_9$ (45 mg, 0.035 mmol) and [2.2.2]crypt (67 mg, 0.18 mmol) were dissolved in ethylenediamine (1.5 mL) in a Schlenk tube. The brown solution was stirred at ambient temperature for 2 hours, then filtered to a glass tube and layered with toluene (3 mL) in the glovebox. The mixed solution in this tube was frozen by liquid nitrogen and sealed by flame gun under dynamic vacuum. The tube was placed in the oven at 60 ℃ for crystallization. After 3 hours, dark brown plate-shaped crystals together with a small amount of elemental tin were found on the wall of the glass tube. For further crystallization the tube was kept still at room temperature for another two weeks. The crystals have been investigated by means of X-ray diffraction studies, were identified: $\{[K[2.2.2]crypt]_3[KCo_{0.68}@Sn_9]\}_n$ (**1**) and (**2**). The yield of the mixture was approximately 8 mg (10%, calculation based on

$K_{4.79}Co_{0.79}Sn_9$ and **1**).

[K([2.2.2]crypt)]$_6$[Sn$_9$]$_{1.21}$[Co@Sn$_9$]$_{0.17}$[Co@Sn$_{10}$]$_{0.62}$·3en·tol (2). From all the preparations described (**1**, **3**, **4**), compound **2** has been obtained as byproduct. Pure compound **2** has been synthesized as follows: $K_{5-x}Co_{1-x}Sn_9$ (55 mg, 0.035 mmol) and [2.2.2]crypt (100 mg, 0.27 mmol) were dissolved in ethylenediamine (1.5 mL) in a Schlenk tube. The brown solution was stirred and filtered to a new Schlenk tube, layered with toluene to crystalize at room temperature. It showed the same unit cell about 24 crystals by random selection. The yield of the crystal was approximately 31 mg (35%, calculation based on $K_{4.79}Co_{0.79}Sn_9$ and **2**).

[K([2.2.2]crypt)]$_5$[Co$_2$@Sn$_{17}$] (3). $K_{5-x}Co_{1-x}Sn_9$ (55 mg, 0.04 mmol) and [2.2.2]crypt (107 mg, 0.28 mmol) were dissolved in ethylenediamine (1 mL) in a Schlenk tube, and the brown solution were stirred for 3 hours at 50 ℃, then filtered to a new Schlenk tube and layered with toluene (3 mL). The tube was laid at ambient temperature to allow for crystallization. After 4 weeks, dark brown/black block-shaped crystals together with a small amount of elemental tin were found on the wall of the glass tube. Determined by Single-crystal X-ray diffraction, two kinds of structures (**2** and **3**) could be identified. The yield of the mixture was approximately 22 mg (25%, calculation based on $K_{4.79}Co_{0.79}Sn_9$ and **3**).

[K([2.2.2]crypt)]$_5$[Co$_2$@Sn$_{17}$]·en·tol (4). $K_{5-x}Co_{1-x}Sn_9$ (45 mg, 0.035 mmol) and [2.2.2]crypt (67 mg, 0.18 mmol) were dissolved in ethylenediamine (1.5 mL) in a Schlenk tube. The brown solution was stirred at ambient temperature for 2 hours, then filtered to a glass tube and layered with toluene (3 mL). The tube was sealed under vacuum, heated in oil bath at 70 ℃ for 3 hours and then stored at ambient temperature. After three weeks, dark brown plate-shaped crystals together with a small amount of elemental tin were found on the wall of the glass tube. The crystals have been identified as **2** and **4** by X-ray single-crystal structure determination. The yield of the mixture was approximately 16 mg (11% calculation based on $K_{4.79}Co_{0.79}Sn_9$ and **4**).

5.3.2.2 Synthesis of Rhodium-centered Compound 5

[K([2.2.2]crypt)]$_6$[Sn$_9$]$_{1.52}$[Rh@Sn$_{10}$]$_{0.48}$·3en·tol (5). The mixture

of the nominal composition "K_3RhSn_6" (50 mg, 0.05 mmol) and [2.2.2]crypt (50 mg, 0.13 mmol) was dissolved in ethylenediamine (1.5 mL) in a Schlenk tube. The orange-brown solution was stirred at ambient temperature for 2 hours, then filtered to another Schlenk tube and layered with toluene (3 mL). After four weeks, dark brown block crystals were found on the wall of the glass tube. Thicker crystals display with black color. The yield of the crystals was approximately 11 mg (4% calculated based on "K_3RhSn_6").

5.3.2.3 Synthesis of Iridium-centered Compound 6

[Rb([2.2.2]crypt)]$_6$[Ir@Sn$_{12}$]$_2$·en·2tol (6). "Rb_3IrSn_{12}" (0.045 g, 0.024 mmol) was dissolved in 1.5 mL of ethylenediamine (green-brown solution) in a test tube inside the glovebox. [2.2.2]crypt (0.038 g, 0.01 mmol) was added and the reaction mixture was stirred for 2 h. The resulting deep brown solution was filtered and layered with toluene (3 mL). After diffusion small black crystals were isolated and examined by X-ray diffraction.

5.3.3 Compounds with Heteroatomic Sb/Sn Clusters

5.3.3.1 Compound 7 with Cobalt-filled Heteroatomic Clusters

[K([2.2.2]crypt)]$_2$[Co$_x$@Sn$_{7-x}$Sb$_{2+x}$] x≈0.58 (7). $K_{4.79}Co_{0.79}Sn_9$ (30 mg, 0.023 mmol, 1 eq.), $SbPh_3$ (20 mg, 0.057 mmol, 2.5 eq.) and [2.2.2]cryptand (20 mg, 0.053 mmol, 2.3 eq.) were mixed in 0.8 mL of ethylenediamine. The red-brown solution was dissolved under sonication, filtered to another glass tube and layered with 2 mL toluene. The glass tube was sealed and heated at 50 ℃ for one hour. After three months, three pieces of black crystals and quantity of precipitates formed.

5.3.3.2 Compound 8 with Unfilled Heteroatomic Clusters

[Rb([2.2.2]crypt)]$_2$[Sb$_x$Sn$_{9-x}$]·3tol·2en x≈2 (8). Rb_4Sn_9 (65 mg, 0.046 mmol, 1 eq.), $SbPh_3$ (35 mg, 0.099 mmol, 2.2 eq.) and

[2.2.2]crypt (35 mg, 0.093 mmol, 2 eq.) were dissolved in 1.5 mL of ethylenediamine. The red-brown solution was stirred and then filtered by tightly packed glass wool. 3.5 mL toluene was added to the filtrate. The whole system stood at 50 ℃ for one hour and kept still at room temperature for crystallization. Over three weeks a few red hexagonal-plate-like crystals formed on the wall of the Schlenk tube. The yield of the crystals was approximately 12 mg (13% calculated based on Rb_4Sn_9).

5.3.4 Compounds with Tetrel-atomic Polyanions

5.3.4.1 Compound 9 with Functionallized Dimer Clusters

$[K(18\text{-crown-6})en_2][K(18\text{-crown-6})]_3[Ge_9(CH{=}CH_2)]_2{\cdot}2en$ (9). $K_{4.79}Co_{0.79}Sn_9$ (60 mg, 0.046 mmol) and bright orange crystal samples $[Ge_9(CH{=}CH_2)_2][K(18\text{-crown-6})]_2{\cdot}en$ (20 mg, 0.015 mmol) were dissolved in 1.5 mL of ethylenediamine (orange-brown solution) in a test tube inside the glovebox. 18-crown-6 (60 mg, 0.227 mmol) was dissolved in toluene (4 mL). The reaction mixture was stirred for 2 h, filtered into a Schlenk tube and layered with the toluene/crown ether solution. After diffusion black crystals were isolated and examined by single crystal X-ray diffraction.

The compound $[Ge_9(CH{=}CH_2)_2][K(18\text{-crown-6})]_2{\cdot}en$ was synthesized by K_4Ge_9 and bis(trimethylsilyl)acetylene ($Me_3Si\text{-}C{\equiv}C\text{-}SiMe_3$) according to the literature.[98]

5.3.4.2 Compound 10 with Different Sequestering Agents

$[K(18\text{-crown-6})]_2[K([2.2.2]crypt)][KSn_9]{\cdot}1.5en$ (10). K_4Sn_9 (50 mg, 0.041 mmol) and $[Co(anthracene)_2][K(18\text{-crown-6})(THF)_2]{\cdot}THF$ (6 mg, 0.007 mmol) were dissolved in 1.5 mL of ethylenediamine. [2.2.2]crypt (40 mg, 0.106 mmol) was dissolved in toluene (3 mL). The reaction mixture was stirred at room temperature for 2 h, filtered into a Schlenk tube and layered with the toluene/crypt solution. After diffusion brown crystals were isolated and determined by X-ray diffraction.

5.3.5 Organometallic Compound with Co(-1)

[Co(anthracene)$_2$][K(18-crown-6)(THF)$_2$]·THF (11): To a deep-blue solution of K[$C_{14}H_{10}$] (3.43 mmol) in THF (30 mL, -78 ℃) was added a bright-blue solution of $CoBr_2$ (0.25 g, 1.15 mmol) in THF (30 mL, -78 ℃). The reaction was stirred overnight and warmed slowly to room temperature, the color of solution gradually changed to deep-pinkish-red. It was filtered to remove KBr, and 18-crown-6 (0.302 g, 1.15 mmol) in THF (10 mL) was added to the filtrate. Hexane (20 mL) was added and the volume was reduced to about 20 mL in vacuum. The brown-black needle-like product was crystallized at -40 ℃ by diffusion of diethyl ether (50 mL) which yields the title compound (Yield: 41% based on $CoBr_2$). Due to the slightly different aftertreatment from the literature,[234] the crystals display acentric space group $P2_12_12_1$ instead of $P1$. The EDX shows an atomic ratio of Co/K close to 1:1 in all the analyzed crystals of [$K(C_{12}H_{24}O_6)(C_4H_8O)_2$][$Co(C_{14}H_{10})_2$]($C_4H_8O$).

6 Appendix

6.1 NMR Spectrum

The ^{119}Sn-NMR spectrum of $K_{4.79}Co_{0.79}Sn_9$ in ethylenediamine in present of cryptand has been tested at room temperature. The chemical shift is in the range of related compounds with empty cluster $[Sn_9]^{4-}$.

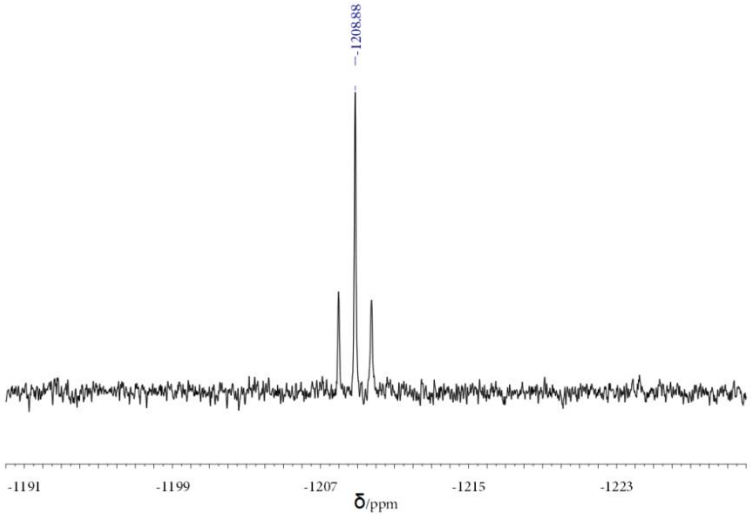

Figure 6.1 ^{119}Sn-NMR spectrum of $K_{4.79}Co_{0.79}Sn_9$ in ethylenediamine with cryptand at room temperature , J(^{119}Sn-^{117}Sn) = 265 Hz. ^{119}Sn was referenced to $SnMe_4$ in C_6D_6 (0 ppm).

6.2 Crystallographic Data

The tables in the appendix contain the refinement information about the crystallographic data of all the characterized compounds. The complete structure parameters with atomic coordinates, displacement parameters and lists of all interatomic distances and angles are shown on the accompanying CD.

6.2.1 $K[K([2.2.2]crypt)]_3[Co_{0.68}@Sn_9]$ (1)

Table 6.1 Crystallographic data of compound **1**.

Compound	$K[K([2.2.2]crypt)]_3[Co_{0.68}@Sn_9]$ (**1**)
Empirical formula	$Sn_9Co_{0.68}K_4N_6O_{18}C_{54}H_{108}$
Formula weight	2394.15g/mol
Measurement temperature	150 (2) K
Wavelength	0.71073 Å
Crystal system	triclinic
Space group	$P\bar{1}$ (No. 2)
Unit cell dimensions	a = 15.7857(3) Å
	b =16.2361(3) Å
	c = 20.2148(4) Å
	α = 98.605(2) °
	β = 104.739(2) °
	γ = 118.328(2) °
Volume	4182.18(15) $Å^3$
Z	2
Density(calculated)	1.901 g/cm^3
μ	3.027 mm^{-1}
F(000)	2324.6
θ range	2.97 – 36.96
Index ranges	$-21 \leq h \leq 22$, $-22 \leq k \leq 22$, $-27 \leq l \leq 28$
Collected reflections	82069
Independent reflections	24370
Data/restraints/parameters	24370/0/833
Goodness-of fit on F^2	0.889
Final R indices [$I>2\sigma(I)$]	R_1 = 0.0314, wR_2 = 0.0681
R Indices for all data	R_1 = 0.0600, wR_2 = 0.0749
largest diff. peak, hole [e $Å^{-3}$]	2.535, -1.191

6.2.2 $[K([2.2.2]crypt)]_6[Sn_9]_{1.21}[Co@Sn_9]_{0.17}[Co@Sn_{10}]_{0.62}\cdot 3en\cdot tol$ (2)

Table 6.2 Crystallographic data of compound **2**.

Compound	$[K([2.2.2]crypt)]_6[Sn_9]_{1.21}[Co@Sn_9]_{0.17}[Co@Sn_{10}]_{0.62}\cdot 3en\cdot tol$ (**2**)
Empirical formula	$Sn_{18}Co_2K_{24}N_{18}O_{36}C_{121}H_{248}$
Formula weight	5020.25 g/mol
Measurement temperature	150 K
Wavelength	0.71073 Å
Crystal system	monoclinic
Space group	$P2_1/c$ (No. 14)
Unit cell dimensions	a = 28.0619(4) Å b = 23.3937(3) Å c = 27.6240(4) Å β = 93.440(1) °
Volume	18101.7 (4) $Å^3$
Z	4
Density(calculated)	1.842 g/cm^3
μ	2.815
F(000)	9824
θ range	6.14-25.50
Index ranges	$-32 \leq h \leq 33$, $-28 \leq k \leq 28$, $-32 \leq l \leq 27$
Collected reflections	130021
Independent reflections	30736
Data/restraints/parameters	30736/174/2083
Goodness-of fit on F^2	0.762
Final R indices [$I>2\sigma(I)$]	R_1 = 0.0475, wR_2 = 0.0851
R Indices for all data	R_1 = 0.1360, wR_2 = 0.0982
largest diff. peak, hole [e $Å^{-3}$]	2.195, -1.242

6.2.3 $[K([2.2.2]crypt)]_5[Co_2@Sn_{17}]$ (3)

Table 6.3 Crystallographic data of compound **3**.

Compound	$[K([2.2.2]crypt)]_5[Co_2@Sn_{17}]$ (**3**)
Empirical formula	$Sn_{17}Co_2K_5N_{10}O_{30}C_{90}H_{180}$
Formula weight	4213.53 g/mol
Measurement temperature	110(2) K
Wavelength	0.71073 Å
Crystal system	monoclinic
Space group	$P2_1/c$ (No. 14)
Unit cell dimensions	a = 15.2473(2) Å
	b = 33.4895(5) Å
	c = 30.9531(5) Å
	β = 110.166(1) °
Volume	14836.5(4) $Å^3$
Z	4
Density(calculated)	1.886 g/cm^3
μ	3.221 mm^{-1}
F(000)	8116
θ range	2.94 - 26.37
Index ranges	$-19 \leq h \leq 19$, $-41 \leq k \leq 41$, $-37 \leq l \leq 38$
Collected reflections	265211
Independent reflections	30254
Data/restraints/parameters	30254/119/1245
Goodness-of fit on F^2	1.055
Final R indices [$I>2\sigma(I)$]	R_1 = 0.0900, wR_2 = 0.2713
R Indices for all data	R_1 = 0.1322, wR_2 = 0.2863
largest diff. peak, hole [e $Å^{-3}$]	2.290, -1.402

6.2.4 [K([2.2.2]crypt)]$_5$[Co_2@Sn_{17}]·en·tol (4).

Table 6.4 Crystallographic data of compound **4**.

Compound	[K[2.2.2]crypt]$_5$[Co_2@Sn_{17}]·en·tol (**4**)
Empirical formula	$Sn_{17}Co_2K_5N_{12}O_{30}C_{99}H_{196}$
Formula weight	4365.77 g/mol
Measurement temperature	123 (2) K
Wavelength	0.71073 Å
Crystal system	monoclinic
Space group	$P2_1/n$ (No. 14)
Unit cell dimensions	a = 17.9334(7) Å
	b = 25.3186(11) Å
	c = 32.3075(15) Å
	β = 93.057(4) °
Volume	14648.3(11)Å^3
Z	4
Density(calculated)	1.980 g/cm^3
μ	3.266 mm^{-1}
F(000)	8452
θ range	2.41 - 25.50
Index ranges	$-21 \leq h \leq 14$, $-30 \leq k \leq 30$, $-39 \leq l \leq 39$
Collected reflections	27251
Independent reflections	10331
Data/restraints/parameters	27251/6/1484
Goodness-of fit on F^2	0.680
Final R indices [$I>2\sigma(I)$]	R_1 = 0.0472, wR_2 = 0.0802
R Indices for all data	R_1 = 0.1343, wR_2 = 0.0921
largest diff. peak, hole [e Å^{-3}]	1.192, -1.001

6.2.5 $[K([2.2.2]crypt)]_6[Sn_9]_{1.53}[Rh@Sn_{10}]_{0.47}\cdot 3en\cdot tol$ (5)

Table 6.5 Crystallographic data of compound **5**.

Compound	$[K([2.2.2]crypt)]_6[Sn_9]_{1.53}[Rh@Sn_{10}]_{0.47}\cdot 3en\cdot tol$ (**5**)
Empirical formula	$Sn_{18}Rh_2K_6N_{18}O_{36}C_{121}H_{248}$
Formula weight	4971.93
Measurement temperature	120 (2) K
Wavelength	0.71073 Å
Crystal system	monoclinic
Space group	$P2_1/c$
Unit cell dimensions	a = 28.0619(4) Å
	b = 23.3937(3) Å
	c = 27.6240(4) Å
	β = 93.4400(10) °
Volume	18101.7(4) $Å^3$
Z	4
Density(calculated)	1.824 g/cm^3
μ	2.811
F(000)	9648
θ range	2.37-25.50
Index ranges	$-33 \leq h \leq 33$, $-28 \leq k \leq 28$, $-25 \leq l \leq 35$
Collected reflections	249938
Independent reflections	33659
Data/restraints/parameters	33659/0/1886
Goodness-of fit on F^2	0.848
Final R indices [$I>2\sigma(I)$]	R_1 = 0.0369, wR_2 = 0.0697
R Indices for all data	R_1 = 0.0809, wR_2 = 0.0750
largest diff. peak, hole [e $Å^{-3}$]	1.621, -1.198

6.2.6 [Rb([2.2.2]crypt)]$_3$[Ir@Sn$_{12}$]·en·2tol (6)

Table 6.6 Crystallographic data of compound **6** and [K([2.2.2]crypt)]$_3$[Ir@Sn$_{12}$]·tol.[126]

Compound	[Rb([2.2.2]crypt)]$_3$[Ir@Sn$_{12}$]·en·2tol (**6**)	[K([2.2.2]crypt)]$_3$ [Ir@Sn$_{12}$]·tol
Empirical formula	$C_{70}H_{132}N_8O_{18}Rb_3IrSn_{12}$	$C_{61}H_{116}IrK_3N_6O_{18}Sn_{12}$
Formula weight	3246.73 g/mol	2955.38 g/mol
Measurement temperature	150 (2) K	150 (2) K
Wavelength	0.71073 Å	0.71073 Å
Crystal system	monoclinic	monoclinic
Space group	*C2/c* (No. 15)	*C$_2$/c*
Unit cell dimensions	*a* = 22.8031(3) Å *b* = 18.2654(3) Å *c* = 48.6766(6) Å *β* = 92.620(10) °	*a* = 22.8031(3) Å *b* = 18.2654(3) Å *c* = 48.6766(6) Å *β* = 92.62(1) °
Volume	20253.0(5) Å^3	20253.0(5) Å^3
Z	8	8
Density(calculated)	2.130 g/cm^3	1.938 g/cm^3
μ	5.702 mm^{-1}	4.39 mm^{-1}
F(000)	12320	
θ range	3.16– 25.50	2.94 - 26.37
Index ranges	-27 ≤ h ≤ 27, -19 ≤ k ≤ 22, -58≤ l ≤ 58	
Collected reflections	166613	114193
Independent reflections	18813	17675
Data/restraints/parameters	18813 /4/957	
Goodness-of fit on F^2	0.805	
Final R indices [$I>2\sigma(I)$]	R_1 = 0.0549, wR_2 = 0.0785	R_1 = 0.043, wR_2 = 0.106
R Indices for all data	R_1 = 0.1317, wR_2 = 0.0905	R_1 = 0.070, wR_2 = 0.113
largest diff. peak, hole [e Å^{-3}]	1.212, -1.752	

6.2.7 $[K([2.2.2]crypt)]_2[Co_x@Sn_{7-x}Sb_{2+x}]$ x≈0.58 (7)

Table 6.7 Crystallographic data of compound **7**.

Compound	$[K([2.2.2]crypt)]_2[Co_x@Sn_{7-x}Sb_{2+x}]$ x≈0.58 (**7**)
Empirical formula	$C_{36}H_{72}Co_{0.58}K_2N_4O_{12}Sn_9$
Formula weight	1931.80 g/mol
Measurement temperature	150 K
Wavelength	0.71073 Å
Crystal system	monoclinic
Space group	*C2/c* (No. 15)
Unit cell dimensions	a = 24.4397(15) Å b = 11.8679(6) Å c = 21.3721(11) Å β = 97.163(7) °
Volume	6150.6(6) $Å^3$
Z	4
Density(calculated)	2.086 g/cm^3
μ	3.917 mm^{-1}
F(000)	3659
θ range	3.05 – 32.62
Index ranges	$-37 \leq h \leq 31$, $-17 \leq k \leq 17$, $-32 \leq l \leq 31$
Collected reflections	66500
Independent reflections	11122
Data/restraints/parameters	11122/6/313
Goodness-of fit on F^2	0.555
Final R indices [$I>2\sigma(I)$]	R_1 = 0.0489, wR_2 = 0.0904
R Indices for all data	R_1 = 0.2940, wR_2 = 0.1139
largest diff. peak, hole [e $Å^{-3}$]	1.603, -1.199

6.2.8 $[Rb([2.2.2]crypt)]_2[Sn_{9-x}Sb_x]\cdot 3tol\cdot 2en$ x≈2 (8)

Table 6.8 Crystallographic data of compound **8**.

Compound	$[Rb([2.2.2]crypt)]_2[Sn_{9-x}Sb_x]\cdot 3tol\cdot 2en$ (**8**)
Empirical formula	$C_{45}H_{86}N_6O_{12}Rb_2Sn_9$
Formula weight	2142.35 g/mol
Measurement temperature	150 (2) K
Wavelength	0.71073 Å
Crystal system	hexagonal
Space group	$P6_3/m$ (No. 176)
Unit cell dimensions	a = 12.2059(1) Å
	c = 26.3856(4) Å
Volume	3404.37(6) $Å^3$
Z	2
Density(calculated)	2.090 g/cm^3
μ	4.716 mm^{-1}
F(000)	2036
θ range	3.01– 25.49
Index ranges	$-20 \leq h \leq 20$, $-20 \leq k \leq 20$, $-44 \leq l \leq 36$
Collected reflections	47885
Independent reflections	2169
Data/restraints/parameters	2169/1/113
Goodness-of fit on F^2	1.106
Final R indices [$I>2\sigma(I)$]	R_1 = 0.0746, wR_2 = 0.1648
R Indices for all data	R_1 = 0.0905, wR_2 = 0.1719
largest diff. peak, hole [e $Å^{-3}$]	2.580, -4.049

6.2.9 [K(18-crown-6)en$_2$][K(18-crown-6)]$_3$ [Ge$_9$(CH=CH$_2$)]$_2$·2en (9)

Table 6.9 Crystallographic data of compound **9**.

Compound	[K(18-crown-6)en$_2$][K(18-crown-6)]$_3$ [Ge$_9$(CH=CH$_2$)]$_2$ ·2en (**9**)
Empirical formula	$Ge_9K_2N_4O_{12}C_{30}H_{67}$
Formula weight	1407.39 g/mol
Measurement temperature	150 (2) K
Wavelength	0.71073 Å
Crystal system	triclinic
Space group	$P\bar{1}$ (No. 2)
Unit cell dimensions	a = 12.6193(7) Å b = 12.6412(7) Å c = 17.1663(9) Å α = 80.451(4) ° β = 81.731(4) ° γ = 72.594(5) °
Volume	2563.9(2) Å^3
Z	2
Density(calculated)	1.823 g/cm^3
μ	5.412 mm^{-1}
F(000)	1394
θ range	3.35 – 27.50
Index ranges	-16 ≤ h ≤ 13, -16 ≤ k ≤ 13, -22≤ l ≤ 22
Collected reflections	57685
Independent reflections	21132
Data/restraints/parameters	21132/0/529
Goodness-of fit on F^2	0.658
Final R indices [$I>2\sigma(I)$]	R_1 = 0.0532, wR_2 = 0.1119
R Indices for all data	R_1 = 0.2200, wR_2 = 0.1278
largest diff. peak, hole [e Å^{-3}]	1.223, -0.774

6.2.10 $[K(18\text{-crown-}6)]_2[K([2.2.2]crypt)]$ $[KSn_9]\cdot 1.5en$ (10)

Table 6.10 Crystallographic data of compound **10**.

Compound	$[K(18\text{-crown-}6)]_2[K([2.2.2]crypt)][KSn_9]\cdot 1.5en$ (**10**)
Empirical formula	$C_{45}H_{96}K_4N_5O_{18}Sn_9$
Formula weight	2219.88 g/mol
Measurement temperature	150 (2) K
Wavelength	0.71073 Å
Crystal system	triclinic
Space group	$P\overline{1}$ (No. 2)
Unit cell dimensions	a = 10.1654(3) Å b = 18.5085(10) Å c = 20.3683(9) Å α = 83.232(4) ° β = 81.475(3) ° γ = 82.427(3) °
Volume	3737.9(3) $Å^3$
Z	2
Density(calculated)	1.972 g/cm^3
μ	3.234 mm^{-1}
F(000)	2142
θ range	3.05 – 25.50
Index ranges	$-12 \leq h \leq 5$, $-22 \leq k \leq 22$, $-24 \leq l \leq 24$
Collected reflections	30342
Independent reflections	13575
Data/restraints/parameters	13575/0/695
Goodness-of fit on F^2	0.961
Final R indices [$I>2\sigma(I)$]	R_1 = 0.0691, wR_2 = 0.1386
R Indices for all data	R_1 = 0.1356, wR_2 = 0.1546
largest diff. peak, hole [e $Å^{-3}$]	1.593, -1.238

6.2.11 [Co(anthracene)$_2$][K(18-crown-6)(THF)$_2$]·THF (11)

Table 6.11 Crystallographic data of compound **11**.

Compound	[Co(anthracene)$_2$][K(18-crown-6)(THF)$_2$]·THF (**11**)
Empirical formula	$C_{52}H_{68}CoKO_9$
Formula weight	935.09 g/mol
Measurement temperature	150 K
Wavelength	0.71073 Å
Crystal system	orthorhombic
Space group	$P2_12_12_1$
Unit cell dimensions	a = 13.0428(10) Å
	b = 13.3557(10) Å
	c = 27.4939(17) Å
Volume	4789.3(6) Å^3
Z	4
Density(calculated)	1.297 g/cm^3
μ	0.501 mm^{-1}
F(000)	1992
θ range	2.96– 26.00
Index ranges	$-16 \leq h \leq 16$, $-16 \leq k \leq 16$, $-33 \leq l \leq 33$
Collected reflections	62002
Independent reflections	9364
Data/restraints/parameters	9364/0/604
Goodness-of fit on F^2	0.765
Final R indices [$I>2\sigma(I)$]	R_1 = 0.0454, wR_2 = 0.0668
R Indices for all data	R_1 = 0.1157, wR_2 = 0.0758
largest diff. peak, hole [e Å^{-3}]	0.955, -0.372

6.3 EDX Analysis Details

Table 6.12 EDX-results of crystal samples in compound **2**.

test	K (%)	Co (%)	Sn (%)
A	21(±3)	3(±1)	75(±6)
B	25(±4)	4(±2)	71(±7)
C	22(±2)	3(±1)	74(±5)
D	22(±3)	2(±1)	76(±6)
E	23(±3)	3(±1)	74(±6)
F	22(±3)	3(±1)	75(±6)
G	21(±3)	5(±2)	74(±6)
H	22(±3)	4(±1)	74(±7)
theoretical value of $K_6Co_{0.8}Sn_{18.7}$	24(6/25.5)	3(0.8/25.5)	73(18.7/24)

Table 6.13 EDX-results of crystal samples in compound **3**.

test	K (%)	Co (%)	Sn (%)
A	20(±3)	5(±1)	74(±6)
B	21(±3)	7(±2)	73 (±6)
theoretical value of $K_5Co_2Sn_{17}$	21(5/24)	8(2/24)	71(17/24)

Table 6.14 EDX-results of crystal samples in compound **4**.

test	K (%)	Co (%)	Sn (%)
A	14(±3)	9(±2)	77(±7)
B	15(±2)	7(±2)	78 (±6)
C	23(±5)	3(±2)	74(±10)
D	19(±5)	9(±4)	72(±9)
theoretical value of $K_5Co_2Sn_{17}$	21(5/24)	8(2/24)	71(17/24)

Table 6.15 EDX-results of crystal samples in compound **5**.

test	K (%)	Rh (%)	Sn (%)
A	13(±4)	5(±2)	83(±11)
B	17(±5)	4(±3)	79(±10)
C	13(±3)	5(±2)	82(±9)
D	24(±6)	6(±3)	71(±10)
theoretical value of $K_6Rh_{0.5}Sn_{18.5}$	24(6/25)	2(0.5/25)	74(18.5/25)

Table 6.16 EDX-results of crystal samples in compound **9**.

sample	K (%)	Ge (%)
A	15(±2)	85(±18)
B	13(±2)	87(±21)
C	13(±2)	87(±21)
D	20(±3)	80(±18)
E	22(±3)	78(±17)
F	15(±2)	85(±23)
theoretical value of K_4Ge_{18}	18(4/22)	82(18/22)

Table 6.17 EDX-results of crystal samples in compound **10**.

test	K (%)	Sn (%)
A	29(±3)	71(±6)
B	35(±4)	65 (±5)
theoretical value of K_4Sn_9	31(4/13)	69(9/13)

Table 6.18 EDX-results of powder samples in compound **11**.

test	K (%)	Co (%)	Br (%)
A	51(±11)	46(±13)	3(±2)
B	48(±11)	48(±14)	4(±4)
theoretical value of KCo	50(1/2)	50(1/2)	0(0/2)

6.4 Abbreviations

Table 6.19 Abbreviations list present in this work.

18-crown-6	1,4,7,10,13,16-hexaoxacyclooctadecane
[2.2.2]crypt	4,7,13,16,21,24-hexaoxa-1,10-diazabicyclo[8.8.8]hexacosane
A	alkali metal
Å	angstrom
BTMSA	Bis(trimethylsilyl)acetylene
dmf	N,N-dimethyl formamide
E	group 14 element
EDX	energy dispersive X-ray analysis
en	ethylenediamine
EPR	electron paramagnetic resonance
GHz	gigahertz
h	hour(s)
HOMO	highest occupied molecular orbital
K	kelvin
kHz	kilohertz
LUMO	lowest unoccupied molecular orbital
mg	milligram
MHz	megahertz
min	minute(s)
mL	milliliter
mm	millimeter
mT	millitesla
NMR	nuclear magnetic resonance
Ph	phenyl ($-C_6H_5$)
T	tesla
THF	tetrahydrofurane
tol	toluene

7 References

(1) Pöttgen, R. *Z. Naturforsch.* **2006**, *61b*, 677
(2) Zhang, J. J.; Xia, Y. Y. *J. Electrochem. Soc.* **2006**, *153*, A1466.
(3) Rylander, P. N. *Hydrogenation methods, Academic Press* New York **1985**.
(4) Narasimhan, C. S.; Deshpande, V. M.; Ramnarayan, K. *Appl. Catal.* **1989**, *48*, L1.
(5) Cheah, K. Y.; Tang, T. S.; Mizukami, F.; Niwa, S.; Toba, M.; Choo, Y. M. *J. Am. Oil Chem. Soc.* **1992**, *69*, 410.
(6) Pouilloux, Y.; Autin, F.; Piccirilli, A.; Guimon, C.; Barrault, J. *Appl. Catal. A-Gen.* **1998**, *169*, 65.
(7) Xu, C.; Tsai, Y. L.; Koel, B. E. *J. Phys. Chem. C* **1994**, *98*, 585.
(8) Larcher, D.; Beaulieu, L. Y.; MacNeil, D. D.; Dahn, J. R. *J. Electrochem. Soc.* **2000**, *147*, 1658.
(9) Cheng, X.-Q.; Shi, P.-F. *J. Alloy Compd.* **2005**, *391*, 241.
(10) Hassoun, J.; Panero, S.; Scrosati, B. *J. Power Sources* **2006**, *160*, 1336.
(11) Yin, J.; Wada, M.; Yoshida, S.; Ishihara, K.; Tanase, S.; Sakai, T. *J. Electrochem. Soc.* **2003**, *150*, A1129.
(12) Wachtler, M.; Winter, M.; Besenhard, J. O. *J. Power Sources* **2002**, *105*, 151.
(13) Benedek, R.; Thackeray, M. M. *J. Power Sources* **2002**, *110*, 406.
(14) Besenhard, J. O.; Yang, J.; Winter, M. *J. Power Sources* **1997**, *68*, 87.
(15) Yang, J.; Winter, M.; Besenhard, J. O. *Solid State Ionics* **1996**, *90*, 281.
(16) Thackeray, M. M.; Vaughey, J. T.; Kahaian, A. J.; Kepler, K. D.; Benedek, R. *Electrochem. Commun.* **1999**, *1*, 111.
(17) Kepler, K. D.; Vaughey, J. T.; Thackeray, M. M. *Electrochem. Solid St.* **1999**, *2*, 307.
(18) Valvo, M.; Lafont, U.; Simonin, L.; Kelder, E. M. *J. Power Sources* **2007**, *174*, 428.

(19) Johannis, A. *C. R. Hebd. Séances Acad. Sci.* **1891**, *13*, 795.
(20) Johannis, A. *C. R. Hebd. Séances Acad. Sci.* **1892**, *114*, 587.
(21) Smyth, F. *J. Am. Chem. Soc.* **1917**, *39*, 1299.
(22) Zintl, E.; Goubeau, J.; Dullenkopf, W. *Z. Phys. Chem.* **1931**, *A 154*, 1.
(23) Zintl, E.; Harder, A. *Z. Phys. Chem.* **1931**, *A 154*, 47.
(24) Fässler, T. F. *Zintl Ions: Principles and Recent Developments, Vol. 140* (Eds.: Mingos, D. M. P., Fässler, T. F.), Springer, Heideberg **2011**, 91.
(25) King, R. B. *Zintl Ions: Principles and Recent Developments, Vol. 140* (Eds.: Mingos, D. M. P., Fässler, T. F.), Springer, Heideberg **2011**, 1.
(26) Laves, F. *Naturwissenschaften* **1941**, *29*, 244.
(27) Housecroft, C. E.; Sharpe, A. G. *Inorg. Chem.* **2005**, *Vol. 2*.
(28) Sevov, S. C. In *Intermetallic Compounds - Principles and Practice*; Wiley VCH, Weinheim **2002**, 113.
(29) Kauzlarich, S. M. *The Chemistry of Metal Clusters*, VCH Publishers, Inc., Weinheim **1996**.
(30) Bol'shakov, K. A.; Bul'onkov, N. A.; Rastorguev, L. N.; Tsirlin, M. S. *Russ. J. Inorg. Chem.* **1963**, *8*.
(31) Hopf, V.; Miiller, W.; Schafer, H. *Z. Naturforsch.* **1972**, *27b*, 1157.
(32) Schnering, H. G. v.; Bolle, U.; Curda, J.; Peters, K.; Carillo-Cabrera, W.; Somer, M.; Wedig, U.; Schultheiss, M. *Angew. Chem. Int. Ed. Engl.* **1996**, *35*, 984.
(33) Klemm, W.; Busmann, E. *Z. Anorg. Allg. Chem.* **1963**, *319*, 297.
(34) Mooser, E.; Pearson, W. B. *Phys. Rev.* **1956**, *101*, 1608.
(35) Wade, K. *J. Chem. Soc. D Chem. Comm.* **1971**, 792.
(36) Mingos, D. M. P. *Accounts Chem. Res.* **1984**, *17*, 311.
(37) Wade, K. In *Advances in Inorganic Chemistry and Radiochemistry Vol. 18*, (Eds.: Emeléus, H. J., Sharpe, A. G.) Academic Press: **1976**;, 1.
(38) Wade, K. *Inorg. Nucl. Chem. Lett.* **1972**, *8*, 559.
(39) Johnston, R. L.; Mingos, D. M. P. *Theoretical Models of Cluster Bonding Vol. 68*; Springer Berlin Heidelberg, **1987**.
(40) Fässler, T. F. *Coordin. Chem. Rev.* **2001**, *215*, 347.
(41) Corbett, J. D.; Edwards, P. A. *J. Am. Chem. Soc.* **1977**, *99*, 3313.
(42) Hauptmann, R.; Hoffmann, R.; Fässler, T. F. *Z. Anorg. Allg. Chem.* **2001**, *627*, 2220.
(43) Sevov, S. C.; Goicoechea, J. M. *Organometallics* **2006**, *25*, 5678.
(44) Rosdahl, J.; Fässler, T. F.; Kloo, L. *Eur. J. Inorg. Chem.* **2005**,

2888.
(45) Fässler, T. F. *Angew. Chem. Int. Ed. Engl.* **2001**, *40*, 4161.
(46) Queneau, V.; Sevov, S. C. *Angew. Chem. Int. Ed. Engl.* **1997**, *36*, 1754.
(47) Von Schnering, H. G.; Baitinger, M.; Bolle, U.; Carrillo-Cabrera, W.; Curda, J.; Grin, Y.; Heinemann, F.; Llanos, J.; Peters, K.; Schmeding, A.; Somer, M. *Z. Anorg. Allg. Chem.* **1997**, *623*, 1037.
(48) Queneau, V.; Sevov, S. C. *Inorg. Chem.* **1998**, *37*, 1358.
(49) Hoch, C.; Wendorff, M.; Röhr, C. *J. Alloy Compd.* **2003**, *361*, 206.
(50) Lehn, J. M. *Accounts Chem. Res.* **1978**, *11*, 49.
(51) Corbett, J. D.; Adolphson, D. G.; Merryman, D. J.; Edwards, P. A.; Armatis, F. J. *J. Am. Chem. Soc.* **1975**, *97*, 6267.
(52) Fässler, T. F.; Hoffmann, R. *J. Chem. Soc. Dalton* **1999**, 3339.
(53) Adolphson, D. G.; Corbett, J. D.; Merryman, D. J. *J. Am. Chem. Soc.* **1976**, *98*, 7234.
(54) Fässler, T. F.; Hoffmann, R. *Chimia* **1998**, *52*, 158.
(55) Scharfe, S.; Kraus, F.; Stegmaier, S.; Schier, A.; Fässler, T. F. *Angew. Chem. Int. Ed. Engl.* **2011**, *50*, 3630.
(56) Scharfe, S.; Fässler, T. F. *Philos. T. R. Soc. A* **2010**, *368*, 1265.
(57) Ugrinov, A.; Sevov, S. C. *J. Am. Chem. Soc.* **2002**, *124*, 10990.
(58) Ugrinov, A.; Sevov, S. C. *Inorg Chem* **2003**, *42*, 5789.
(59) Guloy, A. M.; Ramlau, R.; Tang, Z.; Schnelle, W.; Baitinger, M.; Grin, Y. *Nature* **2006**, *443*, 320.
(60) Hull, M. W.; Sevov, S. C. *J. Am. Chem. Soc.* **2009**, *131*, 9026.
(61) Eichhorn, B.; Kocak, S. *Zintl Ions: Principles and Recent Developments, Vol. 140* (Eds.: Mingos, D. M. P., Fässler, T. F.), Springer, Heideberg **2011**, *140*, 59.
(62) Corbett, J. D. *Chem. Rev.* **1985**, *85*, 383.
(63) Schäfer, H. *Ann. Rev. Mater. Sci.* **1985**, *15*, 1.
(64) Fässler, T. F.; Hoffmann, S. D. *Angew. Chem. Int. Ed. Engl.* **2004**, *43*, 6242.
(65) Kummer, D.; Diehl, L. *Angew. Chem.* **1970**, *82*, 881.
(66) Corbett, J. D.; Edwards, P. A. *J. Chem. Soc. Chem. Comm.* **1975**, 984.
(67) Corbett, J. D. *Structural and Electronic Paradigms in Cluster Chemistry, Vol. 87* (Eds.: Mingos, D. M. P.) **1997**, 157.
(68) Akerstedt, J.; Ponou, S.; Kloo, L.; Lidin, S. *Eur. J. Inorg. Chem.* **2011**, 3999.
(69) Goicoechea, J. M.; Sevov, S. C. *Inorg. Chem.* **2005**, *44*, 2654.

(70) Goicoechea, J. M.; Sevov, S. C. *J. Am. Chem. Soc.* **2004**, *126*, 6860.
(71) Fässler, T. F.; Hunziker, M.; Spahr, M. E.; Lueken, H.; Schilder, H. *Z. Anorg. Allg. Chem.* **2000**, *626*, 692.
(72) Critchlow, S. C.; Corbett, J. D. *J. Am. Chem. Soc.* **1983**, *105*, 5715.
(73) Fässler, T. F.; Hunziker, M. *Inorg. Chem.* **1994**, *33*, 5380.
(74) Fässler, T. F.; Hunziker, M. *Z. Anorg. Allg. Chem.* **1996**, *622*, 837.
(75) Spiekermann, A.; Hoffinann, S. D.; Fässler, T. F. *Angew. Chem. Int. Ed. Engl.* **2006**, *45*, 3459.
(76) Esenturk, E. N.; Fettinger, J.; Eichhorn, B. *J. Am. Chem. Soc.* **2006**, *128*, 9178.
(77) Cui, L.-F.; Huang, X.; Wang, L.-M.; Zubarev, D. Y.; Boldyrev, A. I.; Li, J.; Wang, L.-S. *J. Am. Chem. Soc.* **2006**, *128*, 8390.
(78) Cui, L.-F.; Huang, X.; Wang, L.-M.; Li, J.; Wang, L.-S. *J. Phys. Chem. A* **2006**, *110*, 10169.
(79) Scharfe, S. *Dissertation, Technische Universität München* **2010**.
(80) Xu, L.; Sevov, S. C. *J. Am. Chem. Soc.* **1999**, *121*, 9245.
(81) Downie, C.; Tang, Z.; Guloy, A. M. *Angew. Chem. Int. Ed. Engl.* **2000**, *39*, 337.
(82) Downie, C.; Mao, J.-G.; Parmar, H.; Guloy, A. M. *Inorg. Chem.* **2004**, *43*, 1992.
(83) Yong, L.; Hoffmann, S. D.; Fässler, T. F. *Z. Anorg. Allg. Chem.* **2005**, *631*, 1149.
(84) Yong, L.; Hoffmann, S. D.; Fässler, T. F. *Z. Anorg. Allg. Chem.* **2004**, *630*, 1977.
(85) Wang, J. Q.; Wahl, B.; Fässler, T. F. *Angew. Chem. Int. Ed. Engl.* **2010**, *49*, 6592.
(86) Hauptmann, R.; Fässler, T. F. *Z. Anorg. Allg. Chem.* **2003**, *629*, 2266.
(87) Hauptmann, R.; Fässler, T. F. *Z. Krist-New Cryst. St.* **2003**, *218*, 461.
(88) Ugrinov, A.; Sevov, S. C. *J. Am. Chem. Soc.* **2002**, *124*, 2442.
(89) Ugrinov, A.; Sevov, S. C. *J. Am. Chem. Soc.* **2003**, *125*, 14059.
(90) Ugrinov, A.; Sevov, S. C. *Chem.–Eur. J.* **2004**, *10*, 3727.
(91) Li, F.; Sevov, S. C. *Inorg. Chem.* **2012**, *51*, 2706.
(92) Schrenk, C.; Winter, F.; Pottgen, R.; Schnepf, A. *Inorg. Chem.* **2012**, *51*, 8583.
(93) Schrenk, C.; Neumaier, M.; Schnepf, A. *Inorg. Chem.* **2012**, *51*, 3989.

(94) Schrenk, C.; Helmlinger, J.; Schnepf, A. *Z. Anorg. Allg. Chem.* **2012**, *638*, 589.
(95) Li, F.; Munoz-Castro, A.; Sevov, S. C. *Angew. Chem. Int. Ed. Engl.* **2012**, *51*, 8581.
(96) Hull, M. W.; Ugrinov, A.; Petrov, I.; Sevov, S. C. *Inorg. Chem.* **2007**, *46*, 2704.
(97) Hull, M. W.; Sevov, S. C. *Angew. Chem. Int. Ed. Engl.***2007**, *46*, 6695.
(98) Hull, M. W.; Sevov, S. C. *Inorg. Chem.* **2007**, *46*, 10953.
(99) Chapman, D. J.; Sevov, S. C. *Inorg. Chem.* **2008**, *47*, 6009.
(100) Hull, M. W.; Sevov, S. C. *J. Organomet. Chem.* **2012**, *721*, 85.
(101) Hull, M. W.; Sevov, S. C. *Chem. Commun.* **2012**, *48*, 7720.
(102) Kocak, F. S.; Zavalij, P. Y.; Lam, Y. F.; Eichhorn, B. W. *Chem. Commun.* **2009**, 4197.
(103) Benda, C. B.; Wang, J. Q.; Wahl, B.; Fässler, T. F. *Eur. J. Inorg. Chem.* **2011**, 4262.
(104) Rios, D.; Gillett-Kunnath, M. M.; Taylor, J. D.; Oliver, A. G.; Sevov, S. C. *Inorg. Chem.* **2011**, *50*, 2373.
(105) Kocak, F. S.; Downing, D. O.; Zavalij, P.; Lam, Y. F.; Vedernikov, A. N.; Eichhorn, B. *J. Am. Chem. Soc.* **2012**, *134*, 9733.
(106) Gillett-Kunnath, M. M.; Paik, J. I.; Jensen, S. M.; Taylor, J. D.; Sevov, S. C. *Inorg. Chem.* **2011**, *50*, 11695.
(107) Esenturk, E. N.; Fettinger, J.; Eichhorn, B. *Chem. Commun.* **2005**, 247.
(108) Esenturk, E. N.; Fettinger, J. C.; Eichhorn, B. W. *J. Am. Chem. Soc.* **2006**, *128*, 12.
(109) Goicoechea, J. M.; Sevov, S. C. *Angew. Chem. Int. Ed. Engl.* **2005**, *44*, 4026.
(110) Sun, Z. M.; Zhao, Y. F.; Li, J.; Wang, L. S. *J. Clust. Sci.* **2009**, *20*, 601.
(111) Goicoechea, J. M.; Sevov, S. C. *J. Am. Chem. Soc.* **2005**, *127*, 7676.
(112) Sun, Z. M.; Xiao, H.; Li, J.; Wang, L. S. *J. Am. Chem. Soc.* **2007**, *129*, 9560.
(113) Kocak, F. S.; Zavalij, P.; Lam, Y. F.; Eichhorn, B. W. *Inorg. Chem.* **2008**, *47*, 3515.
(114) Kocak, F. S.; Zavalij, P. Y.; Eichhorn, B. W. *Abstr. Pap. Am. Chem. S.* **2010**, *240*.
(115) Kesanli, B.; Halsig, J. E.; Zavalij, P.; Fettinger, J. C.; Lam, Y. F.;

Eichhorn, B. W. *J. Am. Chem. Soc.* **2007**, *129*, 4567.
(116) Goicoechea, J. M.; Sevov, S. C. *J. Am. Chem. Soc.* **2006**, *128*, 4155.
(117) Gardner, D. R.; Fettinger, J. C.; Eichhorn, B. W. *Angew. Chem. Int. Ed. Engl.***1996**, *35*, 2852.
(118) Teixidor, F.; Luetkens, M. L.; Rudolph, R. W. *J. Am. Chem. Soc.* **1983**, *105*, 149.
(119) Kocak, F. S.; Zavalij, P.; Eichhorn, B. *Chem.-Eur. J.* **2011**, *17*, 4858.
(120) Kesanli, B.; Fettinger, J.; Gardner, D. R.; Eichhorn, B. *J. Am. Chem. Soc.* **2002**, *124*, 4779.
(121) Zhou, B. B.; Goicoechea, J. M. *Chem.-Eur. J.* **2010**, *16*, 11145.
(122) Kramer, T.; Duckworth, J. C. A.; Ingram, M. D.; Zhou, B. B.; McGrady, J. E.; Goicoechea, J. M. *Dalton Trans.* **2013**, *42*, 12120.
(123) Zhou, B. B.; Denning, M. S.; Kays, D. L.; Goicoechea, J. M. *J. Am. Chem. Soc.* **2009**, *131*, 2802.
(124) Wang, J. Q.; Stegmaier, S.; Fässler, T. F. *Angew. Chem. Int. Ed. Engl.* **2009**, *48*, 1998.
(125) Hlukhyy, V.; He, H. Y.; Jantke, L. A.; Fässler, T. F. *Chem.-Eur. J.* **2012**, *18*, 12000.
(126) Wang, J. Q.; Stegmaier, S.; Wahl, B.; Fässler, T. F. *Chem.-Eur. J.* **2010**, *16*, 1793.
(127) Zhou, B. B.; Kramer, T.; Thompson, A. L.; McGrady, J. E.; Goicoechea, J. M. *Inorg. Chem.* **2011**, *50*, 8028.
(128) Scharfe, S.; Fässler, T. F.; Stegmaier, S.; Hoffmann, S. D.; Ruhland, K. *Chem.-Eur. J.* **2008**, *14*, 4479.
(129) Benda, C. B. *Dissertation, Technische Universität München* **2013**.
(130) Eichhorn, B. W.; Haushalter, R. C.; Pennington, W. T. *J. Am. Chem. Soc.* **1988**, *110*, 8704.
(131) Eichhorn, B. W.; Haushalter, R. C. *J. Chem. Soc. Chem. Comm.* **1990**, 937.
(132) Yong, L.; Hoffmann, S. D.; Fässler, T. F. *Eur. J. Inorg. Chem.* **2005**, 3663.
(133) Kesanli, B.; Fettinger, J.; Eichhorn, B. *Chem.-Eur. J.* **2001**, *7*, 5277.
(134) Campbell, J.; Mercier, H. P. A.; Franke, H.; Santry, D. P.; Dixon, D. A.; Schrobilgen, G. J. *Inorg. Chem.* **2001**, *41*, 86.
(135) Schenk, C.; Schnepf, A. *Chem. Commun.* **2009**, 3208.

(136) Zhou, B. B.; Denning, M. S.; Jones, C.; Goicoechea, J. M. *Dalton Trans.* **2009**, 1571.
(137) Goicoechea, J. M.; Sevov, S. C. *Organometallics* **2006**, *25*, 4530.
(138) Zhou, B. B.; Denning, M. S.; Chapman, T. A. D.; Goicoechea, J. M. *Inorg. Chem.* **2009**, *48*, 2899.
(139) Scharfe, S.; Fässler, T. F. *Eur. J. Inorg. Chem.* **2010**, 1207.
(140) Spiekermann, A.; Hoffmann, S. D.; Kraus, F.; Fässler, T. F. *Angew. Chem. Int. Ed. Engl.* **2007**, *46*, 1638.
(141) Spiekermann, A.; Hoffmann, S. D.; Fässler, T. F.; Krossing, I.; Preiss, U. *Angew. Chem. Int. Ed. Engl.* **2007**, *46*, 5310.
(142) Zhou, B. B.; Denning, M. S.; Chapman, T. A. D.; McGrady, J. E.; Goicoechea, J. M. *Chem. Commun.* **2009**, 7221.
(143) Denning, M. S.; Goicoechea, J. M. *Dalton Trans.* **2008**, 5882.
(144)Boeddinghaus, M. B.; Hoffmann, S. D.; Fässler, T. F. *Z. Anorg. Allg. Chem.* **2007**, *633*, 2338.
(145) Yong, L.; Boeddinghaus, M. B.; Fässler, T. F. *Z. Anorg. Allg. Chem.* **2010**, *636*, 1293.
(146) Benda, C. B.; Schaper, R.; Schulz, S.; Fässler, T. F. *Eur. J. Inorg. Chem.* **2013**, *2013*, 5964.
(147) Joseph, S.; Hamberger, M.; Mutzbauer, F.; Hartl, O.; Meier, M.; Korber, N. *Angew. Chem. Int. Ed. Engl.* **2009**, *48*, 8770.
(148) Fässler, T. F. *Abstr. Pap. Am. Chem. S.* **2003**, *226*, U680.
(149) Espinoza-Quintero, G.; Duckworth, J. C. A.; Myers, W. K.; McGrady, J. E.; Goicoechea, J. M. *J. Am. Chem. Soc.* **2013**, *136*, 1210.
(150) Brynda, M.; Herber, R.; Hitchcock, P. B.; Lappert, M. F.; Nowik, I.; Power, P. P.; Protchenko, A. V.; Ruzicuka, A.; Steiner, J. *Angew. Chem. Int. Ed. Engl.* **2006**, *45*, 4333.
(151) Kesanli, B.; Halsig, J. E.; Zavalij, P.; Fettinger, J. C.; Lam, Y. F.; Eichhorn, B. W. *J. Am. Chem. Soc.* **2007**, *129*, 4567.
(152) Esenturk, E. N.; Fettinger, J.; Eichhorn, B. *Polyhedron* **2006**, *25*, 521.
(153) Burns, R. C.; Corbett, J. D. *J. Am. Chem. Soc.* **1982**, *104*, 2804.
(154) Rudolph, R. W.; Wilson, W. L.; Taylor, R. C. *J. Am. Chem. Soc.* **1981**, *103*, 2480.
(155) Critchlow, S. C.; Corbett, J. D. *Inorg. Chem.* **1982**, *21*, 3286.
(156) Gillett-Kunnath, M. M.; Oliver, A. G.; Sevov, S. C. *J. Am. Chem. Soc.* **2011**, *133*, 6560.
(157) Munoz-Castro, A.; Sevov, S. C. *Phys. Chem. Chem. Phys.* **2013**, *15*, 986.

(158) Gillett-Kunnath, M. M.; Munoz-Castro, A.; Sevov, S. C. *Chem. Commun.* **2012**, *48*, 3524.
(159) Lips, F.; Dehnen, S. *Angew. Chem. Int. Ed. Engl.* **2009**, *48*, 6435.
(160) Lips, F.; Holynska, M.; Clerac, R.; Linne, U.; Schellenberg, I.; Pottgen, R.; Weigend, F.; Dehnen, S. *J. Am. Chem. Soc.* **2012**, *134*, 1181.
(161) Lips, F.; Clerac, R.; Dehnen, S. *J. Am. Chem. Soc.* **2011**, *133*, 14168.
(162) Lips, F.; Dehnen, S. *Angew. Chem. Int. Ed. Engl.* **2011**, *50*, 955.
(163) Lips, F.; Schellenberg, I.; Pottgen, R.; Dehnen, S. *Chem.-Eur. J.* **2009**, *15*, 12968.
(164) Waibel, M.; Raudaschl-Sieber, G.; Fässler, T. F. *Chem.-Eur. J.* **2011**, *17*, 13391.
(165) Waibel, M. *Dissertation, Technische Universität München* **2012**, 55.
(166) Gupta, U. *Dissertation, Pennsylvania State University.* **2010**.
(167) Burns, R. C.; Corbett, J. D. *J. Am. Chem. Soc.* **1981**, *103*, 2627.
(168) Critchlow, S. C.; Corbett, J. D. *Inorg. Chem.* **1985**, *24*, 979.
(169) Friedrich, U.; Neumeier, M.; Koch, C.; Korber, N. *Chem. Commun.* **2012**, *48*, 10544.
(170) Xu, L.; Sevov, S. C. *Inorg. Chem.* **2000**, *39*, 5383.
(171) Ababei, R.; Heine, J.; Holynska, M.; Thiele, G.; Weinert, B.; Xie, X. L.; Weigend, F.; Dehnen, S. *Chem. Commun.* **2012**, *48*, 11295.
(172) Vassilev, G. P.; Lilova, K. I. *Arch. Metall Mater.* **2006**, *51*, 365.
(173) Ishida, K.; Nishizawa, T. *J. Phase Equilibia* **1991**, *12*, 88.
(174) Vassilev, G. P.; Lilova, K. I.; Gachon, J. C. *Intermetallics* **2007**, *15*, 1156.
(175) Lang, A.; Jeitschko W. *Z. Metallkde.***1996**, *87*, 759.
(176) Kanatzidis, M. G.; Pöttgen, R.; Jeitschko, W. *Angew. Chem. Int. Ed. Engl.***2005**, *44*, 6996.
(177) Todd, A. D. W.; Mar, R. E.; Dahn, J. R. *J. Electrochem. Soc.* **2006**, *153*, A1998.
(178) Chou, N. H.; Schaak, R. E. *J. Am. Chem. Soc.* **2007**, *129*, 7339.
(179) Wang, X.-L.; Chen, H.; Bai, J.; Han, W. Q. *J. Phys. Chem. Lett.* **2012**, *3*, 1488.
(180) Hlukhyy, V.; Stegmaier, S.; Van Wüllen, L.; Fässler, T. F. *Chem.–Eur. J.* **2014**, accepted.
(181) Burns, R. C.; Corbett, J. D. *Inorg. Chem.* **1985**, *24*, 1489.
(182) Spek, A. L. *J. Appl. Crystallogr.* **2003**, *36*, 7.

(183) Vandersluis, P.; Spek, A. L. *Acta Crystallogr. A* **1990**, *46*, 194.
(184) Jagodzinski, H.; Hellner, E. *Z. Kristallogr.* **1956**, *107*, 124.
(185) Patil, N. G.; Ramakrishnan, S. *Phys. Rev. B* **1997**, *56*, 3360.
(186) Lang, A.; Jeitschko, W. *J. Mater. Chem.* **1996**, *6*, 1897.
(187) Sreeraj, P.; Kurowski, D.; Hoffmann, R. D.; Wu, Z.; Pöttgen, R. *J. Solid State Chem.* **2005**, *178*, 3420.
(188) Sato, H.; Aoki, Y.; Sugawara, H.; Fukuhara, T. *J. Phys. Soc. Jpn.* **1995**, *64*, 3175.
(189) Anand, V. K.; Adroja, D. T.; Hillier, A. D.; Kockelmann, W.; Fraile, A.; Strydom, A. M. *J. Phys.: Condens. Matter* **2011**, *23*, 276001 (12pp).
(190) Anand, V. K.; Adroja, D. T.; Hillier, A. D. *Phys. Rev. B* **2012**, *85*, 014418.
(191) Künnen, B.; Niepmann, D.; Jeitschko, W. *J Alloy Compd.* **2000**, *309*, 1.
(192) Nordmark, E.; Wallner, O.; Häussermann, U. *J. Solid State Chem.* **2002**, *168*, 34.
(193) Tran, V. H.; Bukowski, Z.; Wiśniewski, P.; Tran, L. M.; Zaleski, A. J. *J Phys. Condens. Matter.* **2013**, *25*, 155701.
(194) Schlüter, M.; Häussermann, U.; Heying, B.; Pöttgen, R. *J. Solid State Chem.* **2003**, *173*, 418.
(195) Sreeraj, P.; Wiemhöfer, H. D.; Hoffmann, R.-D.; Skowronek, R.; Kirfel, A.; Pöttgen, R. *J. Solid State Chem.* **2006**, *179*, 355.
(196) Mayer, H. W.; Ellner, M.; Schubert, K. *J. Less Common Met.* **1978**, *61*, P1.
(197) Critchlow, S. C.; Corbett, J. D. *Inorg. Chem.* **1984**, *23*, 770.
(198) Bolle, U.; Tremel, W. *J. Chem. Soc. Chem. Comm.* **1992**, 91.
(199) Lips, F.; Raupach, M.; Massa, W.; Dehnen, S. *Z. Anorg. Allg. Chem.* **2011**, *637*, 859.
(200) Belin, C. H. E.; Corbett, J. D.; Cisar, A. *J. Am. Chem. Soc.* **1977**, *99*, 7163.
(201) Belin, C.; Mercier, H.; Angilella, V. *New J. Chem.* **1991**, *15*, 931.
(202) Spiekermann, A.; Hoffmann, S. D.; Fässler, T. F. *Angew. Chem. Int. Ed. Engl.***2006**, *45*, 3459.
(203) Esenturk, E. N.; Fettinger, J.; Lam, Y. F.; Eichhorn, B. *Angew. Chem. Int. Ed. Engl.* **2004**, *43*, 2132.
(204) Allen, F. H. *Acta Crystallogr. B* **2002**, *58*, 380.
(205) Scharfe, S.; Fässler, T. F. *Z. Anorg. Allg. Chem.* **2011**, *637*, 901.
(206) Ugrinov, A.; Sevov, S. C. *Chem.-Eur. J.* **2004**, *10*, 3727.

(207) Nienhaus, A.; Hoffmann, S. D.; Fässler, T. F. *Z. Anorg. Allg. Chem.* **2006**, *632*, 1752.
(208) Zhelyaskov, V.; Georgiev, G.; Nickolov, Z.; Miteva, M. *Spectrochim. Acta A* **1989**, *45*, 625.
(209) Fukuhara, K.; Tachikake, M.; Matsumoto, S.; Matsuura, H. *J. Phys. Chem.* **1995**, *99*, 8617.
(210) Ozutsumi, K.; Natsuhara, M.; Ohtaki, H. *B. Chem. Soc. Jpn.* **1989**, *62*, 2807.
(211) Leites, L. A.; Bukalov, S. S.; Zabula, A. V.; Lyubetskii, D. V.; Krylova, I. V.; Egorov, M. P. *Russ. Chem. Bull.* **2004**, *53*, 33.
(212) Siebert, H. *Z. Anorg. Allg. Chem.* **1952**, *268*, 177.
(213) Lippincott, E. R.; Tobin, M. C. *J. Am. Chem. Soc.* **1953**, *75*, 4141.
(214) Lannin, J. S.; Maley, N.; Kshirsagar, S. T. *Solid State Commun.* **1985**, *53*, 939.
(215) López-Cruz, E.; Cardona, M. *Solid State Commun.* **1983**, *45*, 787.
(216) Parker, J. H.; Feldman, D. W.; Ashkin, M. *Phys. Rev.* **1967**, *155*, 712.
(217) Williams, J. S.; Haber, B.; Deshmukh, S.; Johnson, B. C.; Malone, B. D.; Cohen, M. L.; Bradby, J. E. *physica status solidi (RRL) – Rapid Research Letters* **2013**, *7*, 355.
(218) Carrillo-Cabrera, W.; Aydemir, U.; Somer, M.; Kircali, A.; Fässler, T. F.; Hoffmann, S. D. *Z. Anorg. Allg. Chem.* **2007**, *633*, 1575.
(219) Carrillo-Cabrera, W.; Cardoso Gil, R.; Somer, M.; Persil, Ö.; von Schnering, H. G. *Z. Anorg. Allg. Chem.* **2003**, *629*, 601.
(220) Kircali, A. *Master Thesis, Koç University* **2007**.
(221) Fässler, T. F.; Hoffmann, R. *Angew. Chem. Int. Ed. Engl.* **1999**, *38*, 543.
(222) Yong, L.; Hoffmann, S. D.; Fässler, T. F. *Z. Krist.-New Cryst. St.* **2005**, *220*, 49.
(223) Brennessel, W. W.; Ellis, J. E. *Inorg. Chem.* **2012**, *51*, 9076.
(224) Hanic, F.; Mills, O. S. *J. Organomet. Chem.* **1968**, *11*, 151.
(225) Zhu, G.; Janak, K. E.; Figueroa, J. S.; Parkin, G. *J. Am. Chem. Soc.* **2006**, *128*, 5452.
(226) Woolf, A.; Chaplin, A. B.; McGrady, J. E.; Alibadi, M. A. M.; Rees, N.; Draper, S.; Murphy, F.; Weller, A. S. *Eur. J. Inorg. Chem.* **2011**, *2011*, 1614.
(227) Elschenbroich, C.; Möckel, R.; Bilger, L. *Z. Naturforsch. Teil B* **1984**, *39*, 375.
(228) Veauthier, J. M.; Chow, A.; Fraenkel, G.; Geib, S. J.; Cooper, N.

J. *Organometallics* **2000**, *19*, 661.
(229) Allen, F. *Acta Crystallogr. Sect. B* **2002**, *58*, 380.
(230) Jilek, R. E.; Jang, M.; Smolensky, E. D.; Britton, J. D.; Ellis, J. E. *Angew. Chem. Int. Ed. Engl.***2008**, *47*, 8692.
(231) Brennessel, W. W.; Ellis, J. E.; Roush, S. N.; Strandberg, B. R.; Woisetschlager, O. E.; Young, V. G. *Chem. Commun.* **2002**, 2356.
(232) Brennessel, W. W.; Ellis, J. E.; Pomije, M. K.; Sussman, V. J.; Urnezius, E.; Young, V. G. *J. Am. Chem. Soc.* **2002**, *124*, 10258.
(233) Brennessel, W. W.; Jilek, R. E.; Ellis, J. E. *Angew. Chem. Int. Ed. Engl.* **2007**, *46*, 6132.
(234) Brennessel, W. W.; Young, V. G.; Ellis, J. E. *Angew. Chem. Int. Ed. Engl.* **2002**, *41*, 1211.
(235) Pöttgen, R.; Hoffmann, R. D.; Sampathkumaran, E. V.; Das, I.; Mosel, B. D.; Müllmann, R. *J. Solid State Chem.* **1997**, *134*, 326.
(236) Sheldrick, G. *Acta Crystallogr. A* **2008**, *64*, 112.
(237) Both synthesis routes were established by Dr. Viktor Hlukhyy.